UNIVERSITA' DEGLI STUDI DI PADOVA

DIPARTIMENTO DI PEDIATRIA

SCUOLA DI DOTTORATO DI RICERCA IN MEDICINA DELLO SVILUPPO E SCIENZE DELLA PROGRAMMAZIONE

INDIRIZZO EMATOONCOLOGIA E IMMUNOLOGIA

XXIV CICLO

TITOLO TESI

Analysis of the epigenetic effects induced by brain microenvironment on glioblastoma and medulloblastoma derived cells through *in vitro* and *in vivo* (Danio rerio) models.

Direttore della Scuola: Ch.mo Prof. Giuseppe Basso

Supervisore: Dott. Luca Persano

Dottoranda: Elena Rampazzo

31 Gennaio 2012

Table of Contents

SUMMARY

Glioblastoma multiforme (GBM) is one of most common and still poorly treated primary brain tumors. One of the biggest challenges in brain tumour research is the possibility of reprogramming cancer cells toward less aggressive phenotypes. To reach this aim however, a more complete understanding of the biology of GBM cells is needed, in particular considering the role played by hypoxia as a signaling pathways regulator. In search for new therapeutic approaches, Bone Morphogenetic Proteins (BMPs) have been demonstrated to induce astroglial commitment in GBM-derived cells in vitro. The mTOR pathway represent a controversial link between the pro-stemness hypoxic pathway and the pro-differentiating BMPs pathway. Indeed, HIF-1α is controlled at the transcriptional and translational level by mTOR and, alike BMP, also mTOR pathway modulates glial differentiation in central nervous system (CNS) stem cells. Here, we investigate the role of mTOR signaling in the regulation of HIF-1α stability in primary GBM-derived cells maintained under hypoxia (2% oxygen). We found that GBM cells, when acutely exposed to high oxygen tension, undergo Akt/mTOR pathway activation and that BMP2 acts in an analogous way. Importantly, repression of Akt/mTOR signaling is maintained by HIF-1α through REDD1 upregulation. On the other hand, BMP2 counter-acts HIF-1α stability by modulating intracellular succinate and by controlling proline hydroxylase 2 (PHD2) protein through inhibition of FKBP38, a PHD2 protein regulator. Despite being encouraging, these data suggested that hypoxia, which is characteristic of the brain niche where GBM reside, strongly counter-acts BMP effects; so a new therapeutic approaches able to counteract tumour growth also in its hypoxic microenvironment is fundamental. In the second part of this study, we reprogrammed primary GBM-derived cells toward a less oncogenic phenotype by activating Wnt pathway in GBM hypoxic microenvironment, that usually correlates with a malignant behaviour of cancer cells. We demonstrate that exogenous Wnt3a ligand mediates neuronal differentiation and proliferation inhibition of GBM cells and that this phenomenon is enhanced under hypoxic conditions by HIF-1α-mediated up-regulation of β-catenin co-factors TCF1 and LEF1. Moreover, we show that Wnt pathway activation inhibits Notch signalling, thus enhancing the pro-differentiating effects exerted by the Wnt activated pro-neuronal genes NEUROD1 and

NEUROG1, and that this occurs mainly in the GBM cancer stem cell subpopulation (CD133+). By using a zebrafish-based protocol for orthotopic xeno-transplantation of primary GBM-derived cells, we show that Wnt pathway activation is able to promote neuronal differentiation of GBM cells by inhibiting Notch signalling also in an in vivo setting.

Conclusions: In this study we elucidate the molecular mechanisms by which two pro-differentiating stimuli, BMP2 and acute high oxygen exposure, control HIF-1α stability. We previously reported that both these stimuli, by inducing astroglial differentiation, affect GBM cells growth. We also found differences in high oxygen and BMP2 sensitivity between GBM cells and normal cells that should be further investigated to better define tumor cell biology. Moreover, we add more information in the epistatic relationship between HIF-1α, Wnt and Notch signalling in GBM-derived cells, demonstrating a Wnt-regulated suppression of Notch activity in the hypoxic microenvironment of GBM tumours.

The third part of my PhD study focused on Medulloblastoma (MDB) which is the most common brain malignancy of childhood. It is currently thought that MDB arises from aberrantly functioning stem cells in the cerebellum that fail to maintain proper control of self-renewal. Additionally, it has been reported that MDB cells display higher endogenous Notch signalling activation, known to promote the survival and proliferation of neoplastic neural stem cells and to inhibit their differentiation. While interaction between Hypoxia Inducible Factor-1α (HIF-1α) and Notch signalling is required to maintain normal neural precursors in an undifferentiated state, an interaction has not been identified in MDB. Here, we investigate whether hypoxia, through HIF-1α stabilization, modulates Notch1 signalling in primary MDB-derived cells. Our results indicate that MDB-derived precursor cells require hypoxic conditions for *in vitro* expansion, whereas acute exposure to 20% oxygen induces tumor cell differentiation and death through inhibition of Notch signaling. Importantly, stimulating Notch1 activation with its ligand Dll4 under hypoxic conditions leads to expansion of MDB-derived $CD133^+$ and $nestin^+$ precursors, suggesting a regulatory effect on stem cells. In contrast, MDB cells undergo neuronal differentiation when treated with γ-secretase inhibitor, which prevents Notch activation.

Conclusions. These results suggest that hypoxia, by maintaining Notch1 in its active form, preserves MDB stem cell viability and expansion.

Significance: We add new insights in the regulation of brain tumour stem cells and contribute to clarify the complex relationship between diverse signalling pathways in controlling GBM cell phenotype.

SOMMARIO

Il Gliobalstoma multiforme (GBM) è il più comune dei tumori cerebrali nell'adulto, con una prognosi ancora oggi particolarmente infausta e senza trattamenti efficaci. Una delle grosse sfide da affrontare nella ricerca sui tumori cerebrali è la possibilità di riprogrammare queste cellule verso un fenotipo meno aggressivo. Per raggiungere questo scopo tuttavia è necessaria una più ampia e completa conoscenza della biologia di questo tumore, in particolare del ruolo dell'ipossia come regolatore delle principali pathways coinvolte nel modulare il fenotipo delle cellule di GBM. Nella ricerca di nuovi approcci terapeutici, le Bone Morphogenetics proteins (BMPs) si sono dimostrate efficaci nell'indurre un differenziamento astrogliale delle cellule di GBM *in vitro*. Il pathway di mTOR rappresenta un collegamento controverso fra il mantenimento della staminalità, mediato dall'ipossia, e il differenziamento mediato dal BMP pathway. Infatti l'Hypoxia Inducible Factor-1α (HIF-1α) è controllato a livello trascrizionale e traduzionale dalla proteina mTOR e, come il BMP, lo stesso mTOR pathway modula il differenziamento gliale delle staminali neurali nel sistema nervoso centrale. In questo studio abbiamo valutato il ruolo del pathway di mTOR nel regolare la stabilità di HIF-1α in cellule primarie derivate da GBM e mantenute in ipossia (2% O_2). Abbiamo dimostrato che, quando esposte ad alte tensioni di ossigeno (20% O_2), le cellule di GBM attivano il pathway di Akt/mTOR e che la somministrazione del BMP2 promuove effetti analoghi. In particolare, abbiamo dimostrato che HIF-1α reprime il pathway di Akt/mTOR attraverso la up-regolazione della proteina Redd1, inibitore di mTOR. In maniera opposta, BMP2 contrasta la stabilità di HIF-1α modulando I livelli intracellulari di succinato e controllando i livelli di proline hydroxylase 2 (PHD2),

attraverso l'inibizione di FKBP38, una proteina regolatoria della PHD2. nonostante siano incoraggianti, questi dati suggeriscono che l'ipossia, caratteristica della nicchia dei tumori cerebrali, contrasta fortemente gli effetti del BMP2; quindi un approccio terapeutico in grado di arrestare la crescita tumorale anche nel suo microambiente ipossico è fondamentale. Nella seconda parte dello studio, l'intento è stato quello di riprogrammare cellule primarie derivate da GBM verso un fenotipo più differenziato e meno aggressivo attivando il Wnt pathway nel loro microambiente ipossico, solitamente correlato con la malignità delle cellule tumorali. Abbiamo dimostrato che la somministrazione esogena del ligando Wnt3a media il differenziamento neuronale e l'inibizione della proliferazione nelle cellule di GBM e che questo fenomeno è più forte in condizioni ipossiche grazie ad una up-regolazione dei co-fattori della β-catenina TCF1 and LEF1. Inoltre, abbiamo dimostrato che l'attivazione del Wnt pathway inibisce il segnale intracellulare di Notch, incrementando gli effetti pro-differenziativi del Wnt che attiva *per-se* i geni pro-neuronali NEUROD1 e NEUROG1. In particolare, questi effetti si esplicano nella sottopopolazione cellulare tumorale staminale (CD133+). Per valutare gli effetti dell'attivazione di questa pathway *in vivo* abbiamo messo a punto un protocollo di xeno-trapianto ortotopico di cellule primarie derivate da GBM in larve di Zebrafish (*Danio Rerio*). Le evidenze ci dimostrano che l'attivazione del Wnt pathway è in grado di promuovere il differenziamento neuronale delle cellule di GBM e di inibire il Notch pathway anche nel contesto di un modello animale.

Conclusione: in questo studio abbiamo delucidato i meccanismi molecolari attraverso cui due stimoli pro-differenziativi, BMP2 e osiigeno, controllino la stabilità di HIF-1α. Abbiamo riportato in precedenti lavori che entrambi questi stimoli inducono il differenziamento astro gliale e bloccano la crescita delle cellule di GBM. Abbiamo inoltre evidenziato le differenze tra cellule tumorali di GBM e cellule staminali neurali sane nella risposta agli stimoli pro-differenziativi, divergenze di risposta che richiedono ulteriori indagini per meglio definire la biologia del tumore. Inoltre, abbiamo delucidato la relazione epistatica che intercorre tra HIF-1α, Wnt e Notch in cellule derivade da glioblastoma, dimostrando come Wnt regoli la soppressione del Notch pathway nel microambiente ipossico dei glioblastomi.

La terza parte del mio progetto di dottorato si è focalizzata su un tumore cerebellare pediatrico di origine neuronale classificato come Medulloblastoma (MDB), che si riscontra essere il più frequente fra i tumori cerebrali pediatrici. Le più recenti ricerche rivelano che il MDB deriva da cellule staminali del cervelletto che proliferano in maniera aberrante perdendo il controllo della loro capacità di auto-rinnovamento. E' stato inoltre riportato che cellule di MDB hanno una elevata attivazione endogena del Notch signalling, noto per promuovere proliferazione e sopravvivenza delle cellule staminali neurali neoplastiche e per inibire il loro differenziamento. Se l'interazione fra HIF-1α e il Notch signalling ha la funzione di mantenere i precursori neurali sani in uno stato indifferenziato, la loro interazione nelle cellule di MDB non è ancora stata caratterizzata. In questo studio abbiamo analizzato se l'ipossia, stabilizzando HIF-1α, modulasse il signalling di Notch1 in cellule primarie derivate da MDB. I nostri risultati indicano che cellule staminali derivate da MDB richiedono un ambiente ipossico per la loro espansione *in vitro*, mentre un'esposizione acuta delle stesse al 20% di ossigeno induce il differenziamento delle cellule tumorali e la loro morte attraverso l'inibizione del Notch1. Da notare che attivando Notch1 con il suo ligando DLL4 in condizioni ipossiche si ha un'espansione di precursori CD133+ e Nestina+ del MDB, suggerendo un effetto regolatorio di questo pathway sulla sotto-popolazione staminale. Al contrario, cellule di MDB vanno incontro a differenziamento neuronale quando trattate con un inibitore della γ-secretase che previene l'attivazione del Notch.

Conclusione: Questi risultati suggeriscono che l'ipossia, attivando il signalling intracellulare di Notch, preserva le cellule staminali di MDB e ne promuove l'espansione.

Significato: Con questo lavoro abbiamo cercato di definire la complessa regolazione che modula il fenotipo delle cellule staminali tumorali e abbiamo contribuito a chiarire la interrelazione fra i diversi signalling pathway che controllano fenotipo e comportamento delle cellule derivate da tumore cerebrale.

INTRODUCTION

The presence of cells with stem like properties in several solid tumours has lead to the "cancer stem cells hypothesis" and nowadays this sub-population of neoplastic cells has become a subject of studies aimed to develop new therapeutic approaches (Vescovi et al., 2006). Understanding the intrinsic properties that characterize cancer stem cells and distinguish them from healthy stem cells is critical for the development of successful and selective therapies. Thus, it is of primary importance to identify the specific cancer stem cells response to signals for proliferation and survival in the stem cell niche. Glioblastoma multiforme (GBM) is the most common malignant tumours occurring in the central nervous system (CNS) and represents 4-10% of the primitive brain malignancy that originate in the cortical region. In particular, GBM is a highly proliferating tumour, characterized by a high tendency to infiltrate surrounding tissues and the presence of extensive areas of necrosis and hypoxia (Rong et al., 2006). Recent evidence indicates that tumours consistently arise from a specific subset of cells defined as cancer stem cells. Dissociated CNS tumour cells express primitive markers (i.e. CD133, Sox2, Musashi1, Bmi1 and Nestin) and exhibit multipotency when placed in defined serum-free stem cell medium (Hemmati et al., 2003; Ignatova et al., 2002; Singh et al., 2003). Additionally, $CD133^{hi}$ cells show the highest frequency of initiating new GBM and MDB tumours when grafted in NOD/SCID mice (Singh et al., 2004). At present, chemo and radiation-therapies target cells characterized by high proliferation rates. Conversely, cancer stem cells seem to be characterized by low rates of division and proliferation, and certain antigens that are currently targeted by some biological treatments may not be expressed on cancer stem cells surface due to their immature state (Guzman and Jordan, 2004; Perez-Caro and Sanchez-Garcia, 2006); thus the cancer stem cell population is spared, causing relapse.

An important parameter we consider in our study is tissue oxygenation. In the human brain, the mean pO_2 measured varies from 3.2% at 22 to 27 mm below the dura, to 4.4% at 7 to 12 mm (Dings et al., 1998). Additionally, high grade gliomas are highly vascularized, with the tendency to infiltrate and they are characterized by extensive areas of necrosis and hypoxia. It is known that lowered oxygen tensions positively

correlate with tumour aggressiveness (Azuma et al., 2003; Jogi et al., 2002) and over-activity of Hypoxia Inducible Factor-1α (HIF-1α) (Smith et al., 2005) is implicated in tumour progression. The correlation between hypoxia and tumor aggressiveness has been causally linked to increased genomic instability (Koshiji et al., 2005), but it is also related to increased survival of proliferating cells by suppression of p53 and its associated cell growth control (Zhang and Hill, 2004). Importantly, hypoxia has been shown to promote de-differentiation of neuroblastoma cells (Jogi et al., 2002; Jogi et al., 2003; Jogi et al., 2004), suggesting that it may reinforce an environment for aggressive tumor growth. It may also prevent a pre-existing stem cell population from differentiating, which is important in light of increasing evidence that cancer is initiated by dysfunctional stem cells (Al-Hajj et al., 2003; Bonnet and Dick, 1997; Singh et al., 2004). The HIF prolyl-hydroxylase 2 (PHD2) protein is the key oxygen sensor setting the low steady-state levels of HIF-1 in normoxia. Indeed, prolyl hydroxylation is a specific modification that provides recognition for the E3 ubiquitin ligase complex containing the von Hippel–Lindau tumour suppressor protein (pVHL) that present HIF-1 to the proteasome (Berra et al., 2003). Thus, it is very important to establish the appropriate cells culture conditions, in order to recreate in vitro an environment that more closely resembles the physiological one.

Additionally, it is known the involvement of signalling molecules, such as bone morphogenetic proteins (BMPs) as crucial mediators of stem cell self renewal and cell fate determination, which appear disrupted in brain cancers. Particularly, BMPs have been shown to be strong inducers of astroglial fates (Chen et al., 2007) while the endogenously secreted BMP-antagonist, noggin (Zimmerman et al., 1996), limits glial differentiation and directs postnatal stem cells to generate neurons (Lim et al., 2008) (Fig.1).

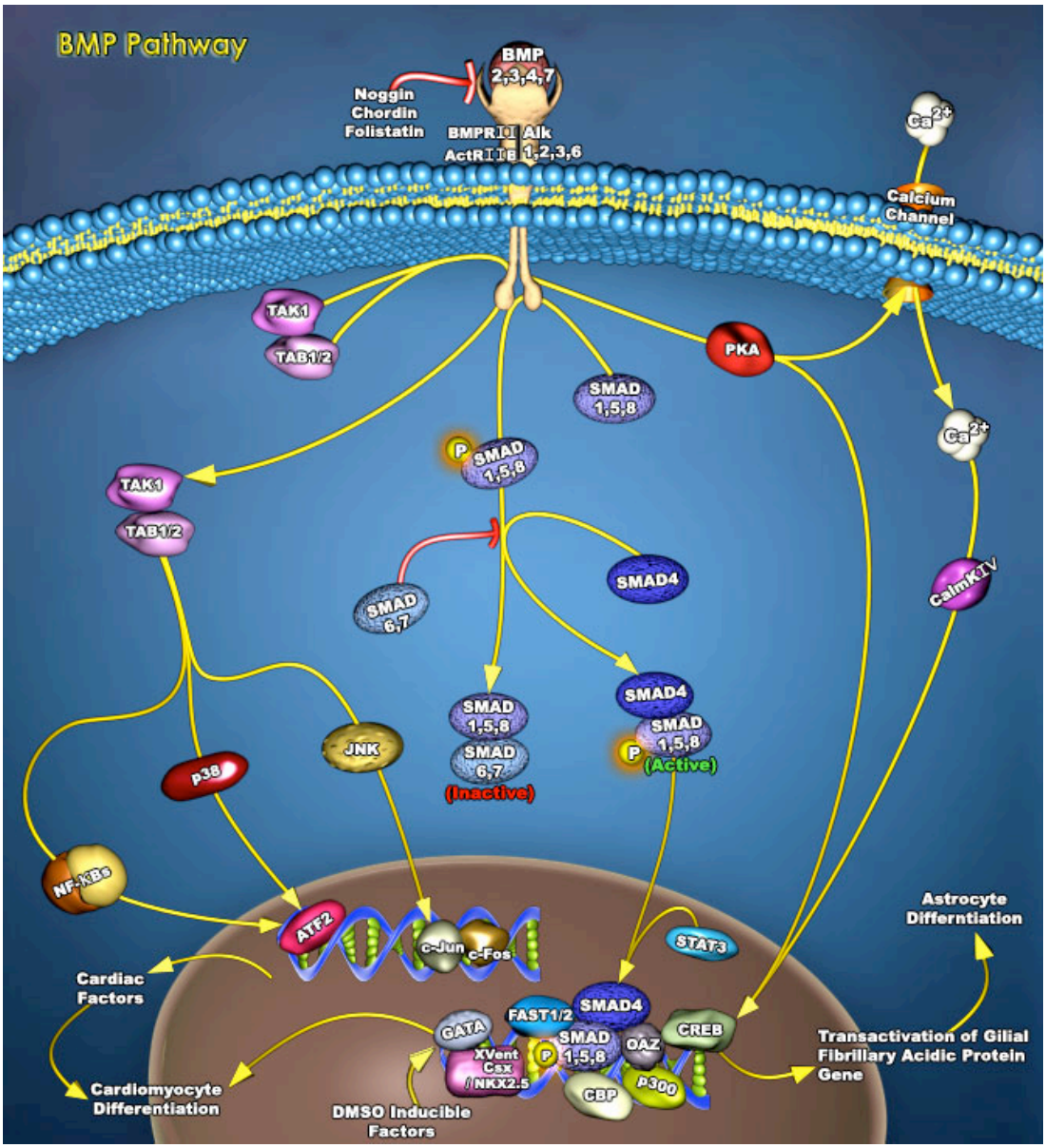

Figure 1. BMP Signaling Pathway.

Recently, Piccirillo et al. showed that BMP4 (and analogously BMP2) can modulate glial differentiation through increase in GFAP expression in primary cultures of glioblastoma (GBM), in particular in the brain tumor inducing population, thus indicating BMPs as potentially useful candidate molecules to promote differentiation of the tumor-initiating cells. We have recently shown (Pistollato et al., 2009a) that BMP2 in vitro treatment, known to promote glial differentiation in GBM derived cells (Piccirillo et al., 2006; Pistollato et al., 2009a), resulted to be less effective under hypoxia, suggesting that hypoxia and also HIF-1α may preserve GBM tumour cell

stemness by de-sensitizing cells to pro-differentiating BMP2 stimulus (Pistollato et al., 2009a; Pistollato et al., 2009b). It has also been reported that epigenetic-mediated dysfunction of the BMP receptor-IB (BMPR-IB) inhibits differentiation of glioblastoma-initiating cells BMPs mediated (Lee et al., 2008). Thus it is necessary to modulate the phenotype and to promote an effective cell cycle arrest of GBM derived cells in their hypoxic microenvironment. Canonical Wnt signalling activation (Fig 2), through β-catenin/TCF-LEF regulatory mechanism, has been recently suggested to promote neurogenesis from NSC in the murine adult hippocampus (Kuwabara et al., 2009), an hypoxic brain zone where reside the adult neural stem cells pool in mice and also in humans (Kuklekov et al., 1999). In the same context, it has been demonstrated that hypoxia can promote canonical Wnt signalling activation and that HIF-1α enhances NSC differentiation and neuronal maturation by co-operating with β-catenin activation (Mazumdar et al., 2010). Nowadays, the role of Wnt activation in regulating brain tumour phenotype remains controversial. Recent studies showed that lithium ($LiCl_2$) potently and specifically blocked glioma cell migration through inhibition of serine/threonine protein kinase glycogen synthase kinase-3 (GSK3), a β-catenin inhibitor (Nowicki et al., 2008). Moreover, the use of other GSK3 inhibitors have been reported to increase β-catenin levels, thus down-regulating stem cell markers, such as Nestin and Sox2 and increasing the fraction of cells expressing β-III-tubulin and GFAP in a cell line-dependent manner (Korur et al., 2009). However, other authors reported that over-expression of Wnt in astrocytic glioma specimens promoted CSCs self renewal and proliferation (Liu et al., 2010; Pu et al., 2009; Sareddy et al., 2009). Thus, the interaction between Wnt pathway and Hypoxic signalling in brain tumours remain to be elucidated.

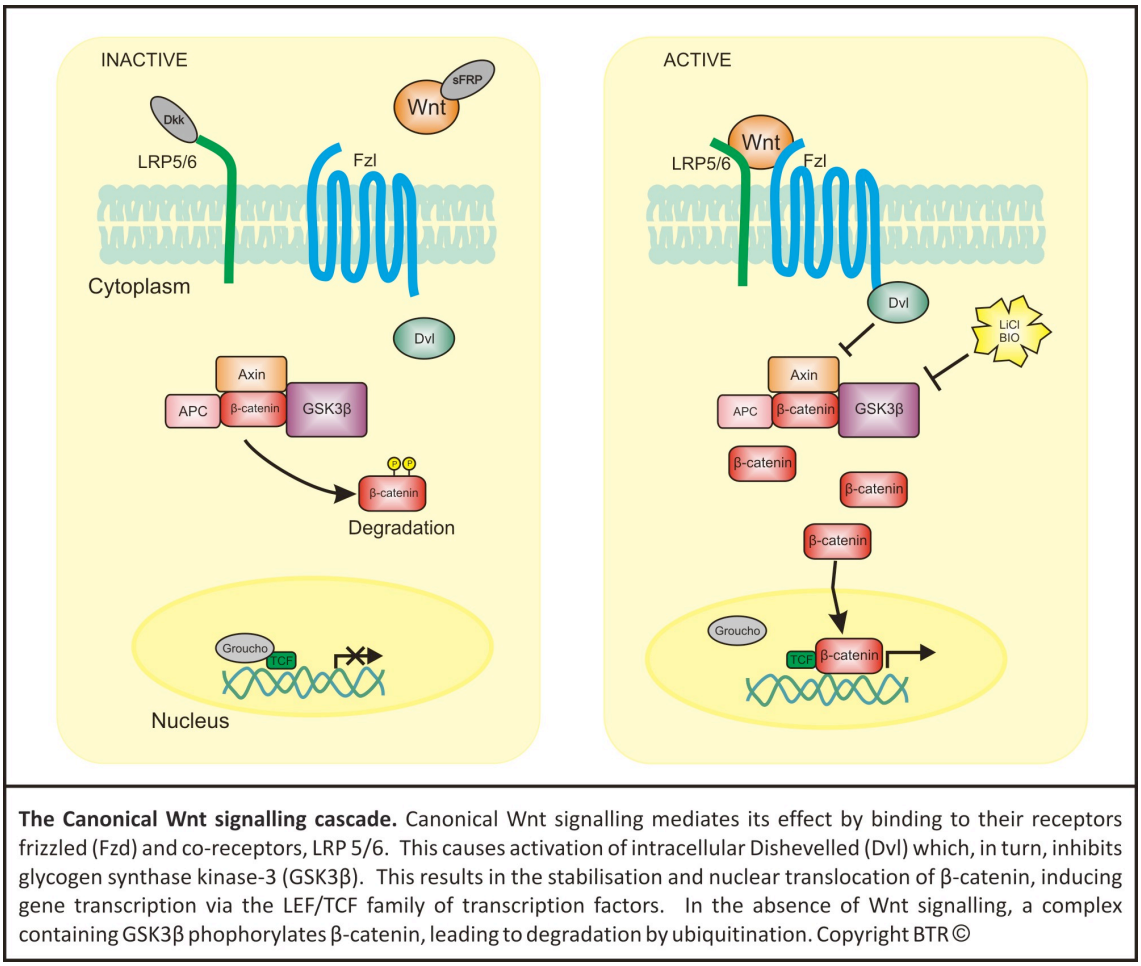

The Canonical Wnt signalling cascade. Canonical Wnt signalling mediates its effect by binding to their receptors frizzled (Fzd) and co-receptors, LRP 5/6. This causes activation of intracellular Dishevelled (Dvl) which, in turn, inhibits glycogen synthase kinase-3 (GSK3β). This results in the stabilisation and nuclear translocation of β-catenin, inducing gene transcription via the LEF/TCF family of transcription factors. In the absence of Wnt signalling, a complex containing GSK3β phophorylates β-catenin, leading to degradation by ubiquitination. Copyright BTR ©

Figure 2. Wnt Signaling Pathway

The small teleost zebrafish (*Danio rerio*) has been extensively used in the past decades as a powerful, easy to use, reliable vertebrate model organism for embryonic and postnatal molecular signaling studies and, lately, as a host for human tumor cell transplantation (FIG 3A-B).

Zebrafish biology allows ready access to all developmental stages, and the optical clarity of embryos and larvae allow real-time imaging of developing pathologies. Owing to the high evolutionary conservation of cell signaling mechanisms in vertebrates, the zebrafish larvae represents an excellent interacting environment that could influence phenotype and behavior of human cells, particularly of those derived from stem cells enriched tumors.

An important consideration to take into account is that in the zebrafish embryo and larvae the oxygen tension profile, at 0.7-1.2 mm in ventral-dorsal direction, ranges from 9% to 5% O2 (Kranenbarg, 2002). Thus, given the important role played by lowered

oxygen in the regulation and maintenance of the brain tumor niche and particularly of brain cancer stem cell sub-populations, the zebrafish larvae could provides a physiologic microenvironment to support the growth and preserve human tumor cells, alternatively to the use of a hypoxic cell culture chamber for *in vitro* studies. Indeed, zebrafish embryos have been recently proposed as a reliable vertebrate model for tumour xeno-transplantation and signalling studies (Geiger et al., 2008; Haldi et al., 2006; Nicoli and Presta, 2007). Moreover, by using zebrafish reporter lines it is possible to evaluate the microenvironmental signalling pathway and their interaction with human cancer cell.

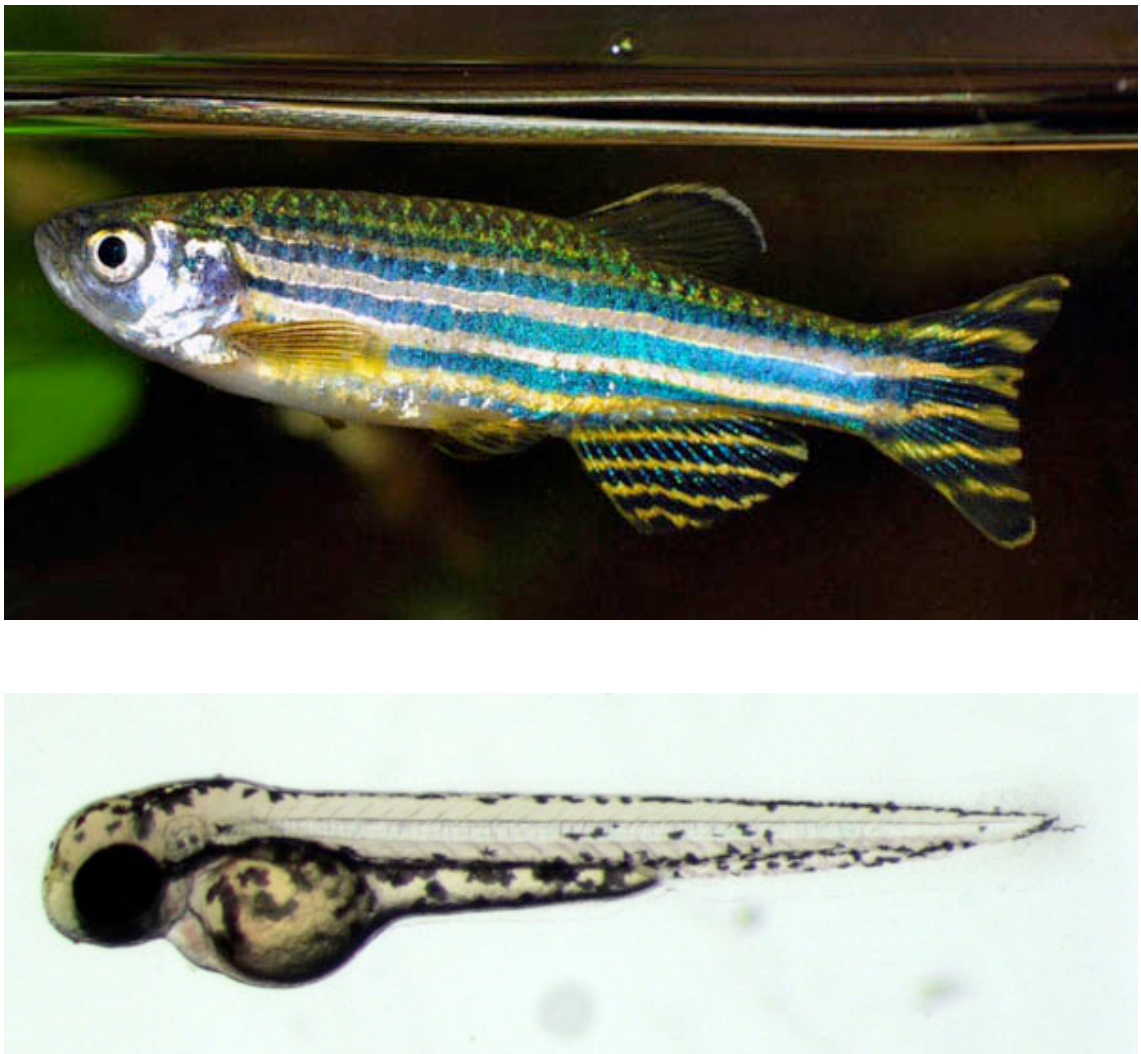

Fig. 3 Zebrafish image. (A) Zebrafish 6 month post-fertilization (B) Zebrafish larva 3 days post-fertilization

PART II: Medulloblastoma

Medulloblastoma is the most common cancerous brain tumor of childhood. It accounts for 20% to 25% of all childhood tumors, and they are malignant, invasive embryonal tumor of the cerebellum, predominantly displaying neuronal differentiation, and an inherent tendency to metastasize via cerebrospinal fluid pathways. Although it is thought that medulloblastomas originate from immature or embryonal cells at their earliest stage of development, the exact cell of origin, or "medulloblast" has yet to be identified. It is currently thought that medulloblastoma arises from cerebellar "stem cells" that have been prevented from dividing and differentiating into their normal cell types.

Additionally, it has been reported that in medulloblastoma cells there is a higher endogenous Notch activation (Fan et al., 2006; Fan et al., 2004; Hallahan et al., 2004; Raffel et al., 1997). Notch is known to promote the survival and proliferation of non-neoplastic neural stem cells and to inhibit their differentiation (Reya et al., 2001; Solecki et al., 2001). Signaling is initiated by ligand binding, followed by intramembranous proteolytic cleavage of the Notch receptor by the γ-secretase complex. Inhibitors of this complex slow the growth of Notch-dependent tumors such as medulloblastoma and T-cell leukemia (Fan et al., 2004; Hallahan et al., 2004). Medulloblastomas also are often characterized by intra-tumoral hypoxia. Recent literature shows that hypoxia and over-activity of Hypoxia Inducible Factor-1α (HIF-1α) correlate with tumor aggressiveness and progression. Hypoxia has a role in normal physiological responses, such as carotid body growth and generation of new neural crest derived glomus cells (Pardal et al., 2007), angiogenesis (Wong and Brem, 2008) and it is implicated in the regulation of crucial signaling pathways, such as bone morphogenetic proteins (BMPs), Akt/mTOR and Notch (Gustafsson et al., 2005; Pistollato et al., 2009a; Pistollato et al., 2009b).

It is known that hypoxia requires notch signalling (Fig. 4) to maintain the undifferentiated cell state in a mouse myogenic cell line C2C12 and mouse embryonic teratocarcinoma cell line P19 (Gustafsson et al., 2005) and notch pathway inhibition in DAOY cells, by pharmacologic inhibitors of γ-secretase, depletes stem-like cells and blocks engraftment (Fan et al., 2006). Here, we sought to investigate whether hypoxia and in particular HIF-1α modulate Notch signalling in primary MDB derived cells.

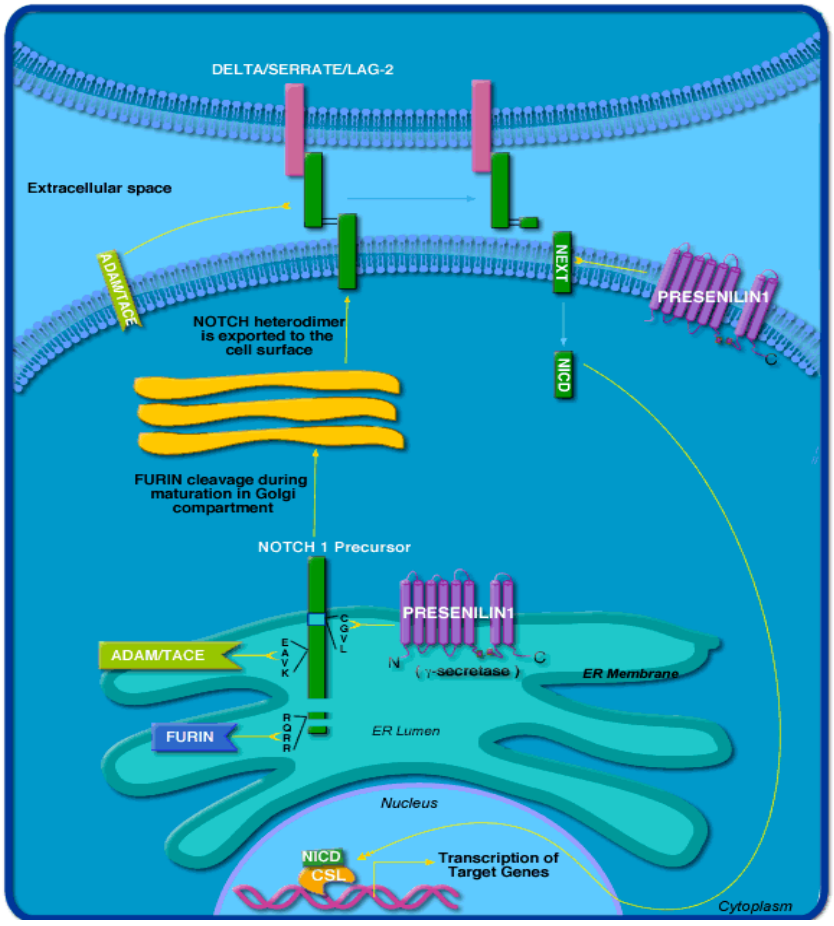

Figure4. Notch Signaling Pathway.

MAIN AIMS OF THE STUDY

1- To better understand the molecular pathways regulated by hypoxic tumour microenvironment in Glioblastoma (GBM) and Medulloblastoma (MDB).
2- To isolate and characterize the cancer stem like cells populations in GBM and MDB based on expression of CD133/CD15 cell surface antigens.
3- To evaluate the regulation of the signalling pathways involved in GBM cells phenotype in different wild type and transgenic Zebrafish larvae following GBM cancer cells transplantation.
4- To evaluate the potential phenotypic reprogramming capacity of Zebrafish (Danio rerio) embryo niche toward transplanted GBM cancer cells.

RESULTS (PART I)

GLIOBLASTOMA

Acute exposure to high oxygen tension promotes Akt/mTOR activation in a time dependent fashion in GBM-derived cells

Since the recent findings that BMP2 mediated glial differentiation of GBM derived cells (Piccirillo et al., 2006) resulted to be less effective under hypoxia, and that acute exposure to high oxygen tension promote intracellular BMP pathway activation (Pistollato et al., 2009a), in the first part of my PhD project I focused on the analysis of the molecular pathway involved in BMP2 and oxygen response in GBM derived cells. It has been previously shown that BMP2 increases Akt serine/threonine kinase activity in serum-deprived 2T3 cells (Ghosh-Choudhury et al., 2002) and Akt/PKB signaling is known to activate mTOR pathway. Importantly, we have recently demonstrated that increasing oxygen tension induces activation of endogenous BMP pathway, through SMAD1/5/8 activation, in GBM-derived cells (Pistollato et al., 2009a). We sought to investigate if a progressive time dependent exposure of GBM cells, that have been constantly maintained under hypoxia (2% oxygen), to an acute 20% oxygen tension, was promoting Akt/mTOR signaling pathway activation. We observed activation of Akt at the level of threonine 308, but not at the level of serine 473 (data not shown), in a time dependent fashion following high oxygen exposure (Figure 5A,C). Also, mTOR phosphorylation at the level of serine 2448 was induced by high oxygen exposure (Figure 5A,D). Under constant hypoxia these activations were inhibited. mTOR is known to regulate several biological cell responses, amongst them: i) translation, through activation of p70S6-Kinase (p70S6K) and inhibition of the inhibitor 4eBP1, ii) cell proliferation, by acting as a cell cycle regulator, iii) cell survival and cell differentiation, by Stat3 activation, iv) angiogenesis, through activation of HIF-1α and Vascular Endothelial Growth Factor (VEGF). We found that all mTOR downstream targets were activated by acute high oxygen exposure in a time dependent manner. Total Akt/mTOR proteins analyses indicated a homogenous expression among conditions both in GBM and normal cells progressively exposed to high oxygen tension (Figure 5A,B). Particularly, Stat3 (Ser727) was activated after 30 min of high oxygen exposure (Figure 5A,E), this indicating gliogenesis (Rajan et al., 2003) and/or activation of pro-

survival response (Fuh et al., 2009). Moreover, while 4eBP1 was only modestly inhibited by oxygen (data not shown), which may be due to alternative regulatory pathways involved in 4eBP1 regulation, p70S6K (Thr389) was highly up-regulated especially after 120 min (Figure 5A,F). These results indicate that activation of Akt/mTOR dependent pro-translational pathways (p70S6K) and gliogenic and pro-survival mechanisms (Stat3) occur in response to acute high oxygen exposure. Moreover, this increase in translation seems to be directed toward cell differentiation, as indicated by increased $p21^{cip1}$ and increased endogenous BMP dependent astroglial commitment as we reported earlier (Pistollato et al., 2009a). In normal SVZ-derived cells Akt was only modestly and not significantly activated by oxygen exposure, while mTOR activation occurred after 1hr; although mTOR downstream targets Stat3 and p70S6k were not activated following mTOR phosphorylation (Figure 5B-F). These results indicate differences in normal and tumour cell response to high oxygen tension exposure.

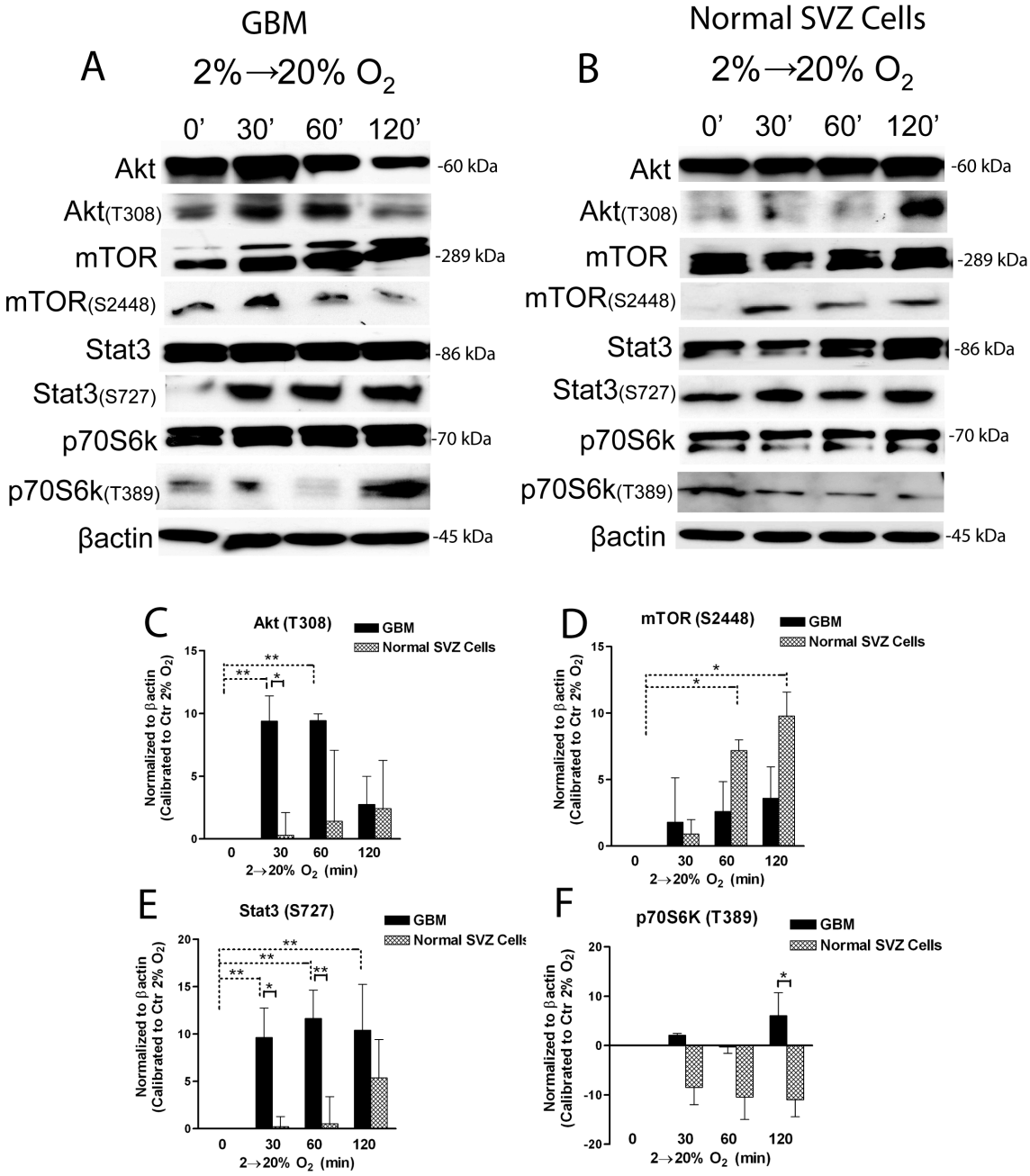

Figure 5. GBM-derived cells undergo Akt/mTOR pathway activation after acute exposure to high oxygen tension. GBM precursors derived cells and normal SVZ derived cells were initially expanded in 2% oxygen, followed by acute exposure to 20% oxygen for 30, 60 or 120 minutes. (A,B) Representative western blot analyses of activated Akt (T308), mTOR (S2448), p70S6K (T389), Stat3 (S727) and total proteins in GBM (A) and normal SVZ cells (B). (C-F) Bar graphs showing mean intensity of indicated proteins normalized to control at 2% oxygen (corresponding to the 0 base line) ± S.E.M. comparing 4 different tumors (black bars), n = 3 for each tumor, with 3 different cultures of normal SVZ-derived cells (lighter bars), n = 3 for each culture. Statistical analyses were done comparing each time point for either GBM or normal cells to its respective T0 (0 min in 20% O2), or as indicated by brackets.

Another protein controlled by mTOR is HIF-1α (Land and Tee, 2007). We found that HIF-1α was rapidly degraded by acute high oxygen exposure, in both GBM and normal SVZ cells (Figure 6A-C). Although, a modest recovery of HIF-1α protein was visible after 2 hr of high oxygen exposure in GBM cells, but not in normal cells (Figure 6A-C), indicating that tumour cells may re-establish HIF-1α level through a hypoxic independent mechanism, possibly controlled by mTOR progressive activation.

We also analyzed REDD1 (RTP801), which has been shown to be strongly induced under hypoxic conditions in a HIF-1α dependent manner (Schwarzer et al., 2005) and recent studies also suggest that REDD1 plays a role in the TSC1/TSC2-mediated inhibition of mTOR (Brugarolas et al., 2004). Accordingly, we found REDD1 downregulated in GBM cells but less intensively in normal SVZ cells, following acute high oxygen exposure (Figure 6A,B,D). Thus, high oxygen dependent Akt/mTOR signaling activation may occur after HIF-1α/REDD1 downregulation.

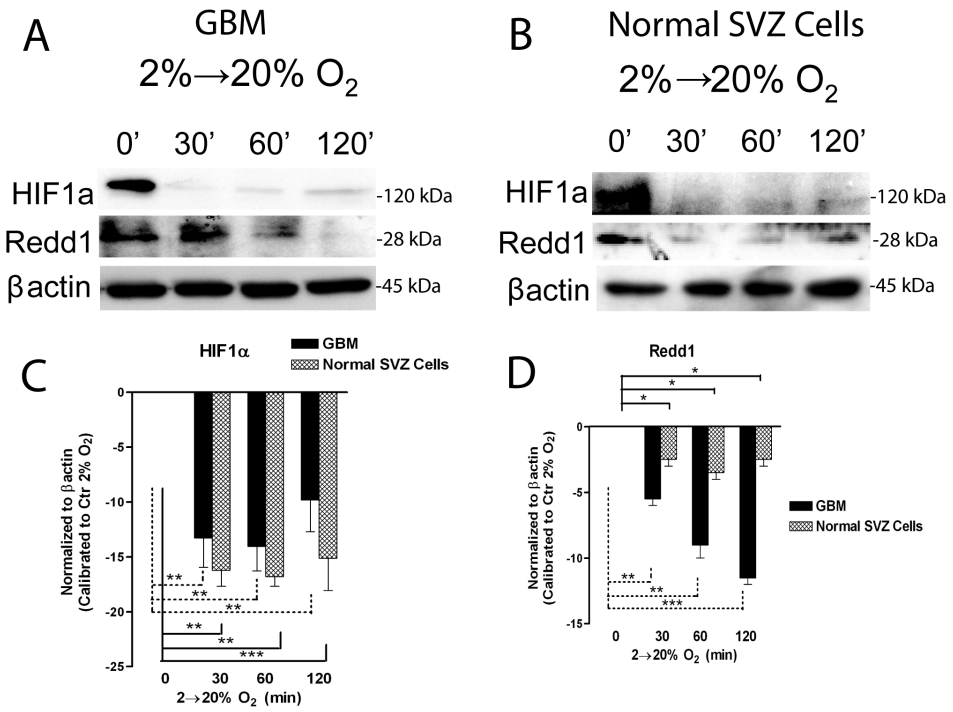

Figure 6. GBM-derived cells undergo transient HIF-1α and REDD1 degradation following acute exposure to high oxygen tension. GBM precursors derived cells and normal SVZ derived cells were initially expanded in 2% oxygen, followed by acute exposure to 20% oxygen for 30, 60 or 120 minutes.

(A,B) Representative western blot analyses of HIF-1α and REDD1 in GBM (A) and normal SVZ cells (B). (C,D) Bar graphs showing mean intensity of HIF-1α and REDD1 normalized to control at 2% oxygen (corresponding to the 0 base line) ± S.E.M. comparing 6 different tumors (black bars), n = 3 for each tumor, with 3 different cultures of normal SVZ-derived cells (lighter bars), n = 5 for each culture.

HIF-1α is required to repress Akt/mTOR signaling activation in hypoxic tumor cells

To understand if HIF-1α mediates the repressive effect of low oxygen on Akt/mTOR signaling, we silenced HIF-1α using a lentiviral vector containing siHIF-1α along with enhanced green fluorescent protein as indicator of efficiency of transduction (siHIF-1α-EGFP) (Figure 7A,D), which was compared to a siLuciferase-EGFP vector (siLUC-EGFP) as a negative control (not shown). By silencing HIF-1α in GBM cells a strong differentiation and eventually cell death occurred after 1 week, as already reported in our previous work (Pistollato et al., 2009a) and these effects were not observed with siLUC-EGFP. Importantly, Akt, mTOR, Stat3 and p70S6K were activated even in HIF-1α silenced cells cultured at 2% oxygen compared to control group and to GBM cells transduced with siLUC-EGFP vector (Figure 7B,C). In normal SVZ cells HIF-1α silencing did not elicit any significant effect and eventually Akt and mTOR inhibition occurred compared to control (Figure 7E,F). HIF-1α silencing correlates with a stronger BMP pathway activity in GBM cells, as shown by SMAD1/5/8 phosphorylation, and BMP pathway is known to activate Akt (Ghosh-Choudhury et al., 2002) and to be correlated to Stat3 regulation in promoting astrogliogenesis (Nakashima et al., 1999). These results indicate that HIF-1α in hypoxic tumor cells may be required to repress convergent signals (SMAD1/5/8 and Stat3) directed to promote an astroglial fate. To prove that HIF-1α downregulation is required in evoking high oxygen dependent Akt/mTOR activation we stabilized HIF-1α by using cobalt chloride ($CoCl_2$, 100 μM), which mimics the effect of hypoxia on HIF-1α, and 12 hr later we exposed cells to high oxygen tension. Performing these experiments directly on HIF-1α silenced cells was not feasible given the scarce viability following HIF-1α silencing. We found that by chemically stabilizing HIF-1α, REDD1 was upregulated and Akt/mTOR pathway was maintained inhibited in GBM derived cells exposed to high oxygen tension (Figure 7G), only p70S6K activation did occur and this may depend on effectors of p70S6K

activation alternative to mTOR. Importantly, normal SVZ cells responded in a different way; indeed, by chemically stabilizing HIF-1α, REDD1 was transiently upregulated and Akt/mTOR pathway was not inhibited, unlike in tumor cells, following exposure to high oxygen tension (Figure 7H), and Akt and Stat3 were eventually upregulated by $CoCl_2$. These results indicate that HIF-1α stabilization, probably through REDD1, prevents high oxygen induced Akt/mTOR activation, and this seems to occur more specifically in GBM derived cells.

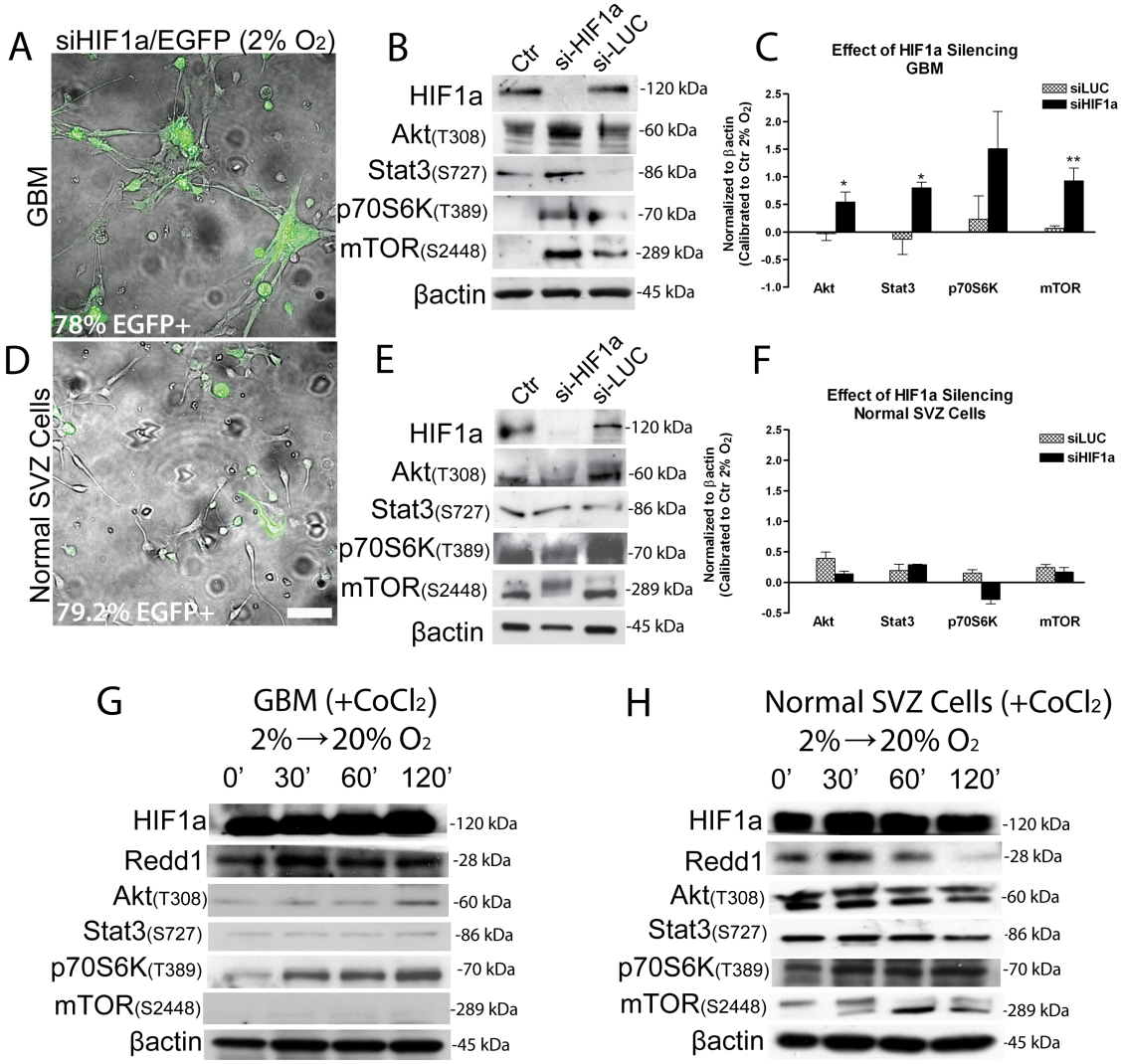

Figure 7. Silencing of HIF-1α promotes Akt/mTOR pathway activation in GBM precursors but not in normal SVZ cells and HIF-1α stabilization by $CoCl_2$ maintains Akt/mTOR pathway inhibited following acute high oxygen exposure. (A,D) Representative pictures of GBM (A) and normal SVZ cells (D) transduced using a lentiviral vector containing siHIF-1α along with enhanced green fluorescent protein (siHIF-1α-EGFP) to test the effects of HIF-1α silencing. Same vector containing siLuciferase

(siLUC-EGFP) was used to test for non-specific effects (pictures not shown). Percentages of EGFP+ cells was determined by using cytofluorimeter (BD, FC500). (B-E) Representative western blot of HIF-1α silenced GBM cells (B) and normal SVZ cells (E), analyzed for HIF-1α, Akt (T308), mTOR (S2448), p70S6K (T389) and Stat3 (S727), along with β-actin as a loading control. (C,F) Bar graphs showing mean intensity of indicated proteins normalized to control at 2% oxygen (not transduced) (corresponding to the 0 base line) ± S.E.M. comparing 2 different tumors (C), n = 2 for each tumor and 1 normal SVZ-derived cell culture (F), n = 2. Asterisks indicate statistically significant differences comparing siHIF-1α to control at 2% oxygen (not transduced). (G,H) Representative western blot analyses of activated Akt (T308), mTOR (S2448), p70S6K (T389), Stat3 (S727) and HIF-1α from GBM (G) and normal SVZ cells (H) that have been pre-incubated 12 hr with CoCl2 (100 μM, Sigma) prior to acute high oxygen exposure. 3 different GBM have been analyzed, n = 2 for each tumor. 20X magnification pictures, bar = 50 μM

Exogenous BMP2, analogously to high oxygen exposure, promotes Akt/mTOR pathway activation and this depends on HIF-1α/REDD1 downregulation

We sought to investigate if exogenous BMP2, alike acute high oxygen exposure, could affect Akt/mTOR pathway activation. While total Akt/mTOR signaling proteins resulted to be homogenously expressed both in GBM and normal cells after BMP2 treatment (Figure 8A and Figure 9A), we found that activation of Akt (Thr308) and also mTOR (Ser2448) occurred with time (Figure 8A,C,D), and, importantly, this activation was accelerated and improved under acute high oxygen exposure, remaining highly activated even after a long term BMP2 exposure (72 hr) (Figure 8B). Importantly, under hypoxia Akt and mTOR were inhibited after short time treatment, resulting activated after 72 hr of BMP2 stimulus. In normal SVZ cells we found that Akt and mTOR were only transiently modulated by BMP2 addition (Figure 9A,C,D) and after 72 hr these activations resulted down-regulated (data not shown). Analyses of mTOR downstream targets, revealed a time dependent increase of Stat3 (Ser727) and p70S6K (Thr389) activation following BMP2 treatment, and these effects were decelerated and decreased by maintaining cells under hypoxia (Figure 8A,E,F), and this occurred transiently also in normal cells (Figure 9,E,F). Also $p21^{cip1}$, involved in cell cycle arrest and induction of differentiation, was found up-regulated by BMP2, but hypoxia inhibited this effects (data not shown).

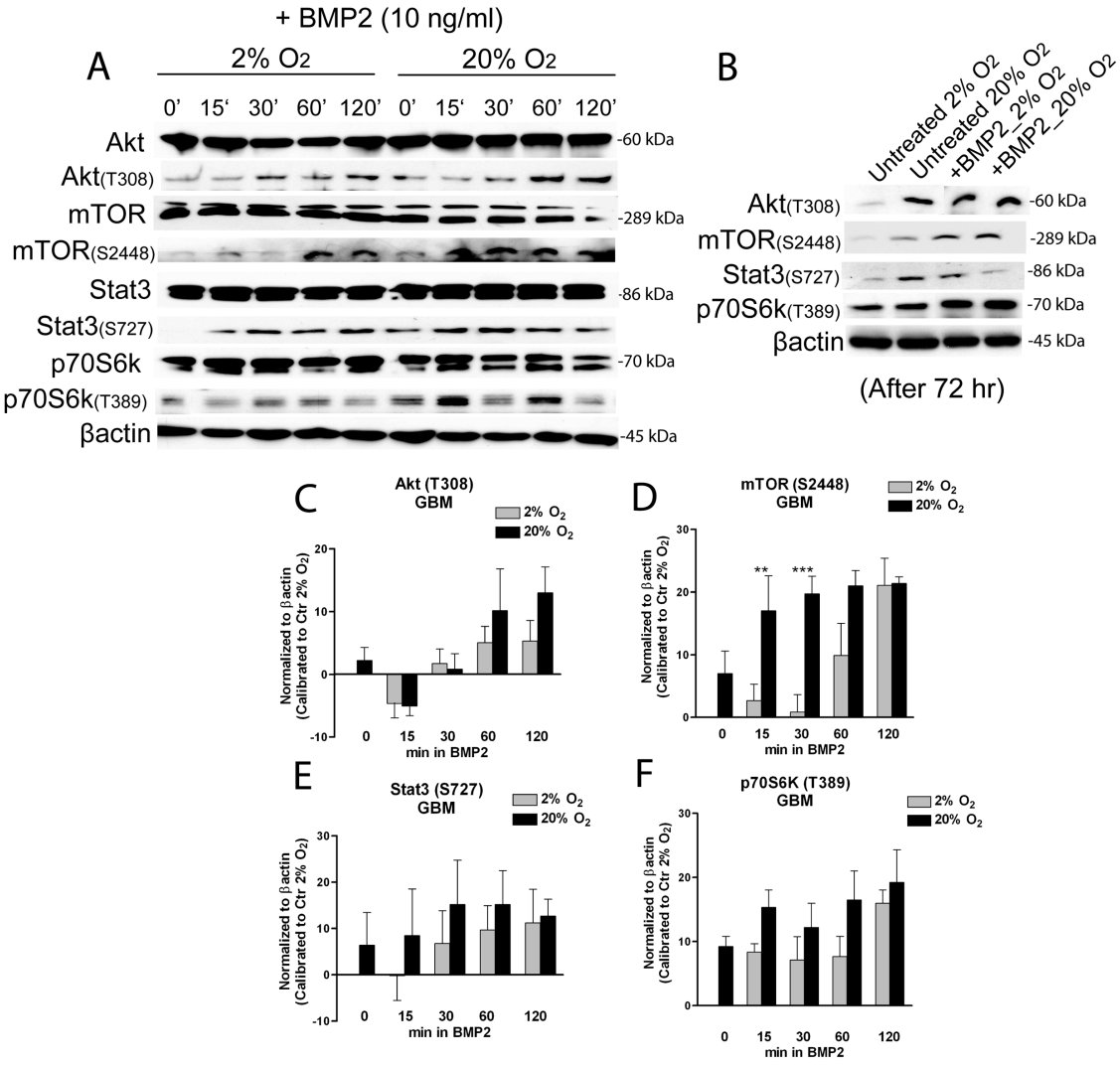

Figure 8. Exogenous BMP2 promotes Akt/mTOR activation in GBM-derived cells and these effects are reduced by hypoxia. (A,B) Representative western blot analyses of activated Akt (T308), mTOR (S2448), p70S6K (T389), Stat3 (S727) and total proteins; GBM-derived cells, initially expanded in 2% oxygen were acutely exposed to 50 ng/ml BMP2 for 0, 15, 30, 60 or 120 minutes, either maintained at 2% or transferred at 20% oxygen (A). Also, some GBM-derived cells were treated with 10 ng/ml BMP2 for longer time (72 hrs) (B). (C-F) Bar graphs showing mean intensity of indicated proteins normalized to control at 2% oxygen (corresponding to the 0 base line) ± S.E.M. comparing 5 different tumors, n = 3 for each tumor.

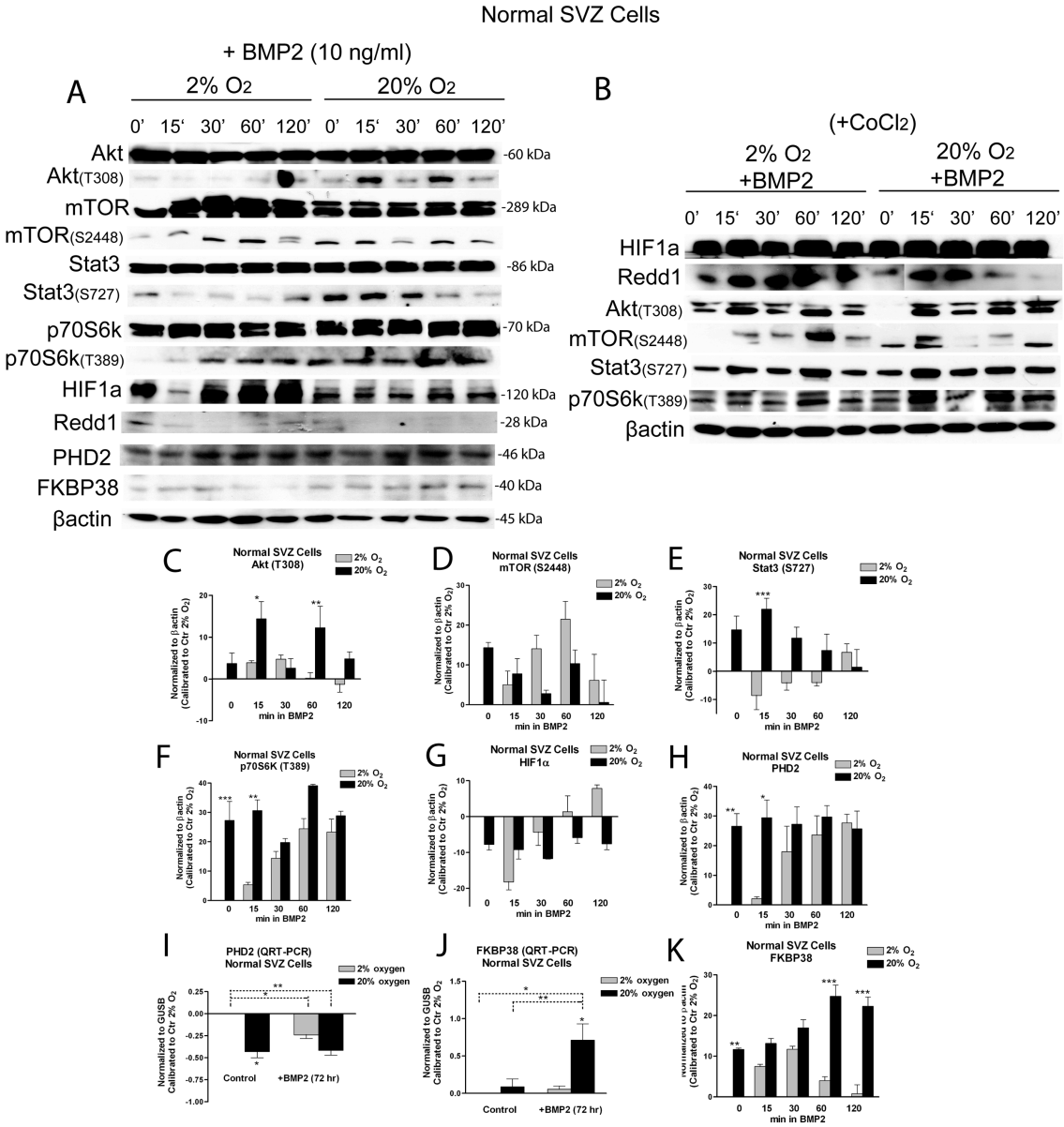

Figure 9. Normal SVZ-derived cells undergo transient Akt/mTOR activation following BMP2 treatment. (A) Representative western blot analyses of indicated proteins; normal SVZ cells, initially expanded in 2% oxygen were treated as described in Fig 4 for GBM cells. (B) Representative western blot analyses of indicated proteins extracted from normal SVZ cells that have been treated for 12 hr with $CoCl_2$ (100 μM, Sigma) either at 2% oxygen or 20% oxygen, starting progressive time course treatment with BMP2 the day after. (C-H, K) Bar graphs showing mean intensity of indicated proteins normalized to control at 2% oxygen (corresponding to the 0 base line) ± S.E.M. comparing 3 different normal SVZ cultures, n = 3 for each one. Statistical analyses were done comparing each time point at 2% O_2 to its respective time point at 20% O_2. (I, J) QRT-PCR analyses of *PHD2* and *FKBP38* normalized to *GUSB* and then calibrated to 2% oxygen control (ΔΔCt Method), mean ± S.E.M. comparing 2 different normal SVZ cultures, n = 3 for each one.

HIF-1α expression is known to be controlled by mTOR (Land and Tee, 2007) and REDD1, mTOR inhibitor, is transcriptionally activated by HIF-1α (Schwarzer et al., 2005). We analyzed if HIF-1α protein was affected following a progressive BMP2 treatment and we found that HIF-1α was strongly down-regulated even under hypoxia following 15 min of BMP2 stimulation in GBM cells (Figure 10A,B). Importantly, HIF-1α level was recovered after 120 min, however not when GBM cells were also acutely exposed to high oxygen. This later stabilization may be consequential to the BMP2 mediated mTOR signaling activation (Figure 8A,B). According to our recent work (Pistollato et al., 2009a), HIF-1α level was reduced after a longer BMP2 exposure (72hrs) (not shown), which is likely correlated to BMP2 dependent glial differentiation in GBM cells. Oppositely, maintenance of HIF-1α expression seems to correlate to tumour cells de-differentiation and normal cells primitiveness. In normal SVZ-derived cells HIF-1α was transiently down-regulated following BMP2 stimulation and with time it was recovered (Figure 9A,G), but its expression did not change after long term (72 hr) treatment (data not shown). Importantly, also REDD1 was down-regulated by BMP2 under hypoxia (Figure 10A,C), and this was only transiently occurring in normal cells (Figure 9A). This suggests that BMP2, analogously to an acute high oxygen exposure, may promote mTOR activation by down-modulating inhibitory REDD1.

As REDD1 is transcriptionally activated by HIF-1α (Schwarzer et al., 2005), we investigated if BMP2 besides modulating HIF-1α protein, promoted also inhibition of HIF-1α transcriptional activity, by using a hypoxia responsive element (HRE)-luciferase reporter construct. Despite physiologic tumour samples variability, we recorded a 40% reduction of HIF-1α transcriptional activity under hypoxia following 8 hr of BMP2 treatment compared to untreated cells. Conversely, in normal SVZ cells BMP2 was operating in an opposite way, promoting a nearly 10% increase of HIF-1α activity (Figure 10D), pointing to differences between normal and tumor cells in BMP2 responsiveness.

We also tested if rapamycin treatment alone or in combination with BMP2 to evaluate if blocking mTOR downstream signaling affected also HIF-1α stability. We found that 72 hr of rapamycin treatment, which did not affect HIF-1α transcriptional activition (data not shown), induced a less pronounced HIF-1α protein reduction, in accordance with

reported results (Yuan et al., 2008), whereas in combination with BMP2 these effects were not further improved (Figure 10E). Normal SVZ cells responded in a similar fashion (data not shown).

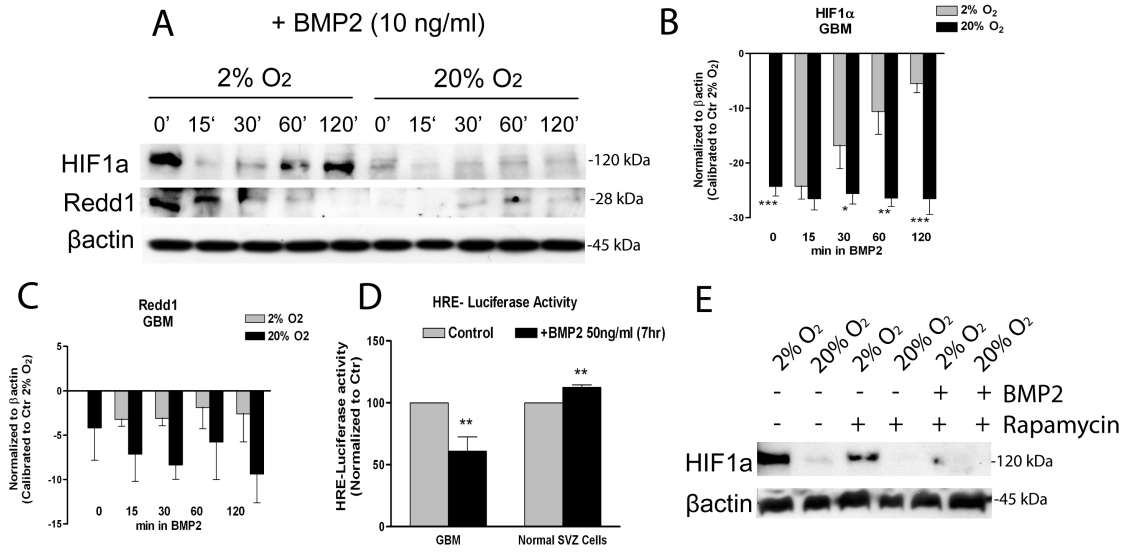

Figure 10. Exogenous BMP2 controls HIF-1α protein level and HIF-1α dependent transcriptional activity even under hypoxia. (A) Representative western blot analyses of HIF-1α and REDD1; GBM-derived cells, initially expanded in 2% oxygen were treated as described in Fig 4. (B,C) Bar graphs showing mean intensity of HIF-1α and REDD1 normalized to control at 2% oxygen (corresponding to the 0 base line) ± S.E.M. comparing 6 different tumors, n = 3 for each tumor. (D) HRE-luciferase assay: GBM cells and normal SVZ-derived cells were transfected either with a HRE-firefly luciferase reporter construct or with a mutated HRE version of the same construct to evaluate aspecific effects. Along with these vectors, also a Renilla luciferase vector has been transfected in order to normalize luciferase detection. Normalization of the data to the mutated HRE vector was done and then values were calibrated to untreated cells (Control). 3 different GBM have been analyzed, n = 2 for each tumor. (E) Representative western blot analysis of HIF-1α in GBM-derived cells, initially expanded in 2% oxygen, then acutely exposed to 100 μM rapamycin alone or in combination with 10 ng/ml BMP2 for 72 hrs. β-actin was used as a loading control. 2 different GBM have been analyzed, n = 3 for each tumor.

To prove that Akt/mTOR activation was due to inhibition of HIF-1α/REDD1 by BMP2, we performed BMP2 treatment on $CoCl_2$ pretreated GBM cells. We found that by stabilizing HIF-1α and consequentially also REDD1, Akt/mTOR signaling was not activated following BMP2 treatment (Figure 11A). p70S6K activation lately occurred, probably due to effectors of p70S6K activation alternative to mTOR, as commented above, and Stat3 (S727) was eventually more stably expressed in $CoCl_2$ treated cells, although it was not modulated by BMP2 during time (Figure 11A). Importantly, in normal SVZ cells, chemically HIF-1α stabilization was only transiently inducing

REDD1 upregulation and Akt/mTOR pathway was not inhibited, unlike in tumor cells, following BMP2 treatment (Figure 9B), and Akt and Stat3 were eventually upregulated. Alternatively to the use of $CoCl_2$, we used the proteasome inhibitor Z-LLF-CHO (Z-LLF, 30 μM) added 30 min prior to 8 or 24 hr of BMP2 time treatment under hypoxia. By preventing proteasomal degradation, BMP2 did not affect HIF-1α protein stability (Figure 11B). Moreover, REDD1 was upregulated and Akt/mTOR signaling was not activated following BMP2 treatment under hypoxia (Figure 11B). These results confirm that HIF-1α degradation and consequentially also REDD1 downregulation are required in BMP2 dependent Akt/mTOR activation, and this preferentially occurs in GBM cells.

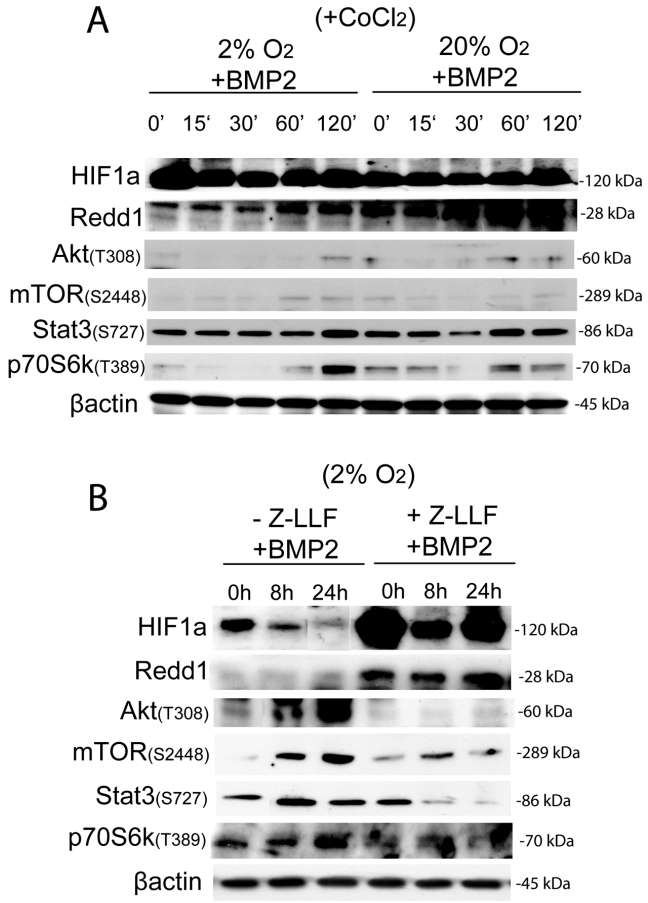

Figure 11. HIF-1α stabilization and consequential REDD1 upregulation maintains Akt/mTOR signaling inhibited in BMP2 treated GBM derived cells. (A) Representative western blot analyses of HIF-1α, REDD1, activated Akt (T308), mTOR (S2448), p70S6K (T389), Stat3 (S727), along with β-actin as loading control ; GBM cells have been treated for 12 hr with $CoCl_2$ (100 μM, Sigma) either at 2% oxygen or 20% oxygen, starting progressive time course treatment with BMP2 the day after. 2 different GBM have been analyzed, n = 1 for each tumor. (B) Representative western blot analyses of indicated proteins extracted from GBM derived cells that have been pre-treated with Z-LLF-CHO, proteasome inhibitor, added 30 min prior to BMP2 treatment (for 8 or 24 hr). 2 different GBM have been analyzed, n = 1 for each tumor.

Exogenous BMP2 promotes increase of PHD2 protein level even under hypoxia by dowregulating FKBP38

As we saw that HIF-1α protein stability was affected following BMP2 treatment, we investigated if proline hydroxylases (PHDs), involved in HIF-1α proline hydroxylation and consequential proteasomal degradation, were modulated by BMP2. PHD2 in particular has been described as the critical oxygen sensor setting the low steady-state levels of HIF-1α in normoxia (Berra et al., 2003). In the same work PHD2 was found up-regulated by hypoxia, providing a HIF-1-dependent auto-regulatory mechanism driven by oxygen tension itself. We found that PHD2 protein was rapidly up-regulated by BMP2, and this occurred more slowly under hypoxia, in both GBM (Figure 12A,C) and normal SVZ cells (Figure 9A,H). Also after a prolonged BMP2 treatment PHD2 protein resulted up-regulated in GBM cells (Figure 12B), which is in accordance to our previous work (Pistollato et al., 2009a) QRT-PCR revealed that while *PHD2* transcript was up-regulated under hypoxia, according to literature (Berra et al., 2003), 72 hr of BMP2 treatment induced a modest but not significant *PHD2* mRNA decrease (Figure 12D). *PHD2* transcript reduction was recorded also in BMP2 treated normal SVZ cells (Figure 9I). Notably, PHD2 promoter is characterized by the presence of HRE consensus sequences directly controlled by HIF-1α (Metzen et al., 2005). Thus, we hypothesize that the observed *PHD2* mRNA reduction may depend on HIF-1α transcriptional inhibition induced by BMP2, as previously described (Figure 10D).

Following-up on our observation that BMP2 mediated PHD2 protein increase was not dependent on de novo protein synthesis (Figure 12D), we sought to investigate if BMP2 was somehow increasing PHD2 protein stability. Peptidyl prolyl cis/trans isomerase FK506-binding protein 38 (FKBP38) has been described as a PHD2 protein regulator by targeting PHD2 to proteasome degradation (Barth et al., 2007). We found that FKBP38 was progressively down-regulated by BMP2 under hypoxia (Figure 12A,E), and this effect was observed also after a prolonged BMP2 treatment (Figure 12B). Conversely to what has been described (Barth et al., 2007), we also found that FKBP38 was up-regulated in hypoxic GBM cells, suggesting that it may be involved in hypoxic HIF-1α stability by promoting PHD2 degradation. QRT-PCR analysis confirmed that *FKBP38* was down-regulated by acute exposure to high oxygen and by BMP2 under hypoxia also at the transcriptional level (Figure 12F). Opposite, this was not occurring

in normal SVZ-derived cells in which BMP2 treatment combined with high oxygen exposure was inducing *FKBP38* up-regulation (Figure 9J), also at the protein level (Figure 9A,K). Thus, we hypothesize that BMP2 may promote PHD2 stabilization by down-modulating FKBP38 expression in GBM cells.

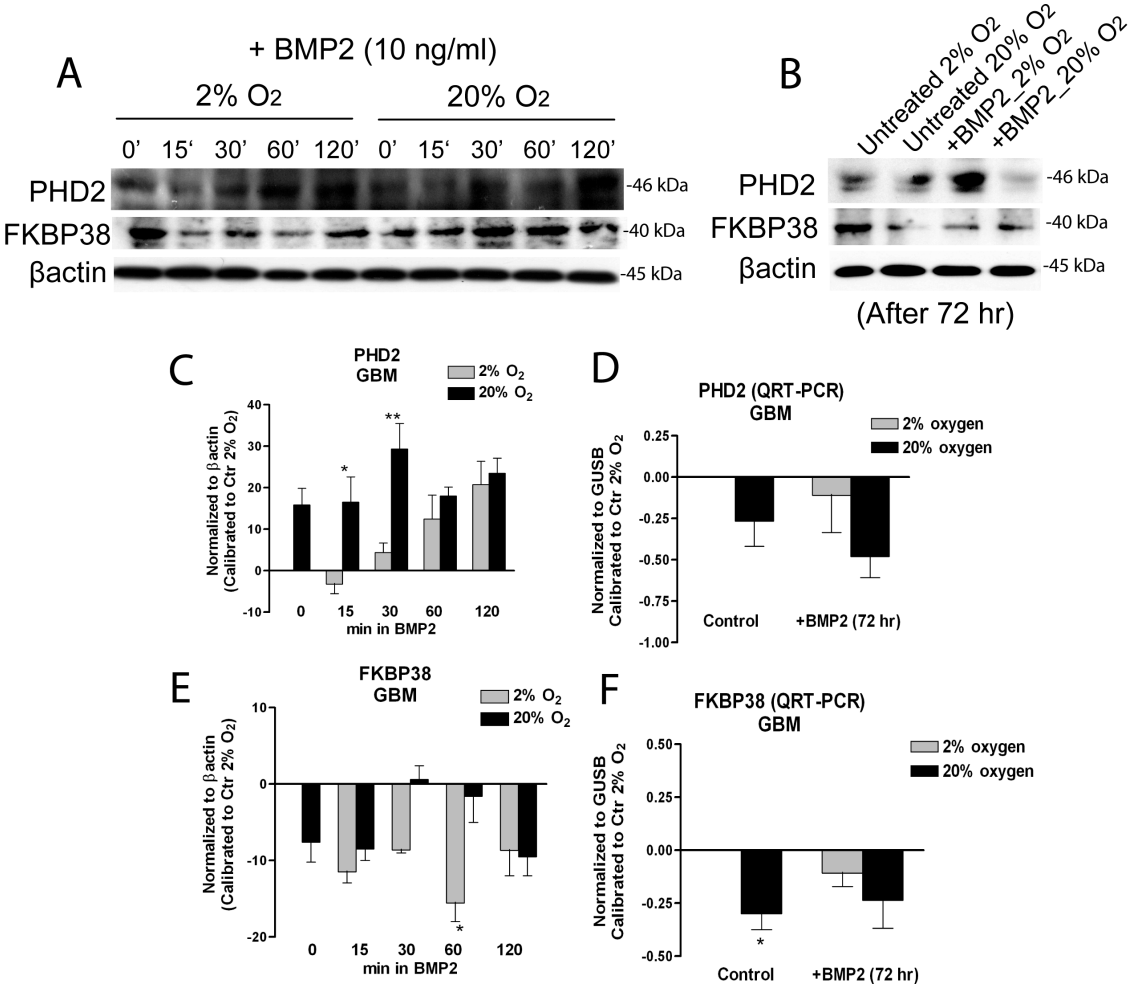

Figure 12. Exogenous BMP2 promotes increase of PHD2 protein level even under hypoxia by dowregulating FKBP38. (A,B) Representative western blot analyses of PHD2 and FKBP38; GBM-derived cells, initially expanded in 2% oxygen were treated as described in Fig 4. Also, some GBM-derived cells were treated with 10 ng/ml BMP2 for longer time (72 hrs) (B). (C,E) Bar graphs showing mean intensity of PHD2 and FKBP38 proteins normalized to control at 2% oxygen (corresponding to the 0 base line) ± S.E.M. comparing 6 different tumors, n = 3 for each tumor. (D,F) QRT-PCR analyses of *PHD2* and *FKBP38,* normalized to *GUSB* and then calibrated to 2% oxygen control (ΔΔCt Method), mean ± S.E.M. comparing 3 different GBM, n = 3 for each tumor.

Exogenous BMP2, by decreasing intracellular succinate, increases PHD2 activity leading to HIF-1α modulation

We finally sought to investigate if BMP2 treatment increased PHD2 activity thus causing HIF-1α modulation. It has been previously reported that impaired SDH activity in several cancer types is associated to HIF-1α stabilization, through a mechanism involving intra-cytoplasmic succinate accumulation and consequential PHD2 inhibition (King et al., 2006). Indeed, SDH is the enzyme complex II bound to the inner mitochondrial membrane that converts succinate to fumarate via FAD reduction to FADH2. Importantly, it has also been shown in other cell models that induction of differentiation by BMPs increases mitochondrial oxidative phosphorylation, as seen by higher SDH activity (Kamegai et al., 1990). We found that BMP2 treatment induced increase of SDH activity in GBM cells (Figure 13A,B). This suggests that pro-differentiating agents, such as BMPs, may promote a metabolic shift toward oxidative phosphorylation in tumor cells and that BMP2, by decreasing intracellular succinate through induction of SHD activation, may increase PHD2 activity leading to HIF-1α modulation. Notably, in normal SVZ cells SDH activation was not changed following BMP2 treatment (Figure14A), this indicating differences in metabolic response to BMP2 treatment between normal and tumor cells. Further addition of exogenous esterificated diethyl-succinate (5 mM, Sigma) either in presence or absence of BMP2 did not induce SDH activation (not shown).

We also tested if additional succinate in combination with BMP2, was promoting a recovery of HIF-1α protein level and/or determining an inhibition of Akt/mTOR signaling in GBM cells. We found that HIF-1α, REDD1 and FKBP38 proteins were upregulated in BMP2/succinate treated cells, even when exposed to 20% oxygen. Moreover, in particular Akt and p70S6K activation were modestly decreased in presence of combined BMP2 and succinate, as compared to BMP2 only treated cells (Figure 13C). This indicates that additional succinate, by upregulating HIF-1α and REDD1, partially inhibits Akt/mTOR activation following BMP2 treatment.

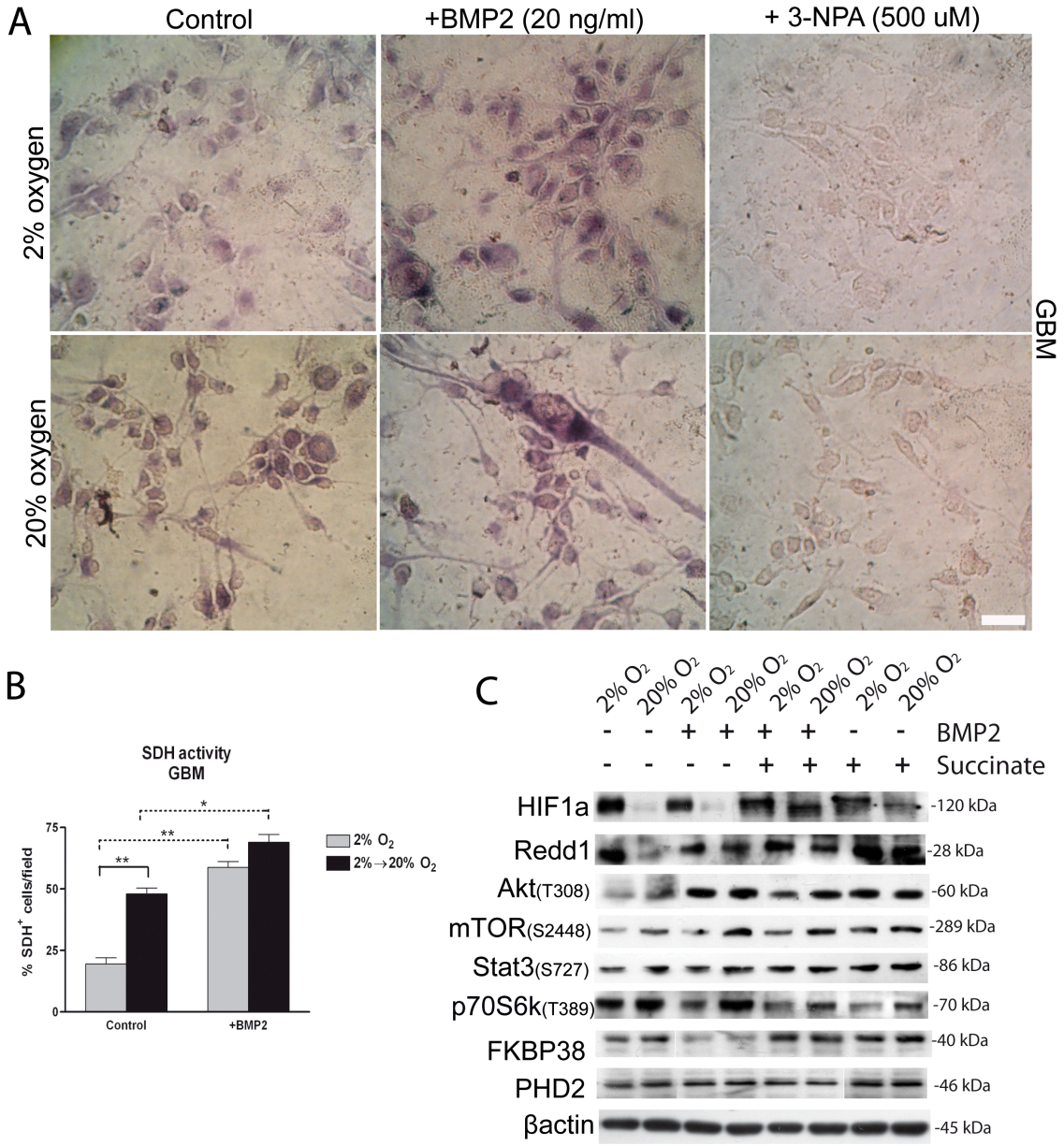

Figure 13. Exogenous BMP2 promotes higher SDH activity and addition of exogenous succinate upregulates HIF-1α/REDD1 and FKBP38 proteins in BMP2 treated cells. (A) Representative citochemical analysis of succinate dehydrogenase (SDH) activity by using NBT reduction methodology. Cells were incubated for 48 hr in presence of either BMP2 (30 ng/ml) or 3-nitropropionic acid (3-NPA) (500 μM, Sigma), known to irreversibly inactivate SDH (negative control). (B) Bar graph showing mean percentage of SDH^+ cells (blue-violet cells) counted from 40X magnification pictures (picture area = 0.02 cm^2), bar = 20 μM. 2 different tumors have been used, n = 2 for each tumor. (C) Representative western blot analyses of indicated proteins extracted from cells that have been treated 72 hr in presence of either BMP2 alone (10 ng/ml), or diethyl-succinate alone (5 mM, Sigma) or combined BMP2 and diethyl-succinate. 2 different GBM have been analyzed, n = 2 for each tumor.

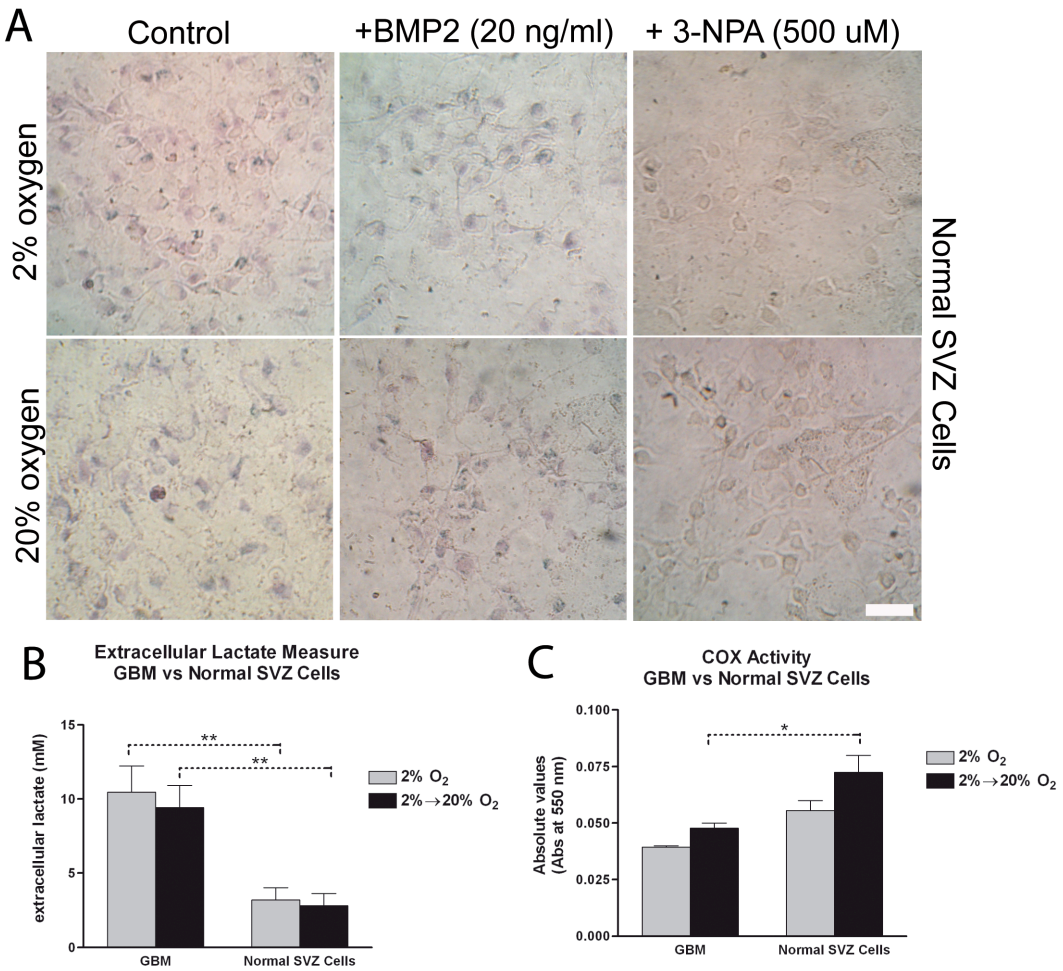

Figure 14. SDH activity does not change following BMP2 treatment in normal SVZ cells and GBM cells are more dependent that normal cells on anaerobic glycolysis. (A) Representative citochemical analysis of succinate dehydrogenase (SDH) activity by using NBT reduction methodology in normal SVZ cells, treated as described in Fig 8A. (B) Bar graph showing extracellular lactate measure comparing 3 different GBM cell cultures and 2 different normal SVZ cell cultures. (C) Bar graph showing cytochrome c oxidase (COX) activity comparing 3 different GBM cell cultures and 2 different normal SVZ cell cultures. Cells have been either maintained under hypoxia or exposed to acute high oxygen tension for 48 hr.

.

Differential BMP receptors expression influence the outcome of BMP2 response

In this work we evaluate that BMP2 is able to mediate astroglial differentiation of GBM derived cells but this effect is reverse by hypoxia where pro-differentiating treatment with BMPs molecules is less effective. Conversely, acute exposure to high oxygen tension greatly increased the BMP2 mediated astroglial differentiation. Moreover, we found that a percentage of GBMs did not respond to BMP2 treatment neither in hypoxia neither at 20% oxygen. A recent work from Fine's group evaluate that almost 20% of GBMs have an impaired differentiation process due to the epigenetic silencing of BMPR1B which is fundamental for the activation of the differentiating cascade(Lee et al., 2008). We sought to investigate endogenous BMP2 and BMPR expression by RQ-PCR and we confirmed previous data about BMPR1B expression which is not transcribed in the 15% of our sample. Moreover, we found all these genes up-regulated in cells cultured under high oxygen tension (Table 1). Thus, the strongest BMP2 mediated effect at 20% of oxygen correlate also with an increased expression of its receptor. These finding highlight the possibility of BMPs molecules to be used as pro differentiating therapies for GBM, but open to way to study pro differentiating molecules able to modulate GBM cells phenotype also in their physiological hypoxic microenvironment.

	2% oxygen	**20% oxygen**	**P Value**
BMP2	1	2.80 (± 0.19)	***
BMPR1A	1	2.64 (±0.522)	*
BMPR1B	1	2.77 (± 0.69)	*
BMPRII	1	1.69 (± 0.18)	*

Table1. RQ-PCR Analysis of BMP2 and BMPR-IA, -IB, -II on GBM samples.

Hypoxia promotes ligand-mediated Wnt pathway activation

Since the recent findings that HIF-1α promoted neuronal differentiation by activating β-catenin co-factors in embryonic and neural stem cells, we evaluated whether Wnt pathway and HIF-1α signal were reciprocally regulated also in GBM-derived cells. For this reason, we transfected GBM cells, constantly maintained in hypoxia (2% oxygen) with a hypoxia-luciferase reporter plasmid (HRE-LUX) or a β-catenin/TCF/LEF-luciferase reporter vector (BAT-LUX) and treated them with exogenous recombinant Wnt3a, a known Frizzled ligand involved in neuronal differentiation (Lie et al., 2005). We found that 24h-treatments with Wnt3a did not alter HIF-1α transcriptional capability (Figure 15A). Conversely, there was a much stronger β-catenin-induced transcriptional activation after Wnt3a treatment in GBM cells maintained in hypoxia rather than 20% O_2 (Figure 15B). Since it has recently been described that hypoxia enhances the expression of β-catenin co-factors TCF-1 and LEF-1 in neural stem cells (Mazumdar et al., 2010), we investigated whether it could mediate β-catenin co-factors regulation also in GBM-derived cells. We analyzed mRNA expression levels of *TCF1*, *TCF3*, *TCF4* and *LEF1* genes and found that only TCF1 and LEF1 transcripts were strongly up-regulated in primary GBM-derived cells at 2% oxygen (Figure 15C). Moreover, we analyzed the expression of the well described GBM cancer stem cell surface marker CD133 (Prominin-1). After Wnt3a stimulus we found percentage of $CD133^+$ cells significantly reduced only in hypoxia (Figure 15D). 20% oxygen decreased $CD133^+$ subpopulation as previously described (Pistollato et al., 2007).

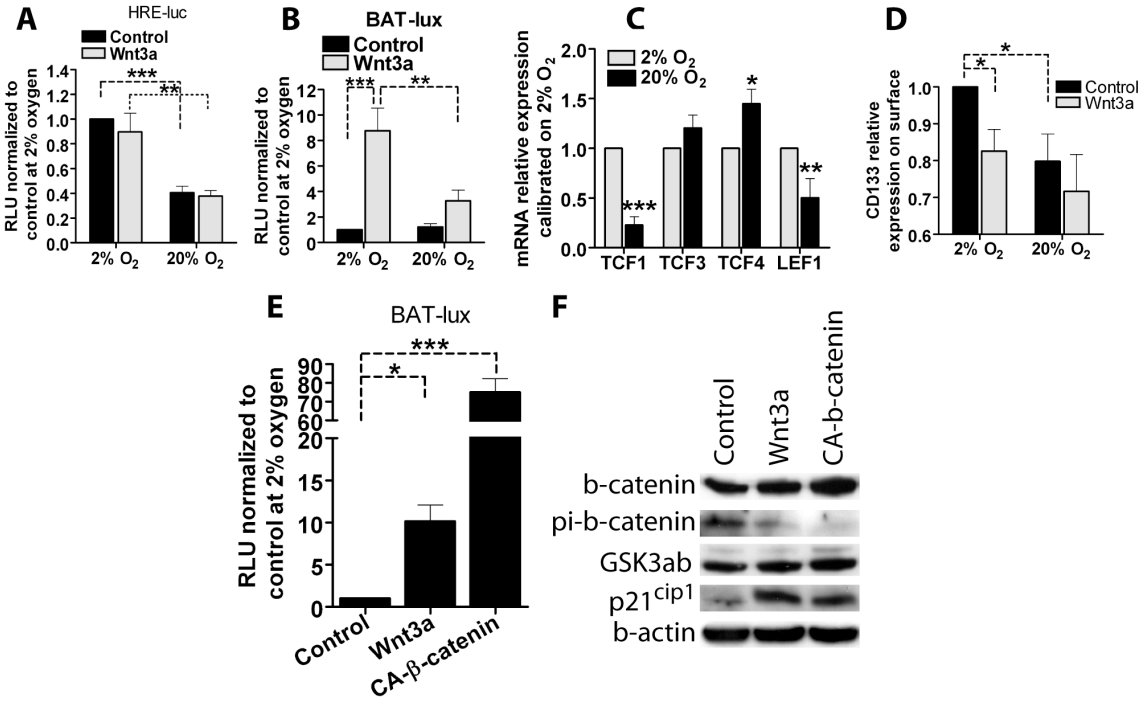

Figure 15: Hypoxia modulates Wnt signalling activation in GBM-derived cells *in vitro*. (A) Bar graph representing luciferase reporter activity of HRE-luc transfected cells, treated with Wnt3a and cultured at 2%O_2 or either 20%O_2. Mean of 6 tumours± S.E.M., n=2 for each tumour (B) Bar graph representing luciferase reporter activity of BAT-lux transfected cells, treated with Wnt3a and cultured at 2%O_2 or either 20%O_2. Mean of 6 tumours ± S.E.M., n=2 for each tumour. (C) RQ-PCR analysis of TCF-1, 3, 4 and LEF-1 in GBM cells maintained in hypoxia or exposed to 20%O_2 tension. Mean of 6 tumours± S.E.M., n=4 for each tumour. (D) Analysis of CD133 cell surface marker expression after Wnt3a treatment of 2% or 20%O_2 cultured cells. Mean of 5 tumours ± S.E.M., n=1 for each tumour. (E) BAT-lux reporter analysis of Wnt3a treated or CA-β-catenin transfected cells at 2%O_2. Mean of 3 tumours± S.E.M., n=2 for each tumour. (F) WB representing the activation status of β-catenin, its regulator GSK3αβ and the differentiation/proliferation marker $p21^{cip1}$ of GBM cells treated with Wnt3a or either transfected with CA-β-catenin plasmid. Analysis repeated on additionally 3 tumours.

Wnt pathway activation induces GBM neuronal differentiation in vitro

To drive Wnt pathway activation in GBM cells we treated them with recombinant Wnt3a or either transfected them with a plasmid encoding for a constitutively active form of β-catenin (CA-β-catenin) that was able to more strongly activate Wnt signalling in BAT-LUX bearing cells (Figure 15E). Total protein analyses confirmed Wnt signalling activation after Wnt3a treatment and CA-β-catenin transfection (Figure 15F). Importantly, addition of Wnt3a and CA-β-catenin induced a significant increase of $p21^{cip1}$, a cell cycle arrest marker (Figure 15F). Immunofluorescence analyses on *in vitro* cultured GBM-derived cells revealed a dramatic phenotypic change after Wnt pathway activation. In particular, GBM cells displayed the induction of neuronal commitment, since we could observe a phenotypic shift of GBM cells from immature/stem cells

(Nestin$^+$) to an increased number of more differentiated (β-III-tubulin$^+$) cells, together with a significant decrease of proliferating cells as measured by Ki67 expression (Figure 16A-D). These effects were observed in cells maintained at 2% oxygen, condition that we found to positively correlate with maintenance of an undifferentiated phenotype (Pistollato et al., 2009a; Pistollato et al., 2007). Moreover, *in vitro* culture of Wnt3a pre-treated GBM cells maintained in hypoxia showed no reversion from the differentiated phenotype within 5 days post Wnt3a withdrawal (Figure 16E). Induction of neuronal differentiation through Wnt signalling activation was confirmed at the transcriptional level by the up-regulation of neuronal maturation and differentiation genes (*NEUROD1*, *NEUROGENIN1* and *β-III-TUBULIN*) (Figure 16F).

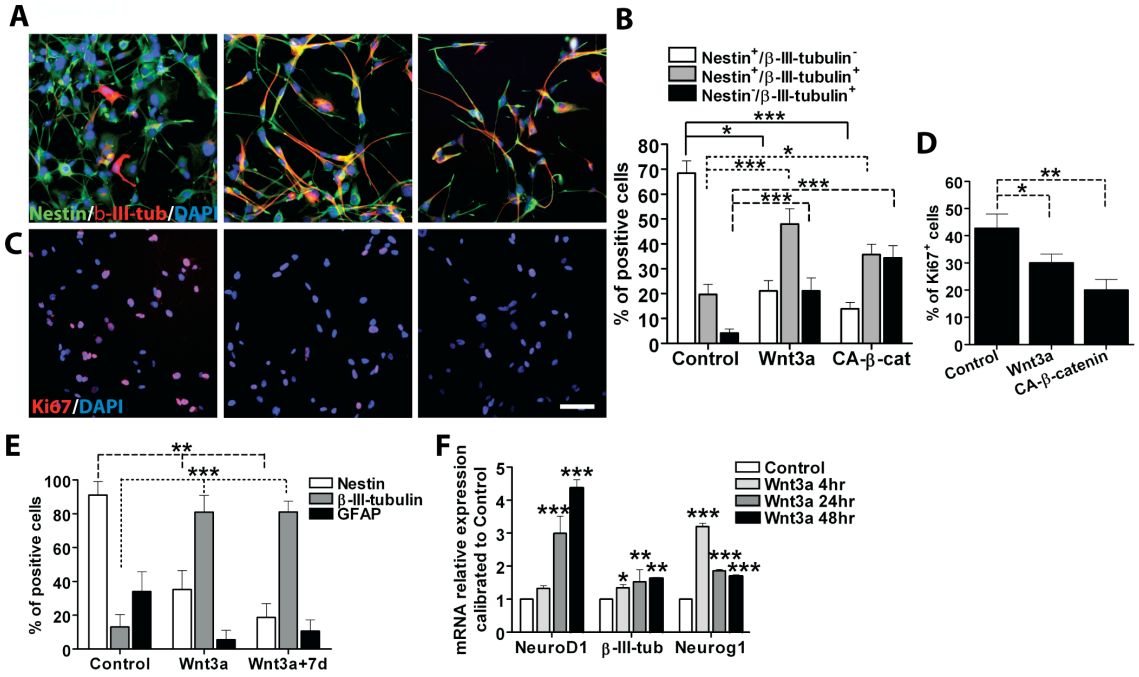

Figure 16. Wnt3a modulates neuronal differentiation of GBM derived cells *in vitro*. (A) Representative immunofluorescence images of GBM cells treated with Wnt3a or transfected with CA-β-catenin and stained for Nestin(green)/β-III-tubulin(red). Bar=100 μm (B) Bar graph reporting relative quantification of images described in panel (A). Mean of 6 tumours ± S.E.M. n=3 for each tumour. (C) Representative immunofluorescence images of GBM cells treated with Wnt3a or transfected with CA-β-catenin and stained for Ki67(red). Bar=100 μm. (D) Bar graph reporting relative quantification of images described in panel (D). Mean of 6 tumours ± S.E.M. n=3 for each tumour. (E) Bar graph reporting relative quantification of immunofluorescence images of GBM cells treated with Wnt3a or after Wnt3a withdrawal and stained for Nestin(green)/β-III-tubulin(red). (F) RQ-PCR analysis reporting mRNA levels of *NEUROD1*, *β-III-TUBULIN* and *NGN1*. Mean of 6 different tumours, n=4 for each tumour. *p<0.05, **p<0.01, ***p<0.001.

Moreover, the hypothesis of induced differentiation was further corroborated by the absence of increased apoptosis in Wnt pathway-activated cells (data not shown). In normoxia, the induction of neuronal differentiation along with growth inhibition

mediated by Wnt pathway activation was less pronounced, if compared to 2% oxygen cultured cells (Figure 17A-D).

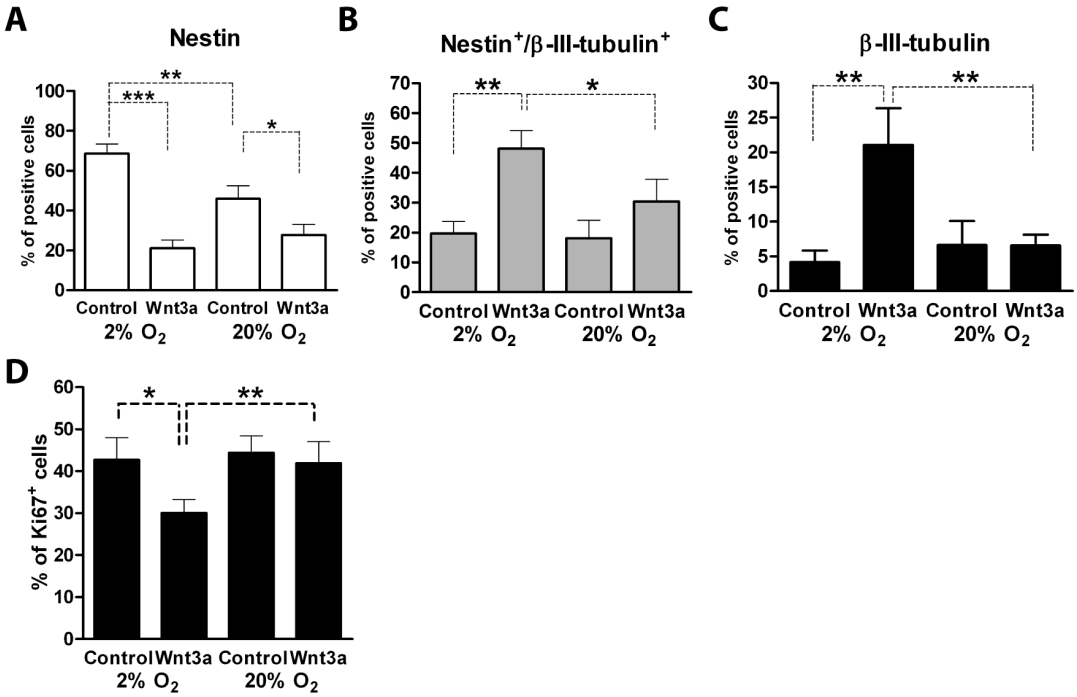

Figure 17. High oxygen tension de-sensitizes GBM cells to Wnt treatment. (A-C) Bar graphs reporting relative quantification of Nestin$^+$/β-III-tubulin$^-$, Nestin$^+$/β-III-tubulin$^+$ and Nestin$^-$/β-III-tubulin$^+$ sub-populations of Wnt3a treated GBM cells at different oxygen tensions. (D) Bar graph showing % of Ki67$^+$ cells of same treated cells. For all graphs mean of 3 tumours ± S.E.M., n=2 for each tumour. *p<0.05, **p<0.01, ***p<0.001.

Wnt-induced differentiation is mediated by Notch signalling inhibition

Since Wnt activation led to a dramatic induction of differentiation, we hypothesized a possible concomitant down-modulation of signalling pathways involved in stem cell maintenance. Notch pathway is known to regulate stem cell fate of adult murine stem cells and medulloblastoma cells by directly interacting with HIF-1α (Gustafsson et al., 2005; Pistollato et al., 2010b). Moreover, its inhibition has been associated to neuronal differentiation in brain stem cells (Cau and Blader, 2009). To confirm this assertion, we treated GBM-derived cells with DAPT, a γ-secretase inhibitor, and Dll4, a Notch ligand recently described as a direct downstream target of Wnt/β-catenin (Corada et al., 2010). Immunofluorescence analysis of sub-populations distribution showed that Notch inhibition promoted the acquisition of a neuronal phenotype (loss of Nestin and increase of β-III-tubulin$^+$ cells) and the decrease of Ki67$^+$ proliferating cells. Moreover, this inhibition occurred mainly at 2% oxygen (Figure 18).

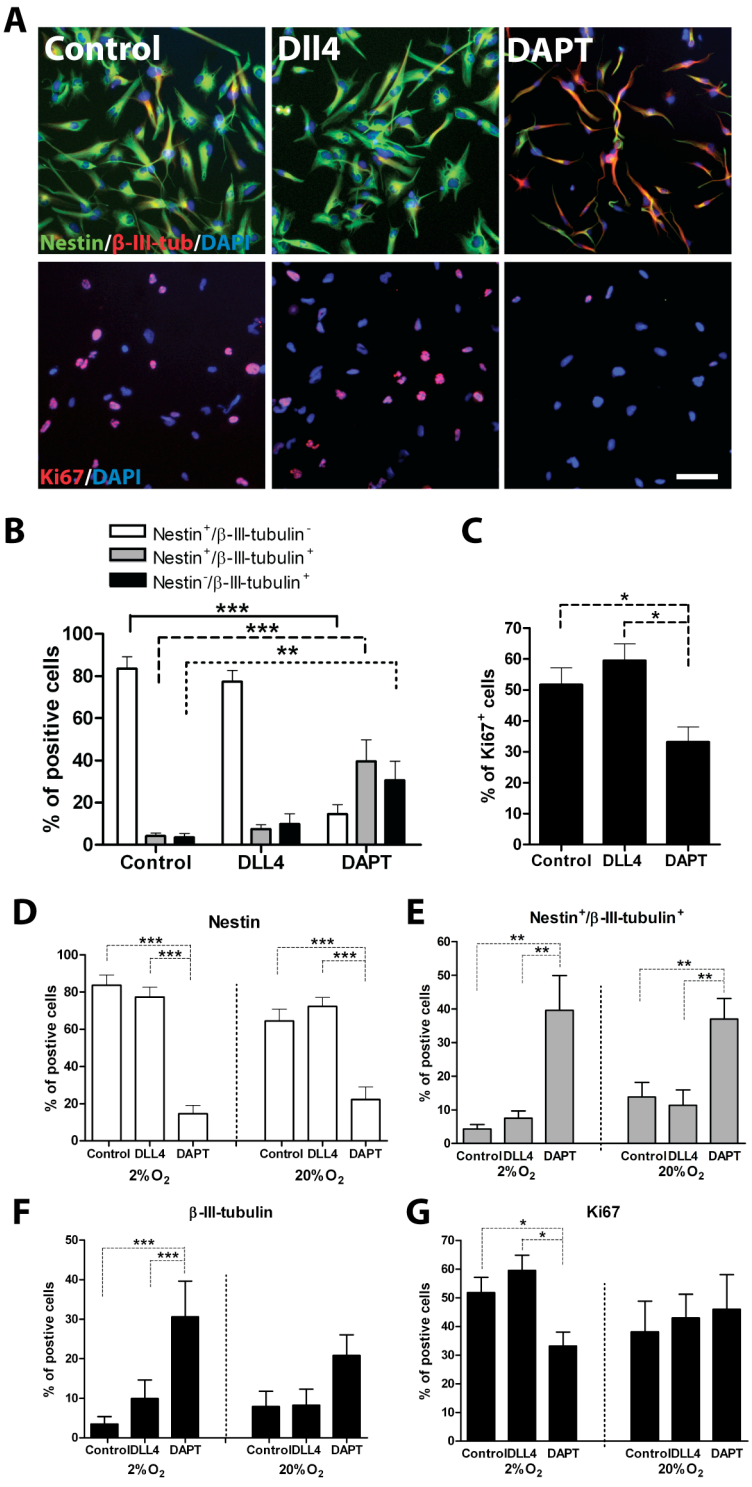

Figure 18. Notch signalling inhibition promote neurogenesis in GBM-derived cells under hypoxia. (**A**) Representative immunofluorescence images of GBM cells treated with Dll4 or DAPT for 96h and stained for Nestin(green)/β-III-tubulin(red) and Ki67(red). bar=100 μm. (**B-C**) Bar graph reporting relative quantification of images described in panel (**A**). Mean of 3 tumours ± S.E.M. n=3 for each tumour. (**D-F**) Bar graphs reporting relative quantification of Nestin$^+$/β-III-tubulin$^-$, Nestin$^+$/β-III-tubulin$^+$ and Nestin$^-$/β-III-tubulin$^+$ sub-populations of Dll4 or DAPT treated GBM cells at different oxygen tensions. (**G**) Bar graph showing % of Ki67$^+$ cells, treated as panel (**A**).

Given the induction of neuronal differentiation after Notch signalling inhibition, comparable to that observed in Wnt pathway activated cells, we hypothesized that these two phenomena should be related. To confirm this hypothesis, we transfected GBM-derived cells with a CBF1-luciferase reporter plasmid and evaluated luciferase signal after Wnt3a treatment or CA-β-catenin transfection. We found that Wnt activation promoted a dramatic inhibition of Notch transcriptional activity (Figure 19A, left) and Notch Intracellular Domain (NICD) activation, with a concomitant decrease of Hes1 expression (Figure 19A, right). We confirmed the Wnt-mediated up-regulation of DLL4 both at transcriptional and protein level and these data were corroborated by the observed increase of MATH1 transcript, known to be over-expressed when Notch is repressed (Gu et al., 2005) (Figure 19A-B). To evaluate the epistatic relationship between Wnt activation and Notch inhibition we tried to rescue the phenotype of Wnt3a treated GBM-derived cells by co-treating them with the Notch ligand Dll4. Analysis of phenotype showed no differences in sub-populations distribution between Wnt3a alone or Wnt3a-Dll4 treated cells (Figure 19C-D), suggesting that Wnt activated intracellular signalling acted upstream of Notch pathway probably by affecting NICD stability.

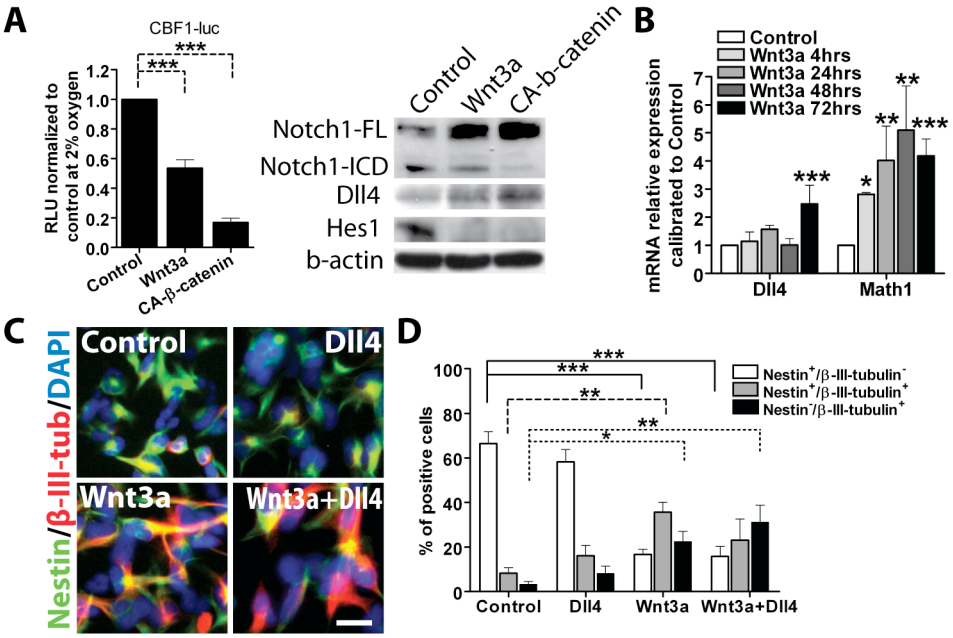

Figure 19. Wnt pathway activation inhibits Notch signalling in GBM derived cells. (**A**) CBF1-luc reporter analysis of Wnt3a treated or CA-β-catenin transfected cells at 2%O_2 and WB of protein extracts from the same cells displaying Notch pathway regulation. Mean of 4 tumours± S.E.M., n=2 for each tumour. (**B**) RQ-PCR analysis reporting relative expression of *Dll4* and *Math1*. Mean of 6 tumours ± S.E.M., n=4 for each tumour. (**C**) Representative immunofluorescence images of GBM cells treated with Dll4, Wnt3a or both for 96 h and stained for Nestin(green)/β-III-tubulin(red) and (**D**) graph reporting relative quantification. Mean of 3 tumours ± S.E.M. n=3 for each tumour. bar=100 μm.

To confirm this hypothesis, we stressed the involved pathways at the intracellular level by transfecting CA-β-catenin in GBM cells over-expressing NICD (Figure 20A). CA-β-catenin/NICD over-expressing cells displayed a delay in the differentiation process, which was however not completely inhibited (Figure 20B-C).

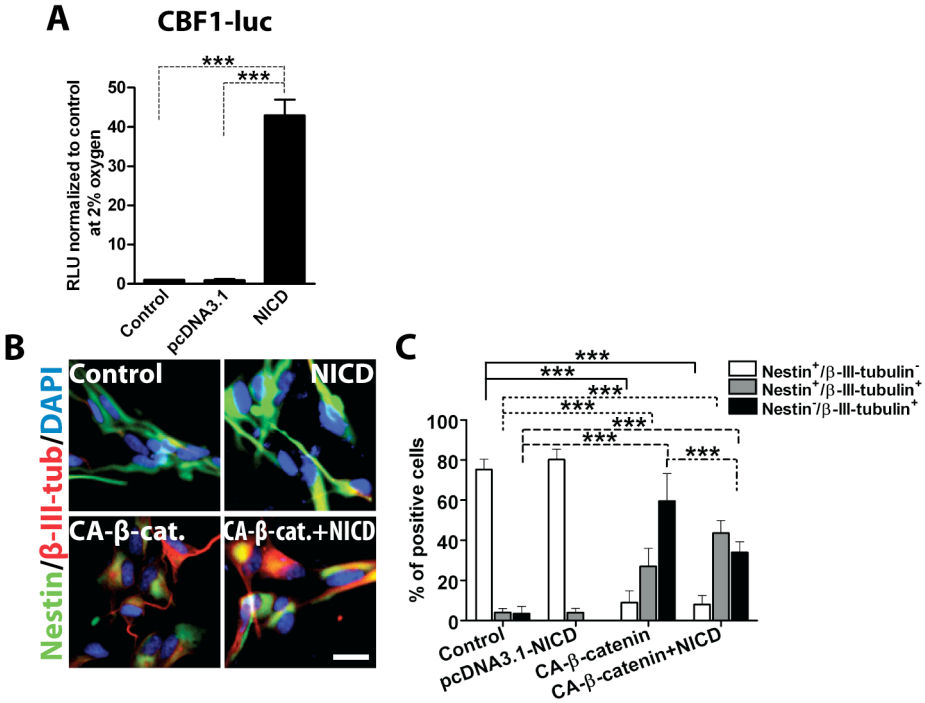

Figure 20. Wnt pathway activation inhibits Notch signalling in GBM derived cells at intracellular level. (A) CBF1-luc luciferase assay on NICD transfected or control cells. (B) Representative immunofluorescence images of GBM cells transfected with NICD, CA-β-catenin or both cultured for 48 h and stained for Nestin(green)/β-III-tubulin(red) and (C) bar graph reporting relative quantification. Mean of 3 tumours ± S.E.M. n=3 for each tumour. bar=100 μm.

As Numb and NumbL are known to inhibit Notch intracellular activity (Gulino et al., 2010) and have been recently proposed to contain β-catenin binding sites in their promoters (Katoh and Katoh, 2006), we evaluated if Wnt3a treatment was able to induce *NUMB* and *NUMBL* transcription. Analysis of *NUMB* and *NUMBL* expression revealed that Wnt3a induced their transcription and increased their protein expression (Figure 21A-B), thus suggesting a potential mechanism for the Wnt-mediated inhibition of Notch signalling observed in primary GBM-derived cells (Figure 19). Indeed, chromatin immuno-precipitation analysis (ChIP) revealed that β-catenin directly binds to *NUMB* promoter after Wnt3a treatment, thus suggesting a direct mechanism of Numb

induction mediated by Wnt signalling activation (Figure 21C). Computational analysis revealed the absence of β-catenin binding sites (TCF/LEF consensus sequences) in the *NUMBL* 5' upstream sequence, indicating that the increased NUMBL protein expression could be probably regulated by an indirect mechanism (data not shown). GBM cells exposed to 20% oxygen displayed a less potent inhibition of Notch signalling after Wnt3a treatment (Figure 21D).

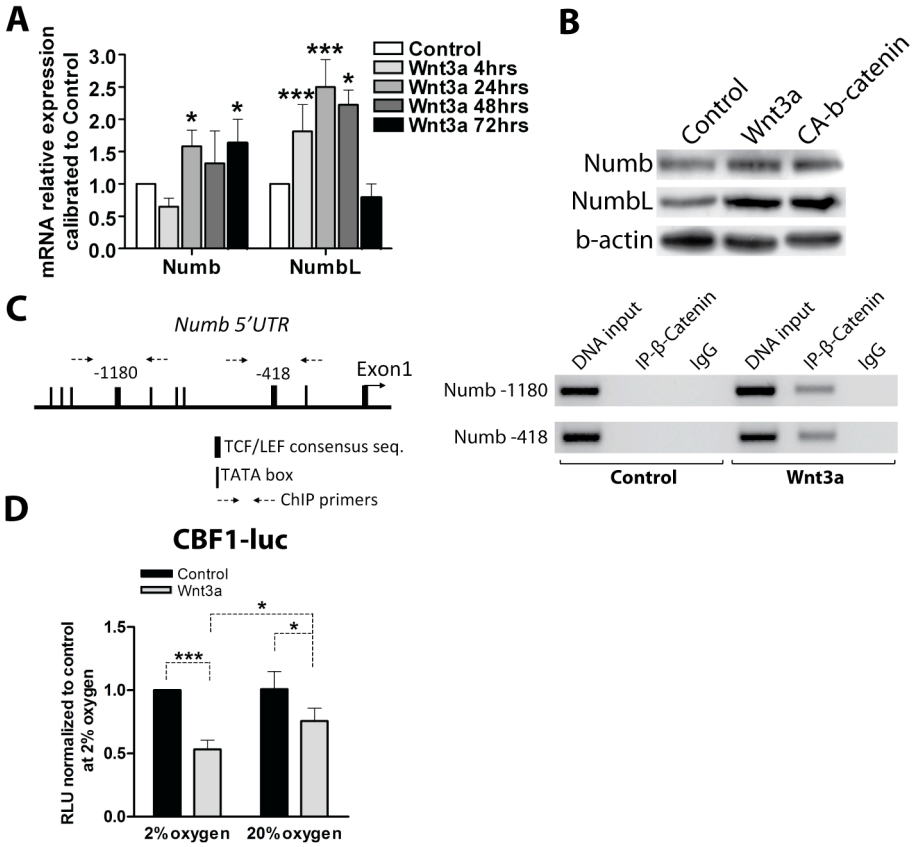

Figure 21. Wnt inhibit notch pathway by NUMB up-regulation. (A) RQ-PCR analysis reporting mRNA levels of *NUMB* and *NUMBL* of Wnt3a treated GBM cells at different time points. (B) NUMB and NUMBL protein expression of Wnt3a treated or CA-β-catenin transfected GBM cells. Mean of 6 tumours ± S.E.M., n=4 for each tumour. (C) Chip analysis of *NUMB* promoter performed on 293T cells treated or not with Wnt3a. The IP was performed by using anti-total β-catenin antibody or an irrelevant antibody as negative control. (D) CBF1-luc luciferase assay conducted on Wnt3a treated GBM cells at different oxygen tensions. For all graphs mean of 3 tumours± S.E.M., n=2 for each tumour. *p<0.05, **p<0.01, ***p<0.001

Wnt pathway activation mostly affects the GBM stem-like cell population

We analysed which sub-population of GBM-derived cells ($CD133^+$ or $CD133^-$) was mostly affected by the pro-differentiating process driven by Wnt pathway activation. Firstly, we sorted $CD133^+$ and $CD133^-$ cells and evaluated their responsiveness to Wnt activation by using the BAT-LUX reporter construct. Starting from a comparable basal level of β-catenin transcriptional activity, Wnt3a- and CA-β-catenin-mediated reporter activation was much stronger in $CD133^+$ cells relative to $CD133^-$ cells (Figure 22A). Moreover, in agreement with previous data of Notch inhibition (Figure 19-20), Wnt3a and CA-β-catenin inhibited Notch transcriptional activity only in $CD133^+$ cells (Figure 22B), thus suggesting that pro-differentiating effects mediated by Wnt pathway activation should be maximal in GBM-derived stem-like cells. In general $CD133^-$ cells displayed a lower level of constitutive Notch signal activation, with no significant phenotypic changes after Wnt3a treatment or CA-β-catenin transfection (Figure 22B-D). Phenotypic analysis carried out on CD133 sorted cells revealed that the differentiation effect mediated by Wnt occurred almost exclusively in stem-like $CD133^+$ cells (Figure 22C-D). As expected, $CD133^-$ untreated cells displayed a more differentiated phenotype relative to $CD133^+$ cells (Figure 22C-D). In agreement with these data, also proliferation was inhibited only in $CD133^+$ cells as showed by Ki67 staining in Figure 22E-F.

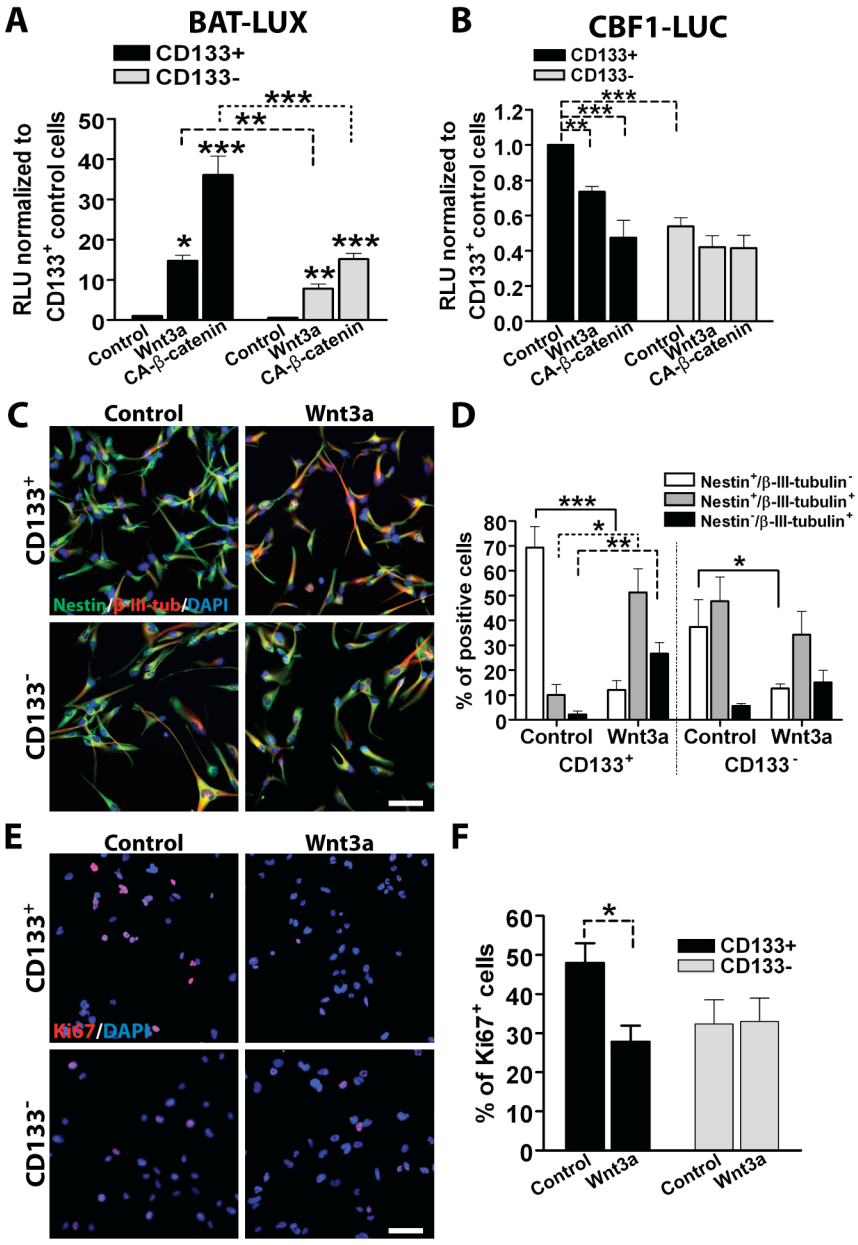

Figure 22. Wnt activation-mediated differentiation primarily affects CD133⁺ GBM derived cells. (A-B) BAT-lux (A) and CBF1-luc (B) reporter analysis of CD133⁺ or CD133⁻ sorted GBM cells treated with Wnt3a or either transfected with CA-β-catenin at 2%O_2. Mean of 4 tumours± S.E.M., n=2 for each tumour. (C-F) Representative immunofluorescence images of CD133± sorted GBM cells treated with Wnt3a for 96 h and stained for (C) Nestin(green)/β-III-tubulin(red) and (E) Ki67(red). bar=100μm. (D,F) Bar graph reporting relative quantification of images in (C) and (E). Mean of 4 tumours ± S.E.M., n=3 for each tumour. *p<0.05, **p<0.01, ***p<0.001.

The most pronounced Wnt3a-mediated differentiation effect (and proliferation inhibition) was observed in CD133⁺ cells maintained at 2% oxygen. Conversely,

CD133$^-$ cells exposed to 20% oxygen were almost insensitive to Wnt3a treatment (Figure 23).

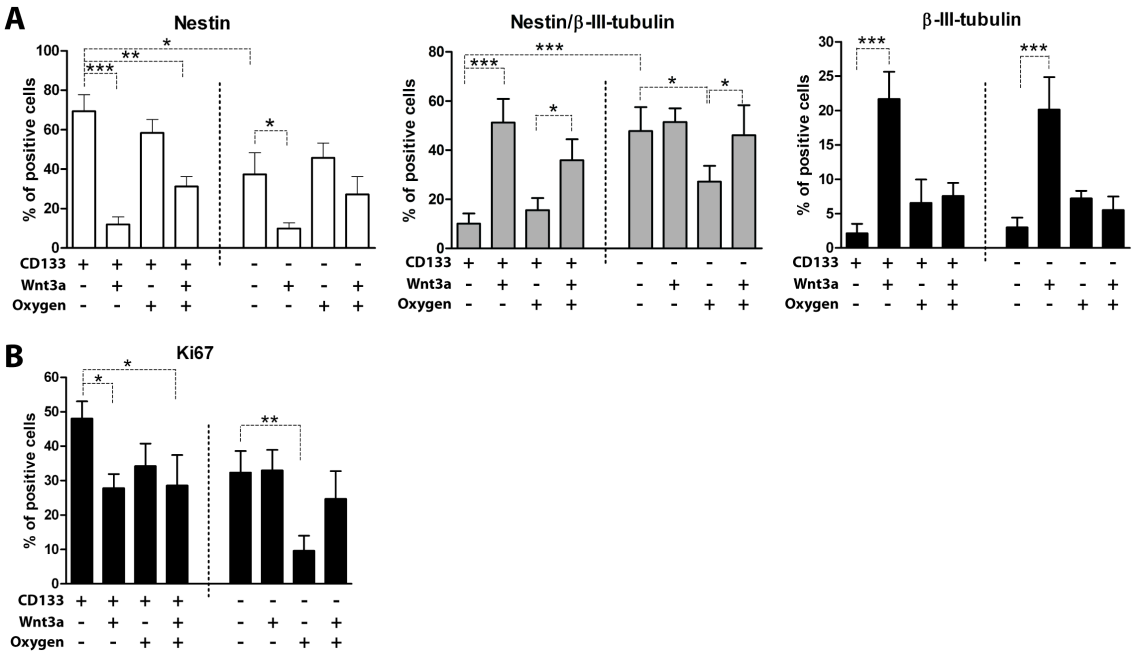

Figure 23. Low oxygen tension enhances Wnt dependent differentiation only in CD133$^+$ GBM-derived cells. (A) Bar graphs reporting relative quantification of Nestin$^+$/β-III-tubulin$^-$, Nestin$^+$/β-III-tubulin$^+$ and Nestin$^-$/β-III-tubulin$^+$ sub-populations of CD133$^+$ and CD133$^-$ sorted cells treated or not with Wnt3a at different oxygen tensions. (B) Bar graph showing % of Ki67$^+$ cells treated as panel (A). For all graphs mean of 3 tumours ± S.E.M., n=10 for each tumour. *p<0.05, **p<0.01, ***p<0.001.

Zebrafish xeno-transplanted GBM cells acquire neuronal phenotype

In parallel to the hypoxic *in vitro* analysis, we evaluated Wnt signalling effects also in an *in vivo* setting. For this purpose we setup a zebrafish-based orthotopic xeno-transplantation procedure of human GBM-derived cells. Since zebrafish brain tissues have been described to be hypoxic (Kranenbarg, 2002) and to express Wnt3a in neural tissues (Clements et al., 2009), we evaluated whether GBM cells phenotype was affected by zebrafish cerebral microenvironment. By using a Wnt-reporter zebrafish strain, we directed the cell injection in a Wnt rich brain site (Figure 24A-B). The correct localization of xeno-transplanted human GBM cells was confirmed by using confocal microscopy analyses (Figure 24B). Xeno-transplanted zebrafish larvae efficiently survived and we could easily track *in vivo* human GBM grafted cells until 5 weeks post injection (6 weeks post fertilization) (Figure 24C). At 4 hours post injection (hpi), GBM cells were characterized by a small, round morphology, typical of undifferentiated brain

tumour cells, and were still localized at the site of injection (Figure 24D). After 48 and 96 hpi GBM cells were recurrently found dispersed within the zebrafish nervous system. Moreover, after 96 hpi, GBM cells increased in cell size and exhibited cellular projections first, and then axonal and neurite outgrowth, typical characteristics of neuronal committed progenitors (Figure 24E-G).

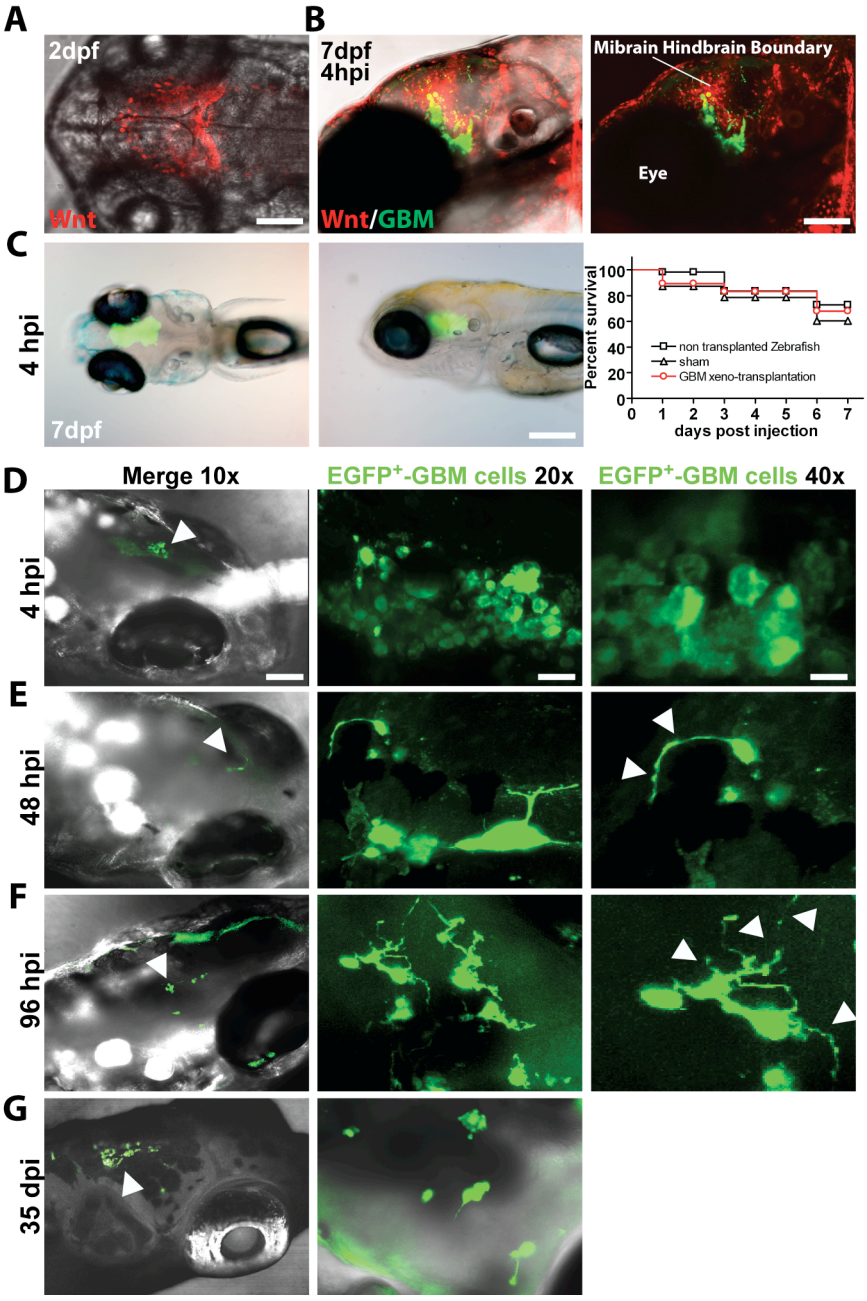

Figure 24. Xeno-transplanted GBM cells acquire a differentiated morphology. (A) Representative images showing mcherry expressing wnt reporter zebrafish cells (red) in the midbrain hindbrain boundary at 2dpf. (B) xeno-transplanted primary GBM derived cells (4hpi) in Wnt activated midbrain hindbrain boundary of 7dpf Wnt-reporter Zebrafish larvae. bar=100 µm. (C) Representative pictures of EGFP transfected primary GBM derived cells grafted into the peri-ventricular zone of 7dpf zebrafish larvae at 4hpi (dorsal view left panel, lateral view right panel). bar=200 µm. Survival graph (right panel) of post-

transplanted zebrafish compared to sham and non-injected larvae bred in the same conditions. Mean of 10 tumours injected ± S.E.M., n=50 for each experimental group. (D-G) Representative images of grafted EGFP expressing GBM cells in live larvae monitored at 4 (D) 48 (E) 96 hpi (F) and 35 dpi (G). White arrows indicate the site where transplanted cells reside in 10x magnification and their cellular projections in 40x magnification. Magnification 10X, bar=100 μm; magnification 20X bar=40 μm; magnification 40X, bar=10 μm.

In order to confirm the neuronal differentiation mediated by the zebrafish brain, we analyzed xeno-transplanted GBM cells phenotype. Immunofluorescence analysis revealed that a progressive loss of Nestin and increase of β-III-tubulin expression occurred in a time-dependent manner, suggesting that the zebrafish brain induced a phenotypic reprogramming of transplanted GBM cells toward neuronal fate (Figure 25A-B). Moreover, expression of Microtubule-associated protein 2 (MAP2), a neuron-specific cytoskeletal protein expressed in post-mitotic differentiated neurons (Sanchez et al., 2000), progressively increased in GBM transplanted cells, confirming the acquisition of a neuronal phenotype (Figure 25C-D). Analysis of Ki67 showed that tumour cells progressively underwent mitotic arrest (Figure 25E-F). To confirm these results, we evaluated the expression of genes related to neuronal differentiation that we previously showed to be up-regulated in GBM cells after Wnt3a treatment (*NEUROD1*, *β-III-TUBULIN* and *NGN1*) and found them up-regulated following xeno-transplantation, confirming the neuronal phenotypic reprogramming of grafted GBM cells (Figure 25G). These results suggest that Wnt ligands-enriched zebrafish brain tissues are able to phenotypically reprogram transplanted GBM-derived cells by directing them toward neuronal differentiation and mitotic arrest, as demonstrated on Wnt3a treated GBM cells *in vitro*.

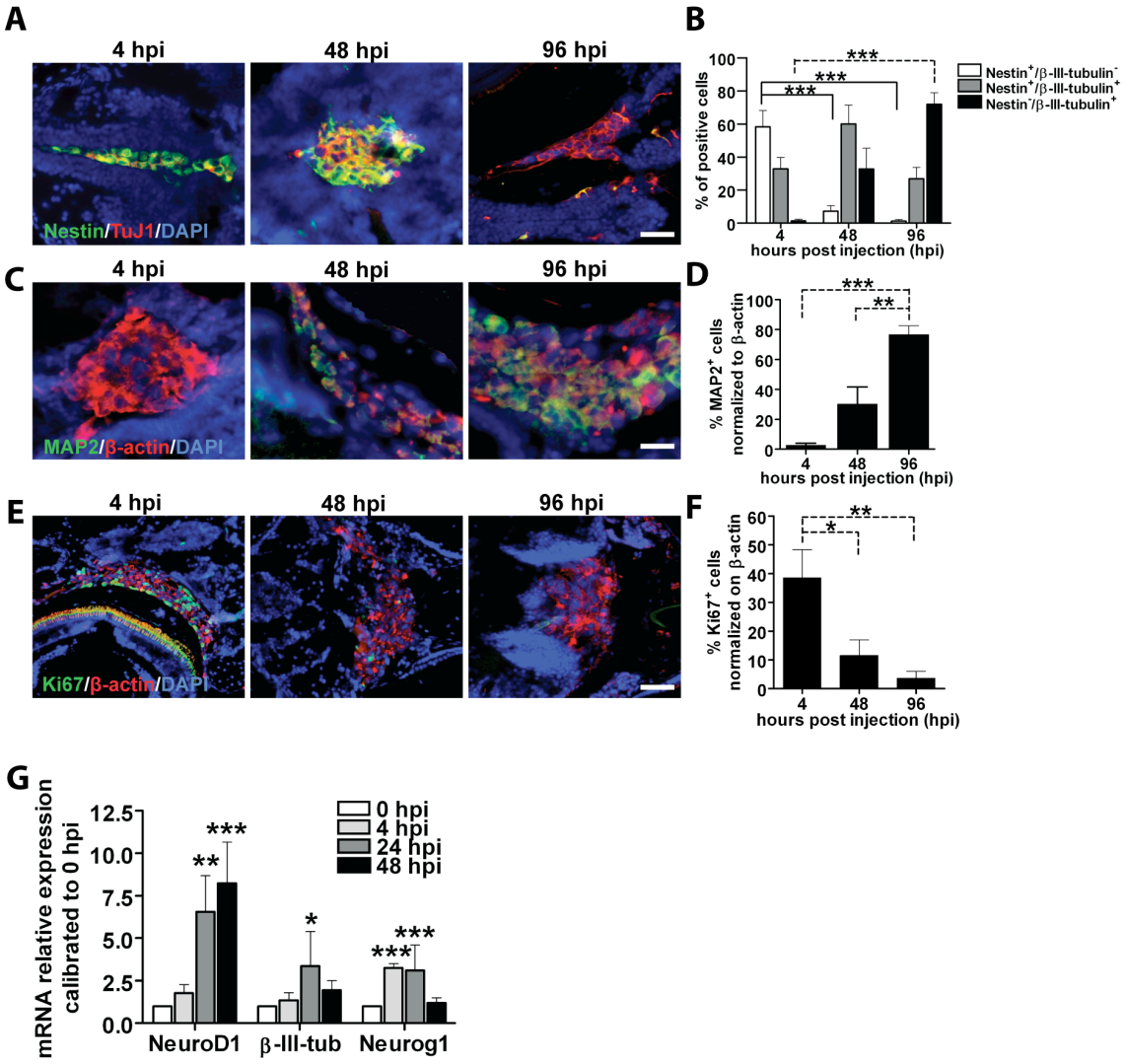

Figure 25. Xeno-transplanted GBM derived cells undergo neuronal differentiation and cell cycle arrest. (A,F) Representative immunofluorescence images of paraffin embedded tissue sections of xeno-transplanted zebrafish larvae at 4, 48 and 96 hpi stained for (A) Nestin(green)/β-III-tubulin(red), (C)MAP2(green)/β-actin(red) and (E) Ki67(green)/β-actin(red). bar=40 μm. (B,D,F) Bar graphs reporting relative quantifications of images shown in (A,C,E). MAP2$^+$ and Ki67$^+$ cells quantification based on % of human β-actin$^+$ cells.bar=40 μm. For all graphs, mean of 10 tumours ± S.E.M., n=10 for each tumour.(G) QRT-PCR analyses of *NEUROD1*, *β-III-TUBULIN* and *NGN1* expression normalized to *GUSB* and then calibrated to control cells (0 hpi) of human GBM cells grafted into zebrafish nervous system, mean ± S.E.M comparing 3 different GBM, n=4 for each tumour.

Gene profile of xeno-transplanted cells points to an induction of a less aggressive phenotype

To add evidences to the involvement of zebrafish Wnt-mediated neuronal differentiation of GBM transplanted cells, we performed whole genome profiling

(GeneChip Human Genome U133 Plus 2.0) of grafted GBM cells. We analyzed gene expression profile (GEP) of human GBM cells after 4, 24 and 48h from transplantation. Microarray data confirmed that zebrafish brain induced a transcriptional reprogram of transplanted GBM cells. Eighty-nine probe sets were retrieved from the intersection of the differentially expressed probe sets along the three time points obtained by two independent experiments (Figure 26A and Suppl. Table1). In particular, we found that *JUN*, *FOS* and *DUSP6* transcription factors were down-regulated following xeno-transplantation. This down-regulation occurred together with a decrease of migration and cellular stress-linked genes such as *COL1A2* and *ITGB1*. According to our phenotypic analyses, also transcription of *KLF6* and *KLF4,* involved in stemness and pluripotency maintenance (DiFeo et al., 2009; Zhang et al., 2010) appeared to be decreased after transplantation. GEP data, showed that GBM cells underwent a dramatic decrease of *VEGF*, *LDHA, GAPDH* and *ALDOA*, indicative of a robust decrease of angiogenesis and glycolysis related genes (Figure 26A-D, Suppl. Table1). Conversely, we observed transcriptional activation of the neuronal developmental genes *GMP6B, CRYAB* and *NEFL*. Moreover, we found a significant increase in the expression of the Wnt-dependent *DKK3* gene (Niehrs, 2006) (Figure 26A-B, Suppl. Table1). This result is in accordance with the observed increase of Wnt related genes *NGN1* and *NEUROD1* occurring inWnt3a treated GBM cells and in grafted GBM cells (Figure 16F and Figure 25G), suggesting a predominant role of Wnt signalling in promoting the acquisition of a neuronal phenotype also in grafted GBM cells.

To investigate whether the induced neuronal differentiation could be primarily dependent on Wnt pathway activation by zebrafish brain tissues, we compared the expression of differentially regulated genes in transplanted cells with mRNA extracted from Wnt3a treated GBM cells *in vitro*. This comparison confirmed that Wnt3a treatment modulated the same gene set observed in GBM transplanted cells (Figure 26B-C).

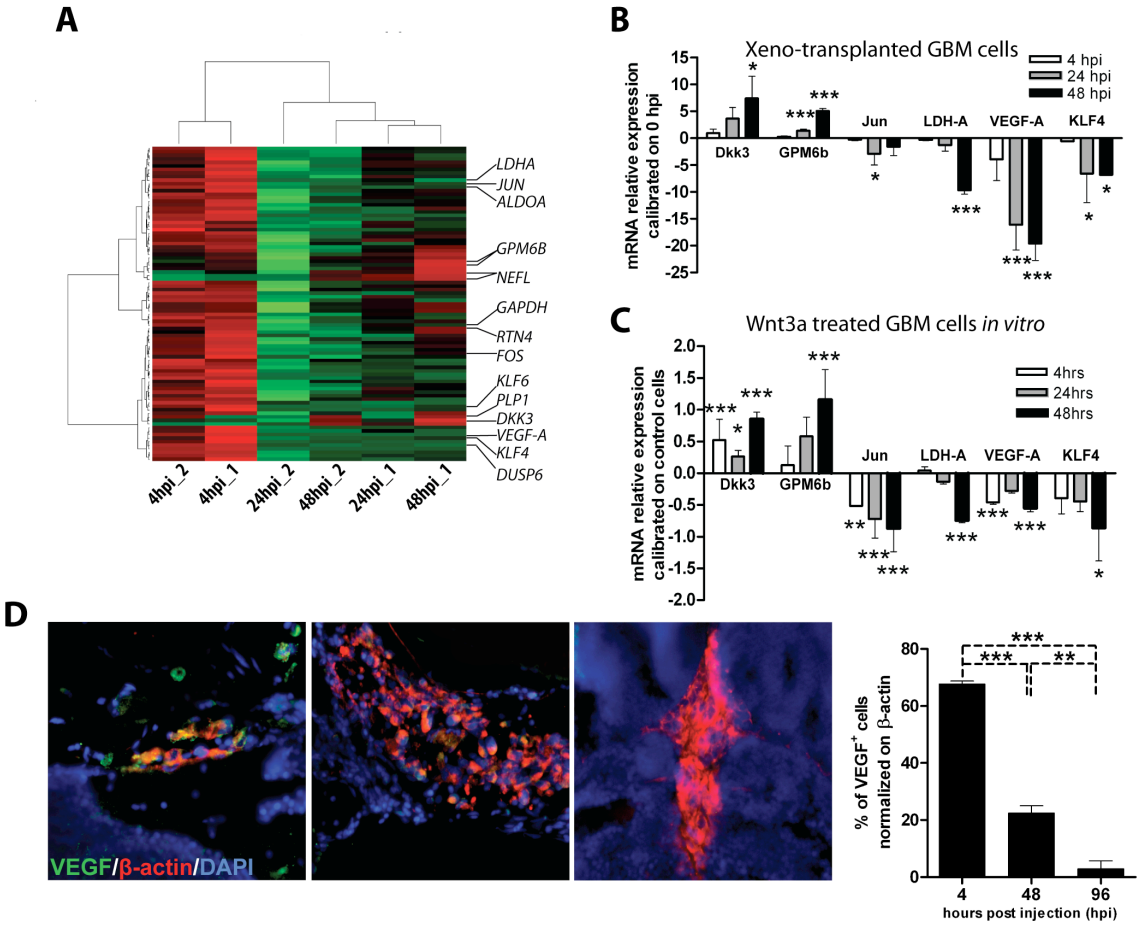

Figure 26. GEP data on xeno-transplanted GBM cells. (A) Heatmap resulting from microarray analysis of two independent experiments of human GBM cells grafted into zebrafish nervous system at 4, 24 and 48hpi. *p<0.05, **p<0.01, ***p<0.001. (B-C) QRT-PCR analyses of *DKK3*, *GPM6B*, *JUN*, *LDHA*, *VEGFA* and *KLF4* expression of xeno-transplanted GBM cells normalized to *GUSB*, then calibrated to control cells (0 hpi) (B) and Wnt3a *in vitro* treated GBM cells (C). (D) Representative immunofluorescence images of tissue sections of xeno-transplanted zebrafish larvae at 4, 48 and 96 hpi stained for VEGF(green)/β-actin(red)) and its relative quantification. bar=40 µm. Mean of 3 tumours ± S.E.M., n=10 for each tumour. **p<0.01, ***p<0.001.

Neuronal reprogramming is dependent on Wnt pathway activation mediated by zebrafish brain

In light of these results, we verified the hypothesized Wnt pathway activation in GBM transplanted cells. We analyzed human β-catenin expression in protein extracts obtained from grafted zebrafish brains after 4, 48 and 96 hpi and found a significant increase in total human β-catenin protein expression from 48 hpi (Figure 27A-B). In order to confirm this result, we evaluated β-catenin mediated transcriptional activity of transplanted GBM cells *in vivo*. Thus, tumour cells were transfected with BAT-LUX reporter vector, transplanted as described and then luciferase activity was monitored. β-

catenin activity-induced luciferase resulted to be up regulated at 24 hpi when compared with non-transplanted cells (Figure 27C). Moreover, by transfecting tumour cells with CBF1-luc reporter vector prior to injection, we confirmed that zebrafish-mediated β-catenin activation led to a concomitant decrease of Notch activity (Figure 27D).

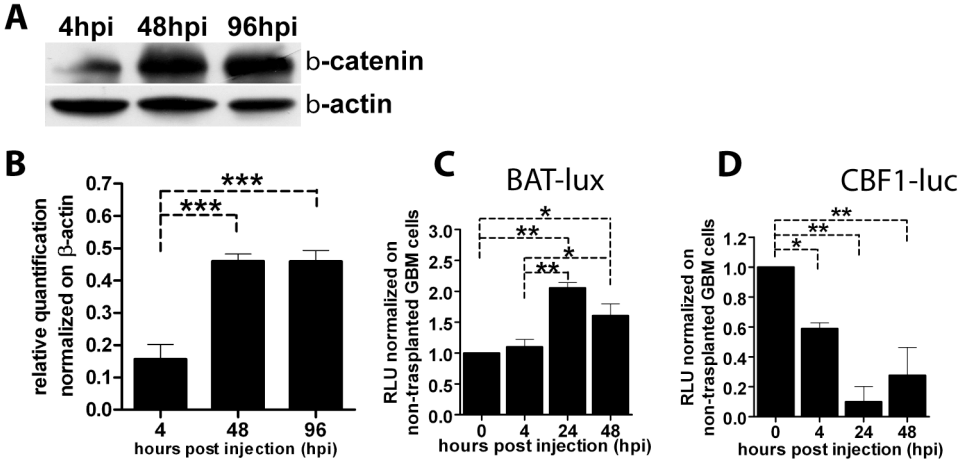

Figure 27. Zebrafish Wnt molecules activate β-catenin and inhibit Notch activity in grafted GBM cells. (A) Representative western blot analyses of human β-catenin in total protein extracts retrieved from zebrafish brains transplanted with GBM cells after 4, 48 and 96 hpi along with human β-actin as loading control. (B) Bar graph reporting relative β-catenin protein quantification normalized on human β-actin. The analysis has been confirmed on additional 3 tumours. For the graph, mean of 4 tumours ± S.E.M., n=3 for each tumour. (C) BAT-lux reporter assay of human GBM grafted cells. Values are expressed in RLU (relative light units) calibrated on not transplanted GBM cells (0 hpi). 3 different GBM have been analyzed, n=4 for each tumour. (D) CBF1-luc reporter assay carried out on same samples as panel (C)

To functionally confirm the pivotal role of Wnt pathway activation in GBM cell differentiation *in vivo*, we transplanted GBM cells in Wnt-ablated transgenic zebrafish, named Tg(*hsp70l:dkk1-GFP*)^{allele} and characterized by the expression of *dikkopf1b* gene (*dkk1*) under the control of heat shock cognate protein 70 promoter. As a consequence of the heat shock, and subsequent *dkk1*-GFP over-expression (Figure 28A) Wnt signalling is inhibited (Stoick-Cooper et al., 2007). GBM cells grafted into the brain of *hsp70l:dkk1-GFP* transgenic zebrafish larvae did not undergo differentiation and maintained their proliferation rate as shown by the expression of Nestin, β-III-tubulin and Ki67 (Figure 28B-E). Interestingly, xeno-transplanted *hsp70l:dkk1-GFP* larvae, when heat shocked to inhibit endogenous Wnt signal, diminished their survival rate compared to non heat shocked transplanted *hsp70l:dkk1-GFP* or sham heat shocked *hsp70l:dkk1-GFP* larvae (Figure 28F).

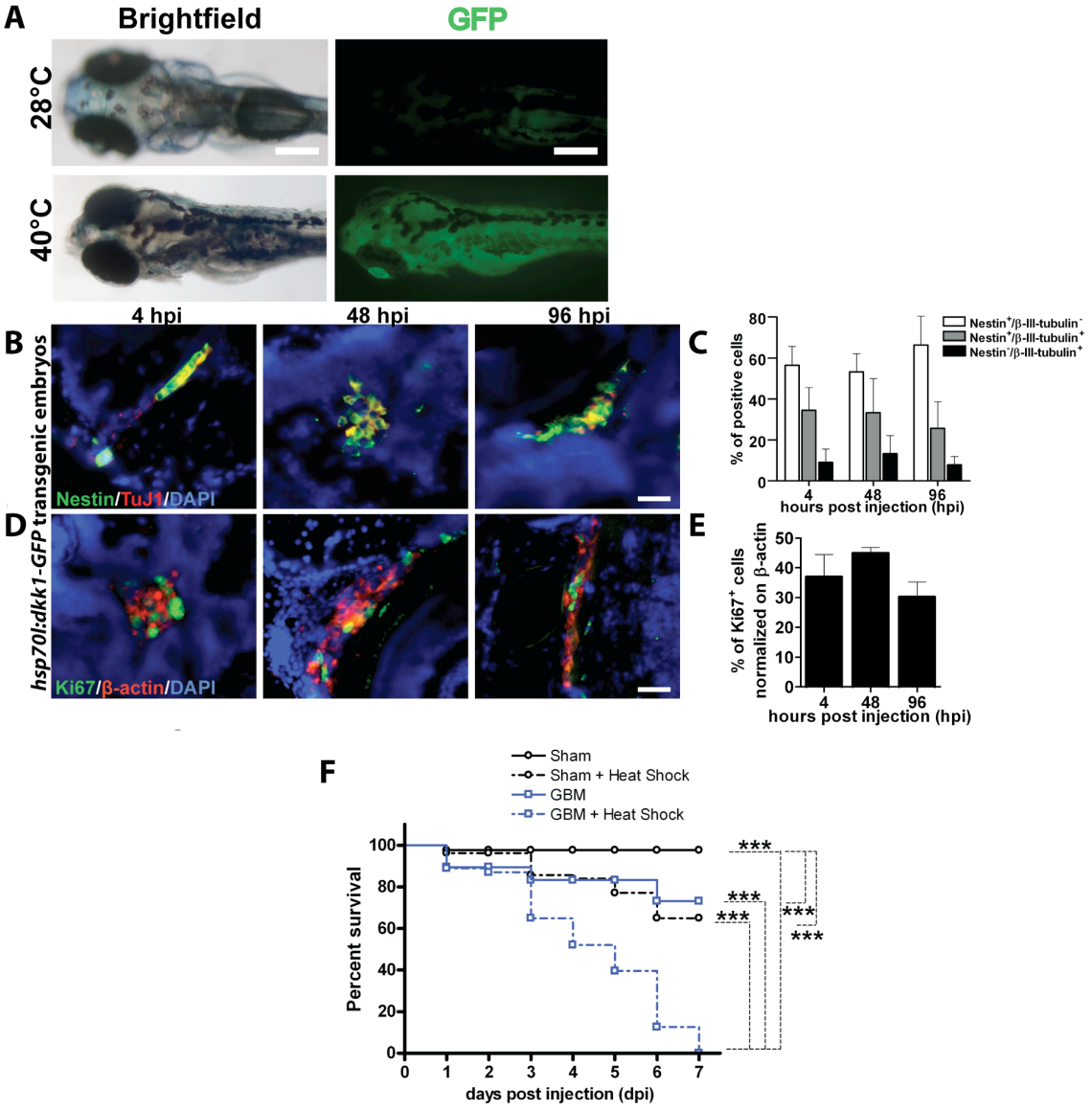

Figure 28. Wnt pathway *in vivo* inhibition prevented neuronal differentiation of grafted GBM cells. (A) Representative images of *hsp70l:dkk1-GFP* larvae maintained at 28°C (upper panels) and after heat shock (40°C) (lower panels). Left panels: live larvae; right panel: transgene expression after heat shock. bar=100 μm. (B-E) *hsp70l:dkk1-GFP* xeno-transplanted larvae at 4, 48 and 96hpi stained for (B) Nestin(green)/β-III-tubulin(red) and (D) Ki67(green)/β-actin(red). bar=40 µm Right panels (C,E) show relative quantification of images described in (B,D). Mean of 6 tumours injected± S.E.M., n=50 for each experimental group. (F) Survival graph of post-transplanted *hsp70l:dkk1-GFP* zebrafish compared to sham larvae ± heat shock bred in the same conditions. Mean of 6 tumours injected ± S.E.M., n=50 for each experimental group. *p<0.05, **p<0.01, ***p<0.001.

In order to further validate these results, xeno-transplanted wild type zebrafish larvae were treated with IWR, a compound known to inhibit Wnt pathway activation *in vivo* and to down-regulate Wnt-controlled genes such as *neurod* (Chen et al., 2009) (Figure 29A). We found that also IWR treatment prevented neuronal differentiation of grafted GBM cells, which maintained an uncommitted and proliferating phenotype (Figure

29B-E). These results demonstrate that zebrafish endogenous Wnt signals promote the neuronal phenotypic reprogramming of xeno-transplanted GBM-derived cells.

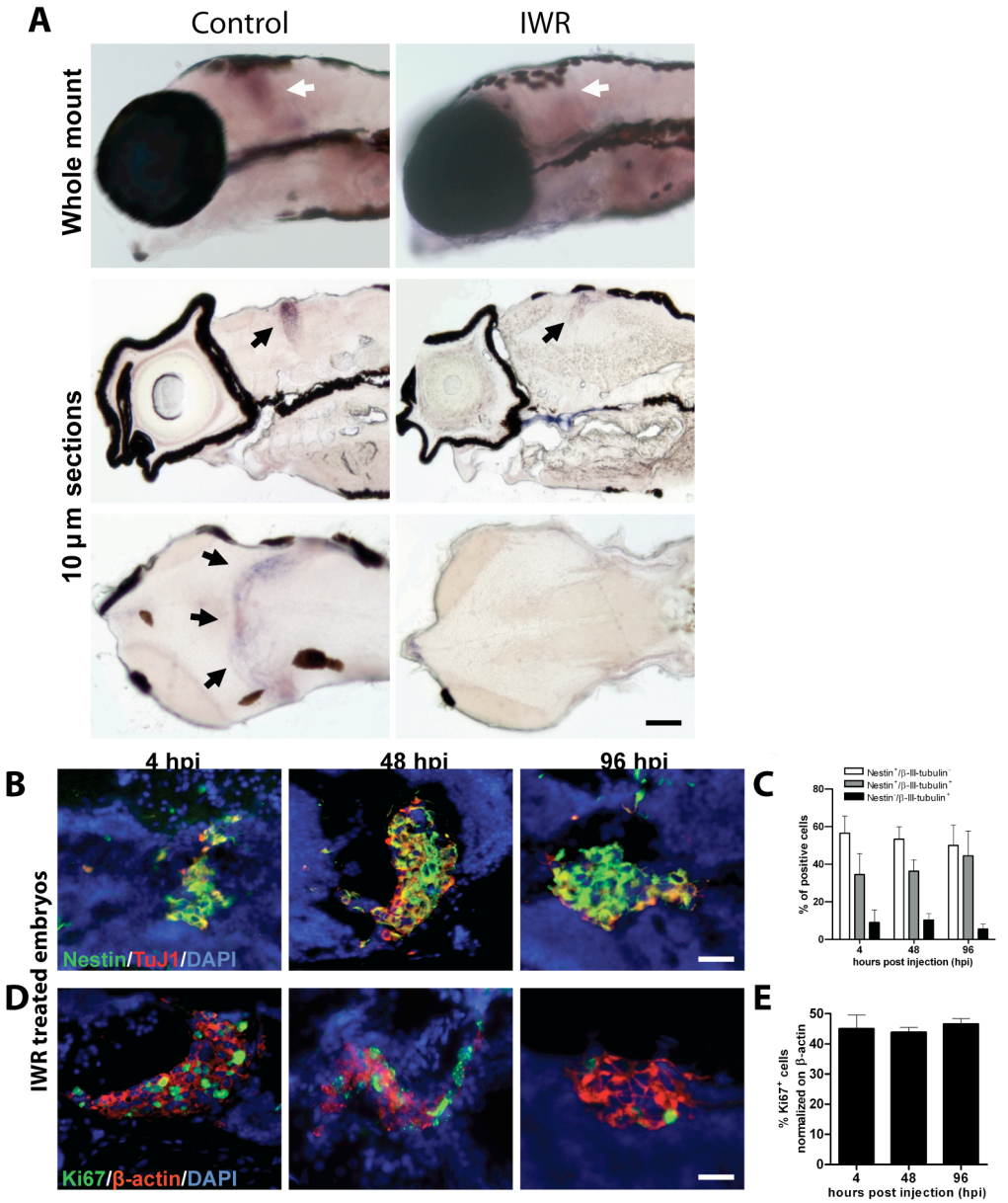

Figure 29. Wnt pathway pharmacological inhibition maintained grafted GBM cells in their undifferentiated proliferating state. (A) Representative images of *neurod* expression by whole mount *in situ* hybridization on control and IWR treated (72h) zebrafish larvae at 9 dpf. Arrows indicate sites of *neurod* expression. Larvae were OCT embedded and post–staining sectioned. The analysis has been confirmed in 3 independent experiments on 150 larvae. bar=100 μm. (B-E) Representative immunofluorescence images of IWR-treated xeno-transplanted larvae stained for Nestin(green)/β-III-tubulin(red) (B) and Ki67(green)/β-actin(red) (D). (C,E) Relative quantification of images described in (B,D).*p<0.05, **p<0.01, ***p<0.001.

Wnt-Notch double reporter zebrafish display a Wnt dependent regulation of Notch signaling in the developing brain

We next evaluated if these mutual regulation between Wnt and Notch pathways regulate also neural *in vivo* development. Our analyses conducted on Wnt-Notch double transgenic zebrafish larvae indicated that this mechanism is involved also in differentiation of zebrafish normal neural precursors. Wnt pathway activated cells in the zebrafish developing brain did not co-activate Notch signalling during time (Figure 30A). Moreover, over-activation of Wnt signalling by $LiCl_2$ treatment, known to activate β-catenin transcriptional activity, was able to expand the Wnt activated neuronogenic zone (midbrain-hindbrain boundary) and to consequently reduce reporter signal from activated Notch pathway (Figure 30B).

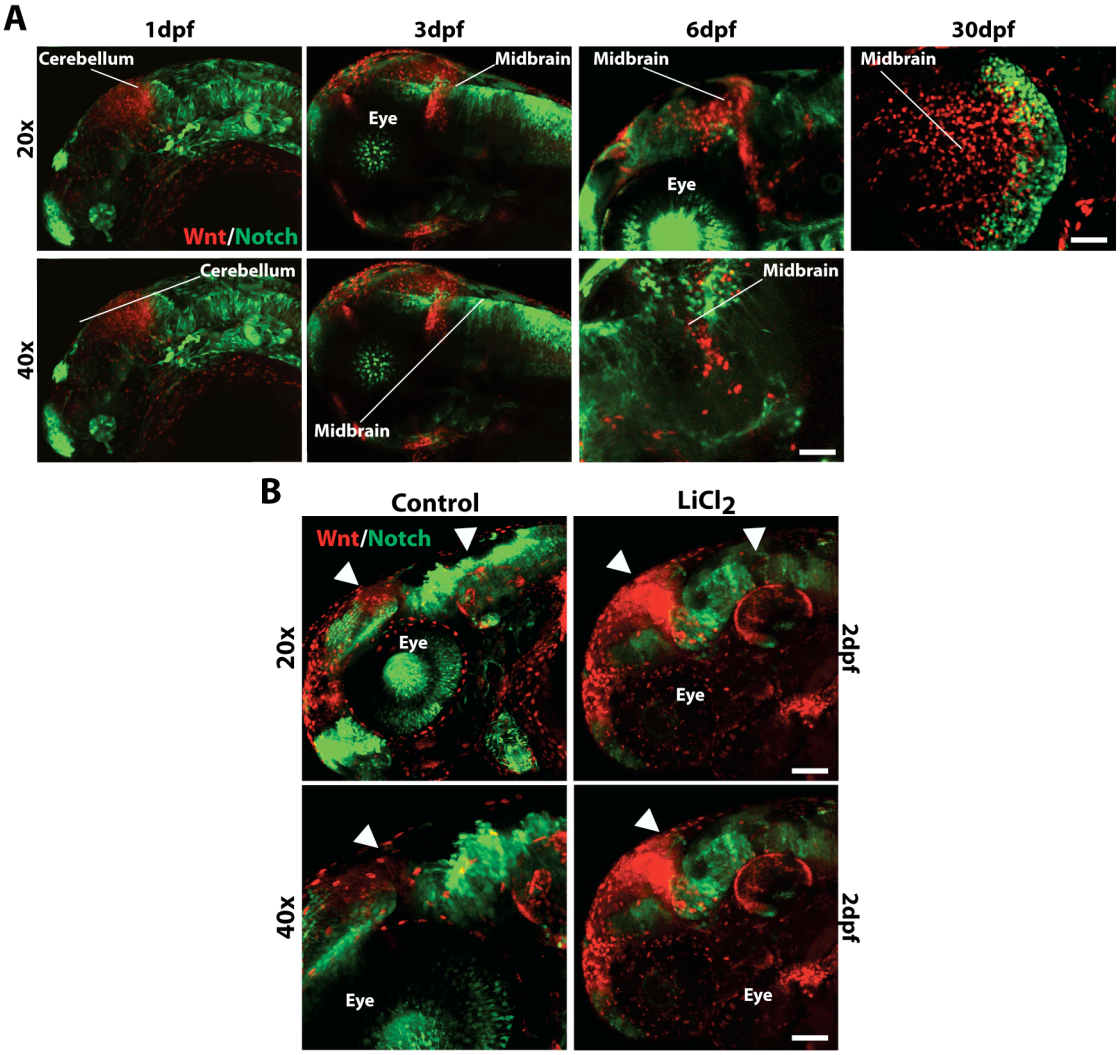

Figure 30. Wnt-Notch double reporter zebrafish display a Wnt dependent regulation of Notch signalling in the developing brain. (A) Representative images of Wnt(red)/Notch(green) transgenic reporter zebrafish showing no co-localization of Wnt/Notch signal in the developing brain. (B) Images of Wnt(red)/Notch(green) transgenic zebrafish treated with the GSK3 inhibitor $LiCl_2$ at different time points. 20X, bar=100 μm. 40X, bar= 10 μm.

DISCUSSION PART I

The pivotal role of the local microenvironment in the initiation and progression of tumours is becoming increasingly clear. HIF-1α and hypoxia have been shown to be implicated in tumour progression (Birner et al., 2001; Garcia, 2006; Gillespie et al., 2007; Holmquist-Mengelbier et al., 2006; Semenza, 2002; Smith et al., 2005). We have recently shown (Pistollato et al., 2009a) that BMP2 in vitro treatment, known to promote glial differentiation in GBM derived cells (Piccirillo et al., 2006), resulted to be less effective under hypoxia, suggesting that hypoxia and also HIF-1α may preserve GBM tumour cell stemness by de-sensitizing cells to pro-differentiating BMP2 stimulus. It has also been reported that epigenetic-mediated dysfunction of the BMP receptor-IB (BMPR-IB) inhibits differentiation of glioblastoma-initiating cells (Lee et al., 2008), but the role of hypoxia in BMP pathway regulation has not been previously considered in other studies. Moreover, HIF-1α expression seems to depend on mTOR signaling control and mTOR seems to be activated also by BMP in murine CNS precursor cells cultured at high density (Chen et al., 2007; Land and Tee, 2007). These observations suggest a convergence of BMP with mTOR in controlling glial differentiation and on the other hand HIF-1α transcriptional activity. In this study we investigated the role of mTOR signaling in the regulation of HIF-1α stability in primary GBM-derived cells compared to normal SVZ-derived cells, maintained under hypoxia, evaluating the effects mediated by acute high oxygen exposure and BMP2. We found that acute exposure to high 20% oxygen tension promotes Akt and mTOR signaling pathways activation, with consequential increase of mTOR downstream targets (Stat3 and p70S6K), whereas hypoxia inhibits these effects. Importantly, under hypoxia, Akt/mTOR pathway results to be inhibited. p70S6K leads to activation of pro-translational responses, which dependably leads to increased differentiation. Accordingly, we also found Stat3, known to promote astrogliogenesis (Rajan et al., 2003), highly activated by acute high oxygen tension. In a previous study it has been

reported that reactivation of Stat3 in PTEN-deficient glioblastoma cells inhibits their proliferation and invasiveness (de la Iglesia et al., 2008). We previously found that after acute high oxygen exposure also SMAD1/5/8 activation, known to induce astrogliogenesis, occurred, analogously to Stat3 activation. Notably, normal SVZ-derived cells underwent mTOR but not analogous Akt, Stat3 and p70S6K activation following high oxygen acute exposure, suggesting differences in oxygen sensitivity between tumour and normal cells. Importantly, after high oxygen exposure HIF-1α was down-modulated, but after 120 min it was partially reconstituted in GBM probably by a mTOR dependent mechanism. Indeed, HIF-1α has been found to be regulated by mTOR via a mTOR signaling motif, this leading to increased angiogenesis (Land and Tee, 2007). Recent studies also indicate that REDD1 (RTP801), induced under hypoxic conditions in a HIF-1α dependent manner, plays a role in the TSC1 (hamartin) / TSC2 (tuberin)-mediated inhibition of mTOR (Brugarolas et al., 2004; Schwarzer et al., 2005), these indicating a reciprocal regulatory control between HIF-1α and mTOR. Here we found that by stabilizing HIF-1α with $CoCl_2$, inhibition mTOR pathway was maintained following acute high oxygen exposure on tumor cells, and this may occur through a negative feedback loop dependent on HIF-1α mediated transcriptional activation of REDD1. Accordingly, we found that silencing of HIF-1α promotes stronger activation of Akt/mTOR even at 2% oxygen, analogously to inducing SMAD1/5/8 activity. Together these results indicate that HIF-1α may be required to repress besides SMAD1/5/8, also Akt and Stat3 activation in hypoxic GBM cells, molecular signals directed toward induction of astroglial fate in neural stem cells (Fukuda et al., 2007).

It has been shown that BMP2 increases Akt serine/threonine kinase activity in serum-deprived 2T3 osteoblasts (Ghosh-Choudhury et al., 2002) and accordingly we found that exogenous BMP2 treatment, analogously to acute high oxygen exposure, induced up-regulation of Akt/mTOR pathway, particularly of Stat3. Importantly, these effects were down-regulated both by hypoxia and by HIF-1α, whose stabilization obtained with either $CoCl_2$ or by using proteasome inhibitor (Z-LLF) was preventing BMP2 induced Akt/mTOR activation, especially in tumor cells. In normal SVZ cells Akt, mTOR and its downstream targets were only transiently modulated by BMP2, indicating a different sensitivity between tumor and normal cells in responsiveness to exogenous BMP2.

Importantly, we also found that after 15 min of BMP2 treatment a rapid down-regulation of HIF-1α protein occurred under hypoxia, but its level was recovered during time in GBM cells. After a longer BMP2 treatment (72 hr), when glial commitment is at a more advanced stage, we previously described (Pistollato et al., 2009a) a reduction of HIF-1α protein, regardless the presence of hypoxia, unlike in normal SVZ cells. We also found that following BMP2 treatment REDD1, HIF-1α downstream target and mTOR inhibitor (Brugarolas et al., 2004; Schwarzer et al., 2005), was down-regulated even under hypoxia. Thus, BMP2, analogously to an acute exposure to high oxygen tension may promote mTOR activation by down-modulating REDD1, as a consequence of HIF-1α dependent transcriptional activity inhibition.

PHD2 is involved in hydroxylation and consequentially degradation of HIF-1α; we found that BMP2 induced increase of PHD2 protein level, in both normal and tumour cells, but this upregulation does not seem to be related to increased protein translation. Moreover, FKBP38, which has been recently described as a PHD2 protein modulator (Barth et al., 2007), was down-regulated both by high oxygen exposure and BMP2 treatment in GBM cells maintained under hypoxia. FKBP38 has been described to bind to mTOR, inhibiting the ability of mTORC1 to signal to downstream targets (Dunlop and Tee, 2009). However, the molecular functions of FKBP38 remain still elusive. We hypothesize that a decrease of FKBP38 following BMP2 and high oxygen exposure may stabilize PHD2 protein level leading to HIF-1α degradation even under hypoxia. FKBP38 down-regulation may also explain mTOR signaling activation under these stimuli. Since several decades it has been shown that solid tumor cells are characterized by intense anaerobic glycolysis, strongly suggestive of an association between mitochondrial dysfunction and cancer. Indeed, a variety of tumor cell types are characterized by an impaired respiratory capacity (Warburg, 1956), and this was confirmed also in our in vitro culture conditions, as shown by increased lactic acid production and decreased cytochrome c oxidase activity (COX) in GBM cells compared to normal SVZ cells. It has also been shown that mTOR pathway is influenced by the intracellular concentration of ATP, independent from the abundance of amino acids (Dennis et al., 2001). Thus, we hypothesize that mTOR signaling down-regulation in our hypoxic GBM cells may be due also to decreased ATP availability. Among mitochondrial dysfunctions, impaired SDH activity in several cancer types has

been associated to non-hypoxic HIF-1α stabilization, through a mechanism involving intracytoplasmic succinate accumulation and consequential PHD2 inhibition (King et al., 2006). Importantly, it has also been shown in other cell models that induction of differentiation by BMPs increases mitochondrial oxidative phosphorylation, as seen by higher SDH activity (Kamegai et al., 1990). Although, this effect has not been clearly described in tumor cells. We found that SDH activity was increased following BMP2 treatment, suggesting that pro-differentiating agents, such as BMPs, may promote a metabolic shift toward oxidative phosphorylation also in tumor cells. Addition of succinate in combination with BMP2, was promoting a recovery of HIF-1α protein, upregulation of REDD1 and consequentially a moderate inhibition of Akt/mTOR signaling, especially of p70S6K. In conclusion, we describe the mechanisms by which BMP2 and, analogously, oxygen tension perturbation, by activating Akt/mTOR signaling, inhibiting FKBP38 and by inducing SDH activity modulate HIF-1α stability and consequentially REDD1 transcription in GBM cells. Together these effects are restrained by preserving the hypoxic niche (Figure 31). Moreover, our results point to discrete differences in high oxygen and BMP2 sensitivity between GBM cells and normal cells that should be exploited to better define tumor cell biology.

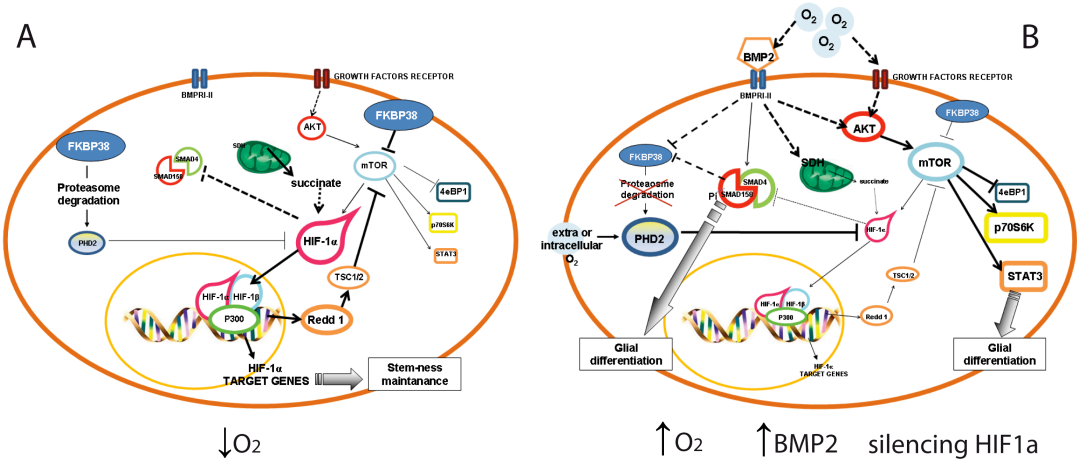

Figure 31: Summary of the hypothetical GBM cell responses to the niche. (A) Under hypoxia, brain tumor cells undergo HIF-1α stabilization, due to PHD2 degradation probably mediated by FKBP38. Consequentially, HIF-1α dependent transcriptional control occurs, with inhibition of Akt/mTOR signaling probably through REDD1 and TSC1/2. Moreover, HIF-1α inhibits SMAD1/5/8 activation. Under hypoxia tumor cells remain in an undifferentiated cell state. (B) Raise of extracellular/intracellular oxygen tension and/or exogenous BMP2, or silencing of HIF-1α, besides activating BMP signaling promotes activation of Akt/mTOR pathway. Consequentially mTOR induces activation of its downstream targets, such as Stat3 (pro-survival, glial differentiation) and p70S6K (pro-translational responses). Under these conditions, HIF-1α, which is also controlled by mTOR at the transcriptional and translational level, is

down-regulated especially in the long term. We showed that HIF-1α degradation is also related to BMP2 dependent increase of SDH activity, this leading to intracellular succinate level decrease and consequential PHD2 activation, in accordance with previous report. We hypothesize that BMP signaling, either independent or dependent on SMAD1/5/8 activation, may also down-regulate FKBP38, thus impeding PHD2 proteasomal degradation and consequentially stabilizing PHD2 protein. Moreover, BMP2 dependent FKBP38 downregulation correlates also to activation of mTOR signaling, as FKBP38 is known to be a mTORC1 inhibitor.

The results of these study have been published on: PLoS One. 2009 Jul 9;4(7):e6206. Molecular mechanisms of HIF-1alpha modulation induced by oxygen tension and BMP2 in glioblastoma derived cells, Pistollato F, Rampazzo E, Abbadi S, Della Puppa A, Scienza R, D'Avella D, Denaro L, Te Kronnie G, Panchision DM, Basso G.

In the first part of the project, I analysed the interplay between oxygen and BMP2 pathway in GBM derived cells, showing that BMP2 in vitro treatment, known to promote glial differentiation in GBM derived cells (Piccirillo et al., 2006; Pistollato et al., 2009a), resulted to be less effective under hypoxia, suggesting that hypoxia and also HIF-1α preserve GBM tumour cell stemness by de-sensitizing cells to pro-differentiating BMP2 stimulus (Pistollato et al., 2009a; Pistollato et al., 2009b). It has also been reported that epigenetic-mediated dysfunction of the BMP receptor-IB (BMPR-IB) inhibits differentiation of glioblastoma-initiating cells BMPs mediated (Lee et al., 2008). Together with these findings, we describe a novel concentric model of the tumour stem cells niche indicating that the more immature cells are localized in the inner core and in the intermediate layer of the tumour mass. Thus, we exploit the hypoxic microenvironment where GBM cells reside (Pistollato et al., 2010a). That said, it is necessary to modulate the phenotype and to promote an effective cell cycle arrest of GBM derived cells in their hypoxic microenvironment.

In the second part of the study, I describe the fundamental role of oxygen tension in modulating GBM derived cells phenotype also in a pro-differentiating process.

Nowadays, the role of Wnt activation in regulating brain tumour phenotype remains controversial. Recent studies showed that lithium ($LiCl_2$) and enzastaurin potently and specifically blocked glioma cell migration and reduced tumorigenicity through inhibition of GSK3 (Kotliarova et al., 2008; Nowicki et al., 2008). Moreover, the use of other GSK3 inhibitors have been reported to increase β-catenin levels, thus down-regulating stem cell markers, such as Nestin and Sox2 (Korur et al., 2009). However,

many authors reported that over-expression of Wnt in glioma tumors promoted CSCs self renewal and proliferation (Liu et al., 2010; Pu et al., 2009; Sareddy et al., 2009). Moreover, it has recently been described that many pro-oncogenes, found to be up-regulated in GBM cells, promoted glioma cell growth and stemness maintenance by activating intracellular Wnt pathway co-factors (Yang et al., 2011; Zhang et al., 2011; Zheng et al., 2010). Interestingly, many oncogenes related to the pro-tumorigenic function of β-catenin interact with specific co-factors and in particular with TCF4. Hypoxia, through the activation of the transcription factor HIF-1α, enhances the expression of the β-catenin co-factors LEF-1 and TCF-1 in embryonic and NSC, thus promoting the canonical β-catenin-dependent Wnt signaling activation (Mazumdar et al., 2010). Our data confirm that the synergistic effect mediated by hypoxia is still functioning also in a cancer setting such as GBM and that this occurs via a conserved mechanism involving the HIF-1α mediated TCF-1 and LEF-1 expression that lead to a higher β-catenin transcriptional activity in hypoxia after exogenous Wnt stimuli. Conversely, we found that TCF4 expression is higher in GBM cells maintained in normoxia. Recent studies on cell differentiation and tissue regeneration point out that the intra-cellular effectors of signalling pathways highly conserved among species, associate with different, lineage specific, co-activators and chromatin remodelling complexes in response to the cellular microenvironment. Thus, these transcription factors tend to occupy specific genomic regions directed by lineage specific master regulators that direct their intracellular function (Trompouki et al., 2011). We suppose that this intriguing model, could function also in GBM. In this paper, we demonstrate that the pro-differentiating effects exerted by Wnt pathway activation are attributable to a concomitant and synergistic mechanism that involve the HIF-1α mediated TCF-1 and LEF-1 expression that lead to a direct over-expression of pro-neuronal genes (*NEUROD1* and *NEUROG1*) and the Notch signalling inhibitors NUMB and NUMBL. Fan and colleagues showed that Notch inhibition selectively depletes glioblastoma CSCs as determined by CD133-high status or dye exclusion (Fan et al., 2010). Moreover, a recent work reported that the Notch inhibitors Numb and NumbL contain TCF/LEF-binding sites in their promoters (Katoh and Katoh, 2006). We confirm the direct interaction between TCF/LEF/β-catenin complex and *NUMB* promoter after Wnt3a stimuli, elucidating the epistatic relationship between Wnt and Notch signalling

in GBM-derived cells, thus defining the Wnt-regulated suppression of Notch-intracellular activity in the hypoxic microenvironment of GBM tumours. Interestingly, our analyses conducted on Wnt-Notch double transgenic zebrafish larvae indicated that this mechanism is involved also in differentiation of zebrafish normal neural precursors. In our previous studies, we demonstrated that microenvironmental hypoxia controls GBM tumour physiology through the regulation of important signaling pathways involved in stemness maintenance and/or differentiation. In particular, we showed that HIF-1α activation has a fundamental role in modulating not only the undifferentiated, aggressive phenotype of GBM cells but also their resistance to current radio-chemiotherapy (Pistollato et al., 2010a; Pistollato et al., 2009b). Moreover, we and others reported the critical role of hypoxia in the functional activation of Notch signaling in normal and cancer stem cells (Gustafsson et al., 2005; Pistollato et al., 2010b; Qiang et al., 2012) and this is apparently in contrast with data presented here. Nevertheless, recent work has revealed intricate connections between Wnt and Notch components, suggesting that activation levels of the single pathways could cooperate in the creation of a molecular machinery able to regulate transition between cell states during development and homeostasis (Munoz-Descalzo et al., 2012). In this work, we surprisingly found that we can promote GBM cells differentiation and growth inhibition also in a hypoxic microenvironment. Indeed, exogenous Wnt stimuli, does not affect HIF-1α transcriptional activity, but, by inhibiting Notch activation, the stemness and proliferation maintenance is compromised opening the way to pro-differentiating factors regulated by the TCF/LEF/β-catenin complex.

To validate this mechanism also *in vivo*, we developed an orthotopic xeno-transplantation model by using primary GBM-derived cancer cells injected in 7dpf zebrafish larvae within brain regions displaying strong presence of Wnt signalling activation. Importantly, zebrafish brain represents a hypoxic microenvironment suitable for GBM cells transplantation, as the oxygen tension profile, at 0.7-1.2 mm in ventral-dorsal direction, ranges from 9% to 5% O_2 in zebrafish embryo (Kranenbarg, 2002). Our data indicate that molecular signals of the developing zebrafish brain are able to reprogram injected human GBM-derived cells toward a quiescent neuronal phenotype, as shown by concerted changes in the expression of stemness, proliferation and neuronal markers. This was confirmed also by obtaining gene expression profile from

xeno-transplanted cells that displayed a less oncogenic phenotype. β-catenin is known to epigenetically regulate chomatin-binding proteins by interacting with crucial chomatin-dependent factors (Mosimann et al., 2009). According to our results, we show that 7dpf zebrafish brain, by releasing Wnt secreted factors, epigenetically reprograms human GBM cells toward neuronal fate, as confirmed also in the *hsp70l:dkk1-GFP* transgenic larvae. In this regard, previous works reported on the role of β-catenin as an important contributing factor to glioma progression (Liu et al., 2010; Pu et al., 2009). However, these studies were conducted on established, commercially available, glioma cell lines maintained at 20% oxygen. Conversely, our data were obtained on primary human GBM-derived cells, which we believe should better reflect the real behaviour of GBM tumour cells. In conclusion, we propose an intriguing model of the epistatic reciprocal regulation between HIF-1α, Wnt and Notch pathways able to promote GBM-derived cell differentiation (Figure 32). Indeed, our data show that hypoxia plays a crucial role in strengthening Wnt-ligand intracellular effects by controlling the expression of β-catenin co-factors TCF-1 and LEF-1. β-catenin stabilization increases levels of Notch inhibitors Numb and NumbL together with pro-neuronal genes expression thus prompting a dramatic differentiation of GBM cancer stem-like cells to a neuronal, less aggressive phenotype. Finally, we point to Wnt signalling activation as a novel molecular strategy to be used in order to induce GBM differentiation and tumour cell growth inhibition.

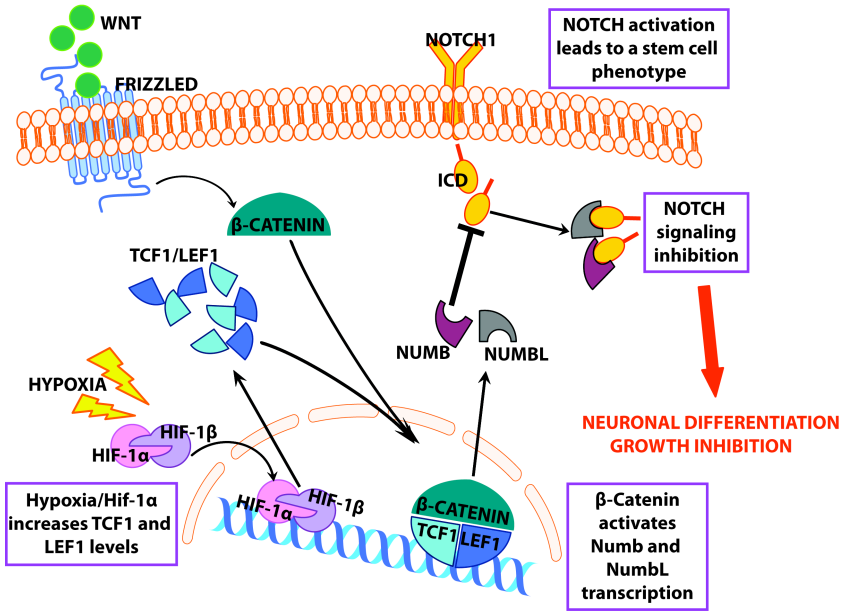

Figure 32. The epistatic relationship between Hif-1α-Wnt- Notch signalling pathway. Cartoon describing the Wnt-dependent Notch signalling regulation proposed in this study.

The results of these study have been submitted to: Plos Biology, Wnt pathway activation promotes differentiation of glioblastoma-derived cells in their hypoxic microenvironment. Elena Rampazzo, Luca Persano, Natascia Tiso, Francesca Pistollato, Enrico Moro, Chiara Frasson, Patrizia Porazzi, Alessandro Della Puppa, Silvia Bresolin, Geertruy Te Kronnie, Francesco Argenton and Giuseppe Basso

RESULTS (PART II)

MEDULLOBLASTOMA

Hypoxia promotes expansion of MDB-derived cells.

We previously reported that normal human subventricular zone (SVZ)-derived neural precursor cells undergo enhanced proliferative expansion in lowered, physiologically relevant 5% oxygen compared with standard laboratory conditions of 20% oxygen (Pistollato et al., 2007). Furthermore, primary glioblastoma-derived cells require an even lower, hypoxic 2% oxygen tension for maximal expansion (Pistollato et al., 2009a; Pistollato et al., 2009b). To determine if MDB-derived neural precursors required the same lowered oxygen tensions for optimal expansion, we performed a similar analysis. We found that 5% and particularly 2% oxygen promoted expansion and long term survival of MDB derived cells (Figure 33A,B). Acute exposure to 20% oxygen for 7 days elicited significant reduction of total cell numbers and, in this condition, MDB cells did not survive for more than two consecutive passages. As previously described, expansion of normal SVZ-derived neural precursor cells was maximally enhanced by 5% oxygen (Figure 33C), but was lower than expansion of MDB.

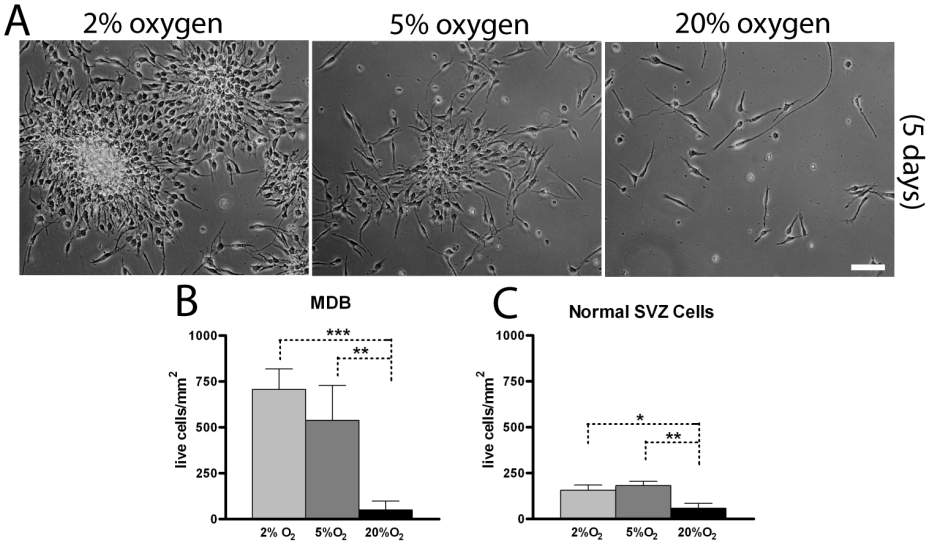

Figure 33. 2% oxygen preserves viability and proliferation of MDB derived cells. (A) Representative pictures of HuTu33 cells expanded at 2%, 5% or 20% oxygen for 7 days. (B,C) Total cell number counts (by trypan blue exclusion) of MDB (B) and SVZ cells (HuSC30 and HuSC23) (C) cultured for 7 days. For (B), mean of 5 different MDB ± S.E.M., n = 2 for each tumor; for (C), mean of 2 different normal SVZ cells cultures ± S.E.M., n = 4 for each cell culture. 10X pictures, bar = 100 μm. *$p < 0.05$, **$p < 0.01$, ***$p < 0.001$.

Acute exposure to high oxygen tension inhibits proliferation and induces neuronal differentiation in MDB-derived neural precursor cells.

In order to determine if the reduced MDB cell expansion in 20% oxygen reflected increased cell death or mitotic arrest, we first analyzed cell growth, expression of the proliferation markers Ki67 and $p21^{cip1}$, and performed cleaved-caspase-3, Annexin-V and TUNEL staining to measure apoptosis levels. We found that MBD derived cells growth was strongly inhibited when cells were cultured at 20% oxygen (Figure 34A) and $Ki67^+$ cells were more abundant in 2% oxygen, indicating higher percentages of actively dividing cells in hypoxic conditions (Figure 35A,F). Conversely, cleaved-caspase3 (Figure 35A,F) and $p21^{cip1}$ (Figure 35B,F) were more frequently expressed in MDB cells exposed to 20% oxygen for 48 hr, consistent with the onset of apoptosis and mitotic arrest. Moreover, analyses of Annexin-V/PI and TUNEL staining revealed a modest, albeit not significant, increase in the percentage of apoptotic cells at 20% oxygen, particularly of $AnnexinV^+/PI^+$ and $TUNEL^+$ apoptotic cells (Figure 34B,C). These results indicate that an acute exposure to increased oxygen tension inhibits proliferation and slightly promotes apoptosis in MDB derived cells.

In order to evaluate if the observed mitotic arrest resulted in cell differentiation, we analyzed MDB-derived cells for the expression of nestin, an intermediate filament which marks multipotent neural stem cells and the lineage-committed progenitors derived from them, but not differentiated neurons, astrocytes and oligodendrocytes (Tohyama et al., 1992). We also measured expression of glial fibrillary acidic protein (GFAP), which marks both astrocytes and some radial glia (Casper and McCarthy, 2006), β-III-tubulin, a marker of immature neurons and their committed progenitors (Memberg and Hall, 1995), and MAP2, a microtubules associated protein that marks differentiated neurons (Heddleston et al., 2009). In 2% oxygen, MDB-derived cells were mainly $nestin^+$ precursors with some $\beta\text{-III-tubulin}^+$ cells, but few if any $GFAP^+$ or $MAP2^+$ cells; exposure to 20% oxygen for 48 hr caused a 2-fold increase in the percentage of $\beta\text{-III-tubulin}^+$ cells, more than 5 fold increase in the percentage of $MAP2^+$

cells and a decrease in nestin$^+$ precursors (Figure 35C,D,E,G). To better characterize this response, we dual-labelled cells with nestin/Ki67 or β-III-tubulin/Ki67, which showed that 20% oxygen reduced the percentages of both nestin$^+$/Ki67$^+$ cells and β-III-tubulin$^+$/Ki67$^+$ (Figure 34D,E). There was a concurrent increase in β-III-tubulin$^+$/Ki67$^-$ cells, consistent with a differentiation of neuronal progenitors to post-mitotic neurons (Figure 34E) and the increase of the MAP2$^+$ cells fraction, as previously shown in Figure 35E,G. Dual labelling with cleaved-caspase3/nestin indicated that, while an increase in apoptotic cells occurred in 20% oxygen compared with 2% oxygen (Figure 35A,F), only a very small percentage of nestin$^+$ cells were apoptotic (Figure 34F). This suggests that the apoptotic response to increased oxygen is selective to neuronal progenitors while the anti-proliferative response is common to multiple precursors, possibly including stem cells. Acute exposure to 20% oxygen did not significantly change the low numbers or absence of GFAP$^+$ (Figure 35D,F) or GFAP$^+$/Ki67$^+$ cells (not shown).

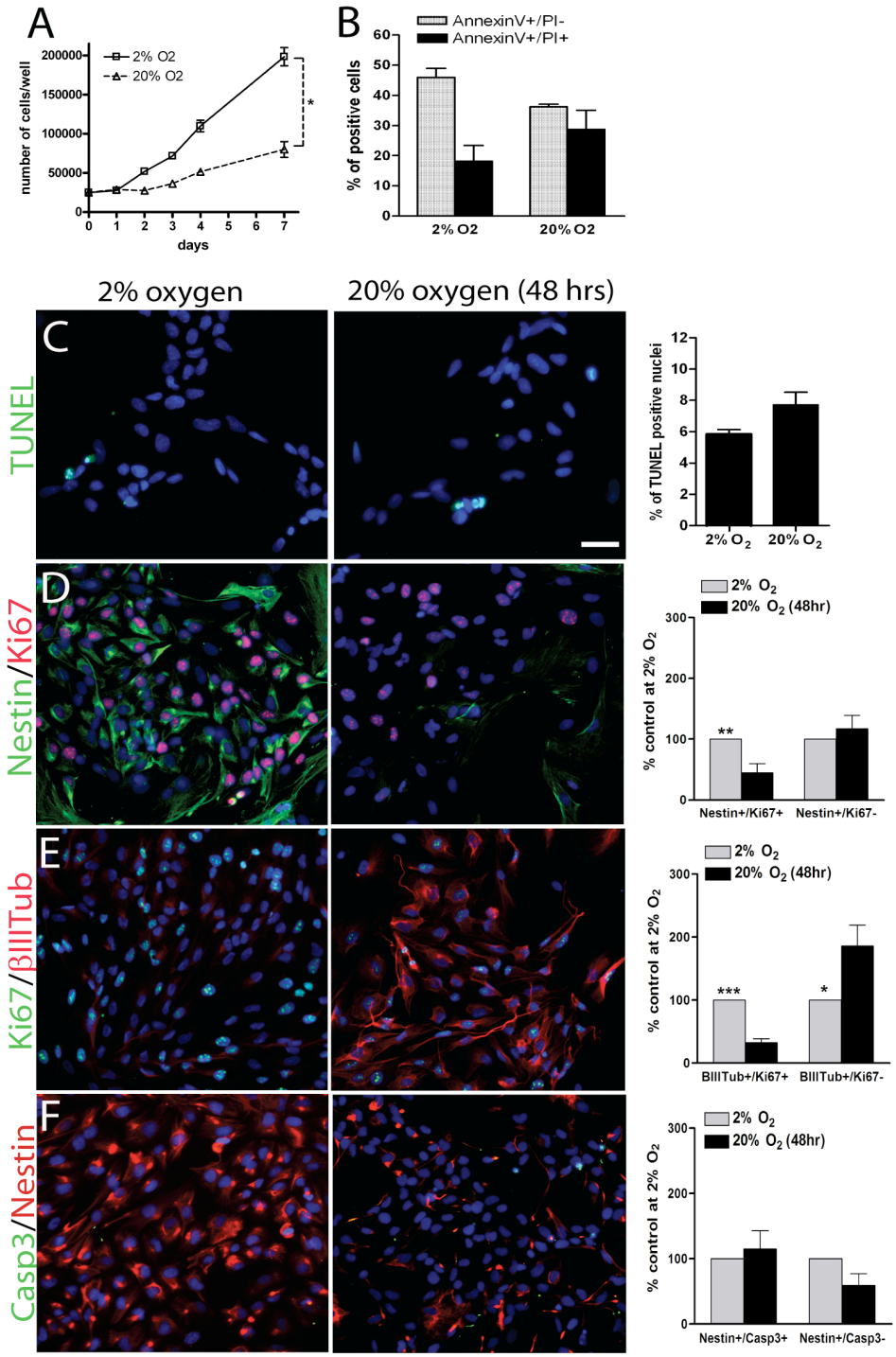

Figure 34. Acute exposure to high oxygen tension inhibits MDB cell growth by decreasing nestin$^+$/Ki67$^+$ and β-III-tubulin$^+$/Ki67$^+$ cells, and promotes low apoptosis levels. (A) Growth curve of FI25 MDB cells plated at a density of 7.2x10^3 cells/cm^2 and counted by trypan blue exclusion. (B) Percentages of AnnexinV$^+$/PI$^-$ and AnnexinV$^+$/PI$^+$ MDB derived cells expanded for 2 days at either 2% or 20% oxygen. Mean of 3 tumors ± S.E.M., n = 2 for each tumor. Representative immunocytochemical images (HuTu33) of (C) TUNEL (green) staining of apoptotic nuclei, (D) nestin (green)/Ki67 (red), (E) Ki67 (green)/ β-III-tubulin (red) and (F) cleaved Caspase3 (green)/nestin (red) staining of MDB cells plated as described in figure 2A. Corresponding percentages of (C) TUNEL$^+$ nuclei, (D) Nestin$^+$/Ki67$^+$, Nestin$^+$/Ki67$^-$, (E) β-III-tubulin$^+$/Ki67$^+$, β-III-tubulin$^+$/Ki67$^-$, (F) Nestin$^+$/Casp3$^+$, Nestin$^+$/Casp3$^-$, relative to total live DAPI$^+$ nuclei in the right panels. Values in D,E,F were normalized to control at 2% oxygen.

For all graphs, mean of 3 different MDB ± S.E.M., n = 3 for each tumor. 10X pictures, bar = 100 μm. *p < 0.05, **p < 0.01, ***p < 0.001.

To confirm the observed neuronal commitment of MBD derived cells following acute exposure to high oxygen tension, we analyzed the expression of a series of genes reported to be differentially modulated during neuronal differentiation of cerebellar neural progenitors (Calabrese et al., 2007). In particular, the stem cells related gene Sox2 disclosed a dramatic down-regulation after 48 hr of 20% oxygen exposure (Figure 35H). On the contrary genes involved in the regulation of the mid-hindbrain regions and the generation of the external granular layer (EGL) of the developing cerebellum (EN1 and Math1),in the formation of granule neuron precursors (Neurod1 and NSCL1), in the migration of more differentiated neuron precursors (β-III-tubulin) and their differentiation to post mitotic neurons (MAP2), were all up-regulated after 2 days at 20% oxygen (Figure 35H). Pax6, involved in several stages of migration of differentiating neurons, did not vary its expression (Figure 35H). All these data confirm the observed neuronal differentiation of MDB derived cells when exposed at high oxygen tensions and their progressive acquirement of a non cycling neuronal phenotype.

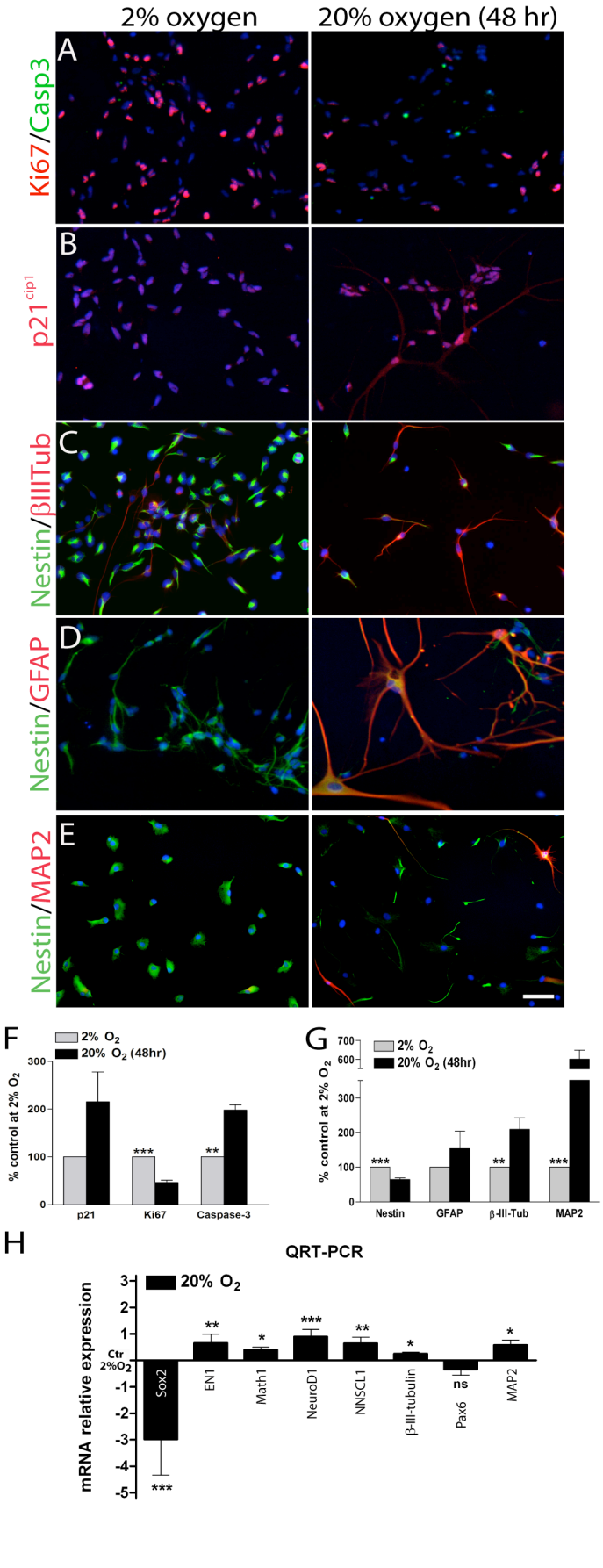
2% oxygen
20% oxygen (48 hr)
A
Ki67/Casp3
B
p21 cip1
C
Nestin/βIIITub
D
Nestin/GFAP
E
Nestin/MAP2
F
2% O2
20% O2 (48hr)
% control at 2% O2
300
200
100
0
***
**
p21
Ki67
Caspase-3
G
2% O2
20% O2 (48hr)
% control at 2% O2
700
600
300
200
100
0
***
**
***
Nestin
GFAP
β-III-Tub
MAP2
H
QRT-PCR
20% O2
mRNA relative expression
3
2
1
Ctr
2%O2
-1
-2
-3
-4
-5
***
**
*
***
**
*
ns
*
Sox2
EN1
Math1
NeuroD1
NNSCL1
β-III-tubulin
Pax6
MAP2

Figure 35. Acute exposure to high oxygen tension promotes neuronal differentiation, mitotic arrest and eventually cell death in MDB derived cells. (A) Representative immunocytochemical images (HuTu33) of (A) Ki67 (red)/cleaved-Caspase3 (green), (B) $p21^{cip1}$ (red), (C) nestin (green)/ β-III-tubulin (red), (D) nestin (green)/GFAP (red) and (E) nestin (green)/MAP2 (red) staining of MDB cells expanded for 2 days at either 2% or 20% oxygen. Quantifications in (F,G); for all graphs, mean of 5 different MDB ± S.E.M., n = 3 for each tumor. (H) QRT-PCR analyses of *SOX2*, *EN1*, *MATH1*, *NEUROD1*, *NSCL1*, β-*III-tubulin*, *PAX6* and *MAP2*, normalized to *GUSB* and then calibrated to 2% oxygen control. Mean ± S.E.M of 4 different MDB. *p < 0.05, **p < 0.01, ***p < 0.001, ns: not significant.

Recent studies have shown that brain tumor progenitors preferentially localize near vasculature but are also present in surrounding hypoxic tissues (Gilbertson and Rich, 2007). Vasculature is a source of signals for CNS stem cell self-renewal (Netto et al., 2008), but is also a delivery vehicle for oxygen, thereby presenting two potentially antagonistic signals for precursor proliferation (Liao et al., 2009). We performed immunohistochemical analyses of MDB tumor tissues to determine if neural precursor numbers co-varied with tumor areas of low or high microvascular density (MVD), measured by CD34 expression (Bruick and McKnight, 2001). Staining indicated that MDB areas with low MVD had high HIF-1α expression (Figure 36A,B and Table 2), were more enriched in $nestin^+$ cells and had few β-$III\text{-}tubulin^+$ cells (Figure 36C,D, left panels and Table 2), when compared to tumor areas with high MVD (Figure 36C,D, right panels and Table 2). $GFAP^+$ cells were barely detectable in the analyzed MDB samples (not shown).

To verify that HIF-1α molecule was not just accumulated but also that HIF-1α signaling was actually activated in MDB tissues, we analyzed the expression of a well known HIF-1α downstream target gene, carbonic anhydrase IX (CAIX) (Gaiano and Fishell, 2002) together with CD34. This confirmed that tumor areas with a low MVD had a higher proportion of $CAIX^+$ cells (Figure 36E and Table 2). These *in vivo* results are consistent with our *in vitro* findings that hypoxia preferentially promotes expansion and survival of MDB-derived precursor cells, while an acute exposure to a higher oxygen tension promotes neuronal differentiation. Consistent with our data, it has been reported that restricted oxygen conditions increase the cancer stem cell fraction and promote acquisition of a stem-like state (Gilbertson and Rich, 2007)

.

Tumor Area	CD34	HIF-1α	CAIX	Nestin	β-III-tubulin
Low MVD	0.71 ± 0.12	42 ± 7.61	82.5 ± 4.79	58.33 ± 1.27	4.29 ± 1.91
High MVD	13.5 ± 1.2	0.64 ± 0.28	26.17 ± 6.91	4.2 ± 1.59	63.33 ± 4.35

Values represents mean of 5 different MDB samples ± SEM. HIF-1α, CAIX, Nestin and β-III-tubulin values are expressed as percentages of total $DAPI^+$ cells. CD34 values are expressed as number of $CD34^+$ vessels/field. MVD, microvessel density.

Table 2. $HIF\text{-}1\alpha^+$, $CAIX^+$, $Nestin^+$ and $\beta III\ tubulin^+$ cells percentage in MDB areas with low and high MVD (referred to figure 36)

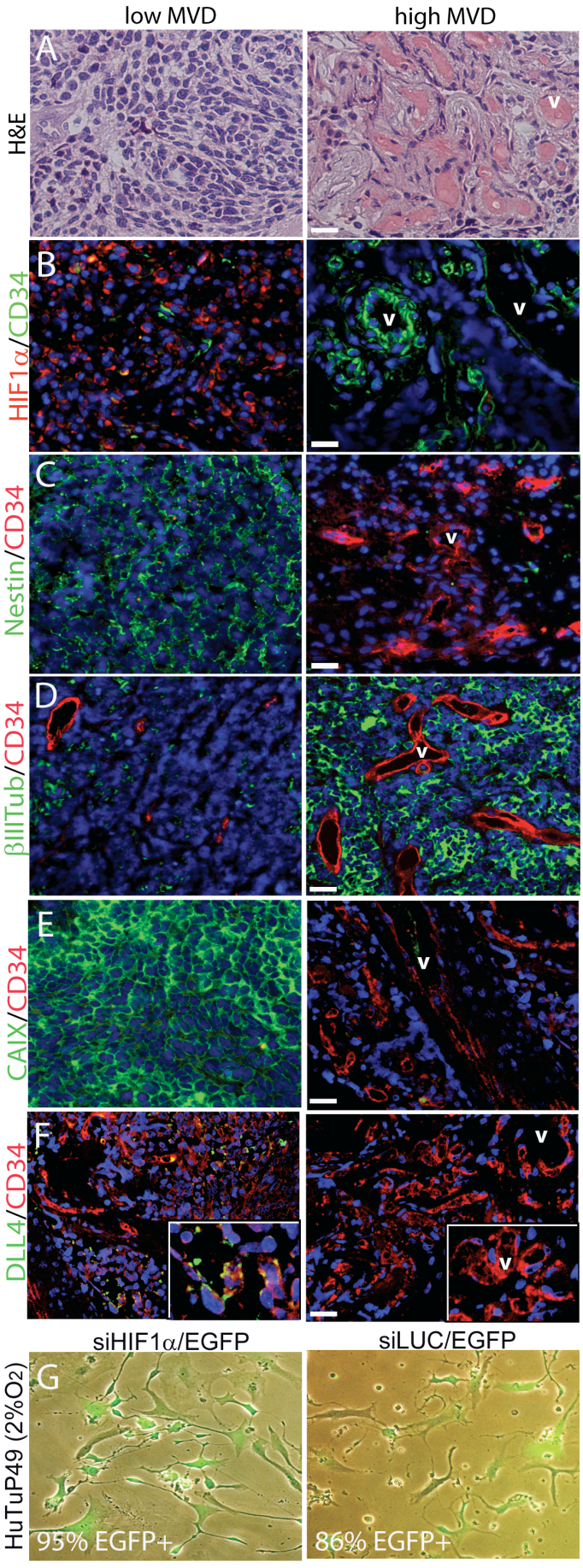
low MVD
high MVD
A
H&E
v
B
HIF1α/CD34
v
v
C
Nestin/CD34
v
D
βIIITub/CD34
v
E
CAIX/CD34
v
F
DLL4/CD34
v
v
siHIF1α/EGFP
siLUC/EGFP
G
HuTuP49 (2%O2)
95% EGFP+
86% EGFP+

Figure 36. HIF-1α, CAIX and Dll4 are more highly expressed in tumor areas with low MVD. (A) Haematoxylin and eosin (H&E) staining of MDB tissues; v, vessels are mainly visible in tumor areas characterized by high MVD (microvessel density). Representative immunohistochemical images of (B) HIF-1α (red)/CD34 (green), (C) nestin (green)/CD34 (red), (D) β-III-tubulin (green)/CD34 (red), (E) CAIX (green)/CD34 (red) and (F) CD34 (red)/Dll4 (green) staining MDB tissues (14213-2 and 14223-2). Tumor areas were analyzed based on low MVD (left panels) and high MVD (right panels). For quantification, see Suppl. Table 2 (G) Representative pictures of transduced MDB cells (HuTuP49) at 3 days post-transduction (dpt). Percentages of $EGFP^+$ cells were determined by flow cytometry. 10X pictures, bar = 100 μm, 60X insets (in F), bar = 20 μm, 20X pictures, bar = 40 μm.

Acute exposure to high oxygen tension inhibits Notch signaling in MDB derived cells.

We then sought to determine the molecular mechanisms by which increased oxygen tension promotes neuronal differentiation of MDB cells. HIF-1α is rapidly degraded by proteolysis in response to increasing oxygen tension, which explains its actions as a signal transducer of hypoxia (Bruick and McKnight, 2001); we also found that this rapid degradation occurred in MDB-derived precursors in response to acute 20% oxygen exposure (Figure 37A). Notch signaling supports the survival, proliferation and prevents differentiation of normal and tumor-derived neural stem cells (Fan et al., 2004; Gaiano and Fishell, 2002; Hallahan et al., 2004; Solecki et al., 2001; Weng et al., 2004). Signaling is initiated by the binding of Delta or Jagged ligands to Notch receptors, which leads to intramembranous proteolytic cleavage of the Notch receptor (from a 270 kDa to a 110 kDa protein) by the γ-secretase complex, yielding an activated Notch Intracellular Domain (NICD) that translocates to the nucleus to regulate target gene transcription. We found that Notch signaling was inhibited by acute exposure to 20% oxygen (Figure 37A), as shown by the decrease of NICD (110 kDa) after 30 min exposure to 20% oxygen. We also found that Delta-like-4 (Dll4), a Notch ligand, was transiently down-regulated within 30 min in 20% oxygen (Figure 37A). Analysis of Notch1-transcriptional activity using a luciferase reporter assay revealed a significant decrease in Notch1 activation when MDB cells were acutely exposed to 20% oxygen (Figure 37B). We then analyzed Dll4 expression in MDB tissue and found that Dll4 expression was high in tumor areas characterized by low MVD, but was not detectable in presence of high MVD (Figure 36F). This is consistent with a previous report showing that Dll4 expression is induced by vascular endothelial growth factor (VEGF)-A and hypoxia (Williams et al., 2006).

One Notch1 target gene is the basic-helix-loop-helix transcription factor Hes1, which is known to inhibit neurogenesis and maintain the neural stem cell identity (Kageyama et al., 2008). We found that acute exposure of MDB cells to 20% oxygen caused Hes1 down-regulation along with β-III-tubulin up-regulation (Figure 37A). This is consistent with a role for downstream Notch target genes in mediating the cell fate responses to changing oxygen tension.

HIF-1α is required to maintain Notch1 activation.

To investigate whether HIF-1α is required to maintain Notch1 in its active form, we silenced HIF-1α with a lentiviral vector bearing a siRNA specific for HIF-1α (Arsham et al., 2002; Favaro et al., 2008; Indraccolo et al., 2002; Razorenova et al., 2005) (Figure 36G). Experiments were performed in 2% oxygen to model conditions in which HIF-1α is normally active. Silencing of HIF-1α caused MDB-derived precursors to show morphological differentiation and eventually die by 5-7 days post-transduction (nearly 85% cell death, not shown). In contrast, sham silencing with luciferase siRNA did not induce cell death, thus excluding a non-specific effect of viral infection (not shown). This indicates that HIF-1α stability may be required to preserve MDB cell viability. During the early stages of morphological differentiation, we found that components of the Notch1 pathway were down-regulated after HIF-1α silencing; these included total and activated (NICD) Notch, Hes1 and Dll4; sham silencing with luciferase siRNA had little effect on Notch or NICD, but did cause some non-specific down-regulation of Dll4 and Hes1 relative to the unchanged β-actin loading control. In contrast, β-III-tubulin expression increased after silencing HIF-1α, consistent with increased neuronal differentiation (Figure 37C). These results provide evidence that HIF-1α is required to maintain the activation of Notch1 signaling in MDB-derived precursor cells.

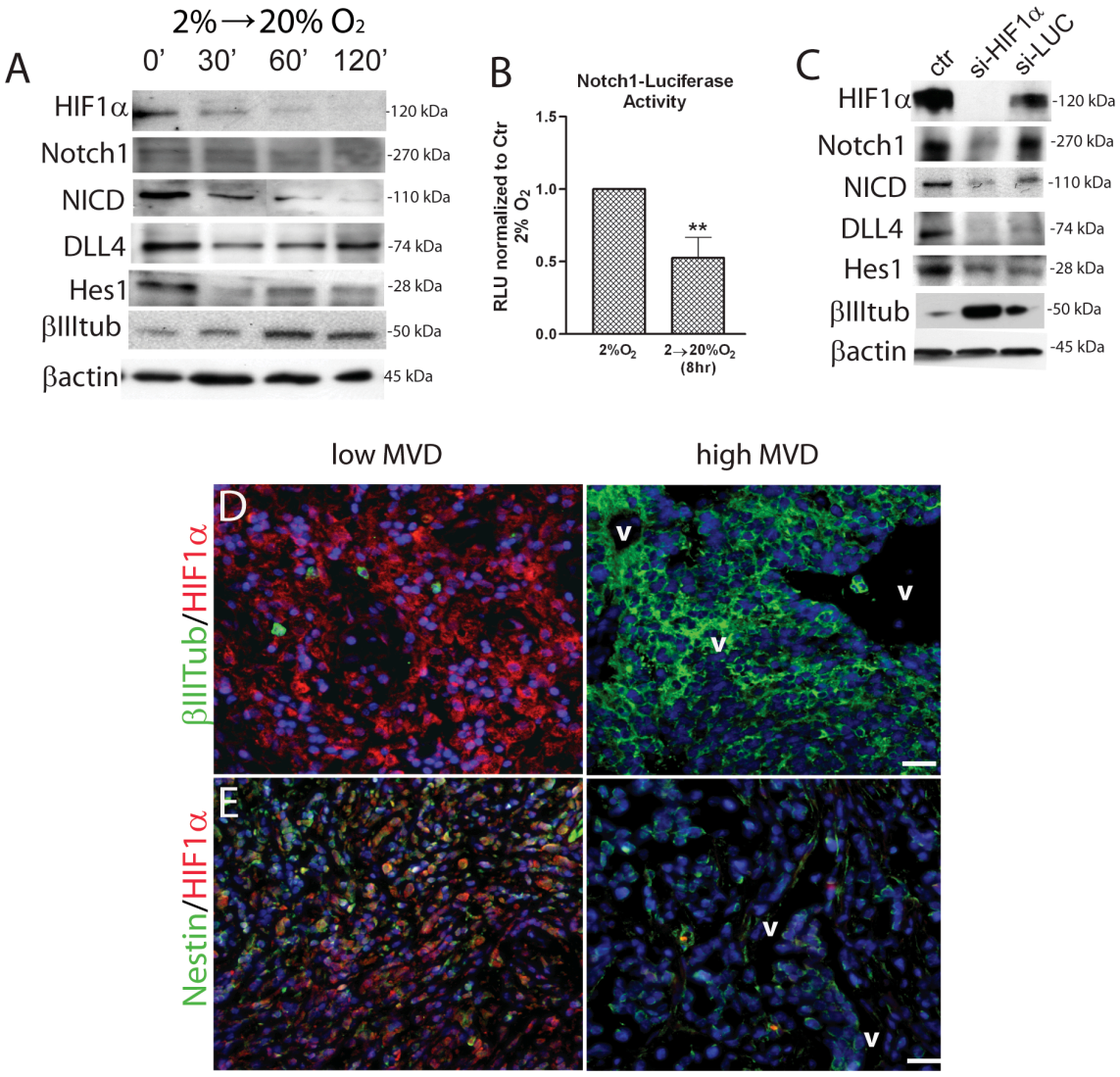

Figure 37. Acute exposure to high oxygen tension promotes Notch1 pathway inhibition and HIF-1α is required to maintain Notch1 signaling activated. (A) Representative western blot analyses of HIF-1α, Notch1, NICD, Dll4, Hes1, β-III-tubulin and β-actin of MDB cells acutely exposed to 20% oxygen for 30, 60 or 120 minutes. (B) Notch1-Luciferase transfected MDB cells, have been either left at 2% oxygen or acutely exposed to 20% oxygen for 8 hrs. The graph reports mean of 3 different MDB. (C) Representative western blot analyses of cells that had been transduced with a siHIF-1α/EGFP or si-LUC/EGFP bearing vectors. (D,E) Representative immunohistochemical images of (D) HIF-1α (red)/β-III-tubulin (green), (E) HIF-1α (red)/nestin (green) staining of MDB tissues. See quantification in Suppl. Table 2. Magnification 10X, bar = 100 μm. *$p < 0.05$, **$p < 0.01$, ***$p < 0.001$. RLU, relative light units; v, vessels; MVD, microvessel density.

HIF-1α and Notch1 are co-expressed in MDB precursor cells.

Immunohistochemical analysis of MDB tissues indicated that the majority of HIF-1α$^+$ cells co-expressed Notch1 and Hes1 (merged images in Figure 38A,B and Table 3).

Moreover, the HIF-1α downstream target gene CAIX, was found to be expressed in the majority of both HIF-1α$^+$ and Notch1$^+$ MDB cells (Figure 39A,B). In accordance to our data, a previous report described that direct interaction between NICD and HIF-1α occurs in several cell types, such as cortical embryonic stem cells, satellite cells, C2C12 and mouse embryonic teratocarcinoma cell line P19, and HIF-1α is recruited to Notch-responsive promoters upon Notch activation under hypoxic conditions (Gustafsson et al., 2005). Hes1 localization was primarily nuclear and co-localized in the same cells as HIF-1α (Figure 38B). The majority of nestin$^+$ precursor cells resulted to express Notch1 (Figure 38C), and both CD133$^+$ cells, representative of tumor stem cell fraction, and nestin$^+$ cells expressed HIF-1α (Figure 38D,E) (quantification in Table 3).

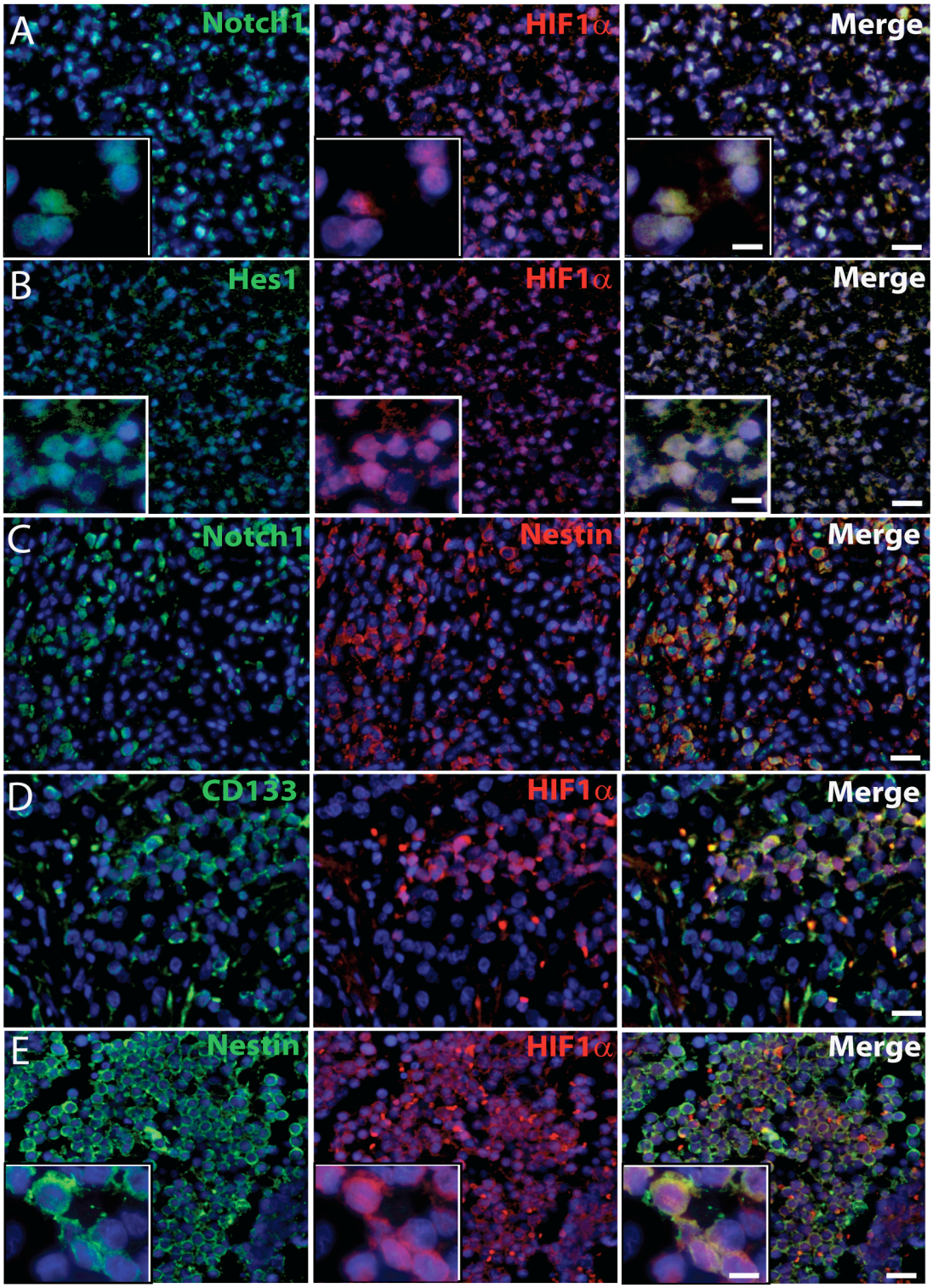

Figure 38. Notch1, Hes1 and HIF-1α are co-expressed in nestin$^+$ and CD133$^+$ MDB cells *in vivo*. Representative immunohistochemical images of (A) HIF-1α (red)/Notch1 (green), (B) HIF-1α (red)/Hes1 (green), (C) nestin (red)/Notch1 (green), (D) HIF-1α (red)/CD133 (green) and (E) HIF-1α (red)/nestin (green) staining of MDB tissues. Insets in panel A, B show nuclear localization of Notch1 (left, A), HIF-1α (middle, A, B and E), and Hes1 (left, B) and cytoplasmic localization of nestin (left, E). 10X pictures, bar = 100 μm (for A,B,C,D,E), 60X insets, bar = 20 μm (in A,B merge). See quantification in Table 2.

HIF-1α status	Nestin	β-III-tubulin	CD133	Notch1	Hes-1
HIF-1α$^+$	57.92 ± 6.35	2.33 ± 1.2	46.88 ± 5.97	78.57 ± 7.05	84.7 ± 7.06
HIF-1α$^-$	4.2 ± 1.59	63.33 ± 4.35	5.57 ± 1.02	8.86 ± 4	8.71 ± 3.71
Values represents mean of 5 different MDB samples ± SEM. Data are expressed as percentages of total DAPI$^+$ cells.					

Table 3. Phenotypic identity of HIF-1α$^+$ and HIF-1α$^-$ MDB cells (referred to figure 38)

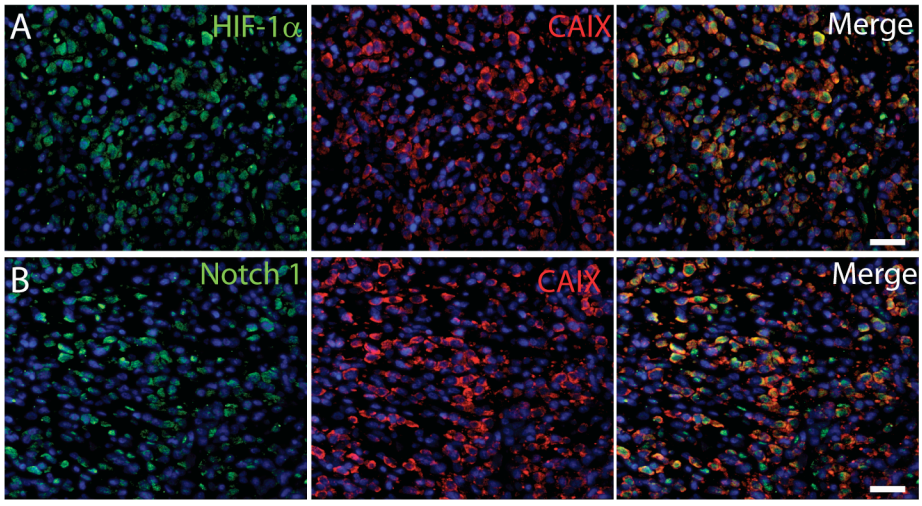

Figure 39. HIF-1α and Notch1 are expressed by CAIX$^+$ MDB cells. Representative immunohistochemical images of (A) HIF-1α (green)/CAIX (red) and (B) Notch1 (green)/CAIX (red) staining MDB tissues. 10X pictures, bar = 100 μm (in merge).

Modulation of Notch1 signaling affects HIF-1α protein stability and transcriptional activity.

Next, we sought to investigate whether exogenous modulation of Notch pathway in MDB derived cells was differentially regulated in 2% oxygen compared to 20% oxygen. We treated cells for 72 hr with immobilized Dll4 (R&D, 2μg/ml) or with DAPT

(Calbiochem, 10μM), a γ-secretase inhibitor that prevents Notch cleavage and activation (Ikeuchi and Sisodia, 2002; Martys-Zage et al., 2000; Schroeter et al., 2003). Analyses of total protein confirmed that Notch1 pathway was more strongly activated in 2% oxygen, as shown by an increase of 110 kDa NICD; addition of Dll4 increased this activation as well as Hes1 expression in both oxygen tensions (Figure 40A). Conversely, β-III-tubulin was slightly down-regulated by Dll4 in 2% oxygen, while Dll4 protein level did not significantly change among conditions (Figure 40A). In contrast, DAPT treated cells underwent inhibition of Notch1 signaling, especially when acutely exposed to 20% oxygen (Figure 40A). In order to verify if DAPT treatment promoted either increased MDB cell differentiation or apoptosis, we tested cleaved caspase3, PARP and $p21^{cip1}$ expression; we found increase of $p21^{cip1}$ protein level in DAPT treated cells in 2% oxygen, while levels of cleaved caspase3 (not shown) and cleaved PARP did not significantly change (Figure 40A).

We then analyzed whether HIF-1α protein stability was altered by Notch1 activation or inhibition. Surprisingly, we found that HIF-1α protein did not change following Dll4 stimulation, but was reduced in DAPT treated cells (Figure 40A) maintained under hypoxia. Moreover, we found that the level of PHD2, a proline hydroxylase that is a direct sensor of oxygen tension and is responsible for initiating HIF-1α protein degradation, was higher following DAPT treatment in 2% oxygen (Figure 40A). We previously showed the involvement of the peptidyl prolyl cis/trans isomerase FKBP38 in controlling PHD2 degradation. Indeed, it has been shown that PHD2 protein abundance depends on the membrane-associated localization of FKBP38 (Barth et al., 2007). Thus, we wanted to determine if a similar PHD2 modulation of HIF-1α protein levels occurred in MDB cells following DAPT or Dll4 stimulus. We found that Dll4 stimulation in both oxygen tensions promoted up-regulation of FKBP38 (Figure 40A). In contrast, DAPT promoted a strong reduction of FKBP38 (Figure 40A). Even though this is not a direct measure of higher PHD2 activation, it indicates that increased PHD2 protein stability is a consequence of Notch inhibition and that this could be mediated by FKBP38.

In order to measure the interaction between HIF-1α and its cognate consensus sequence (HRE), we used a hypoxia responsive element (HRE)-luciferase reporter assay. We found that 8 hr of Dll4 treatment induced a significant increase of HIF-1α dependent

transcriptional activity in 2% oxygen, in contrast to the effects mediated by DAPT (Figure 40B). Also, a Notch1-luciferase reporting assay confirmed Dll4-dependent activation in both 2% and 20% oxygen, while DAPT decreased Notch1 signaling more effectively in 2% oxygen Figure 40C). This is probably due to the fact that endogenous Notch1 signaling was already inhibited in MDB cells acutely exposed to 20% oxygen (Figure 37B and Figure 40C). Together these results suggest that Notch1 signaling is preferentially activated in MDB-derived cells in hypoxic conditions, and also that Dll4 and DAPT control HIF-1α mediated transcriptional activity. They also indicate that inhibition of Notch1 signaling by DAPT causes HIF-1α down-regulation, probably by PHD2 up-regulation.

Furthermore, QRT-PCR analyses revealed that *HES1* transcript was up-regulated by Dll4 only in cells maintained in 2% oxygen (figure 40D), while *HEY1*, another Notch1 downstream target gene involved in the progression of glioblastoma (Hulleman et al., 2009), was more highly expressed after Dll4 treatment, regardless of oxygen tension (not shown). Conversely, *HES1* expression was decreased by DAPT, confirming the effectiveness of DAPT in inhibiting Notch1 pathway activation in 2% and 20% oxygen. Analysis of *DLL4, HIF-1α* and *PHD2* gene expression did not show significant differences among conditions (not shown), suggesting that the observed modulations in protein expression levels do not necessarily reflect transcriptional changes.

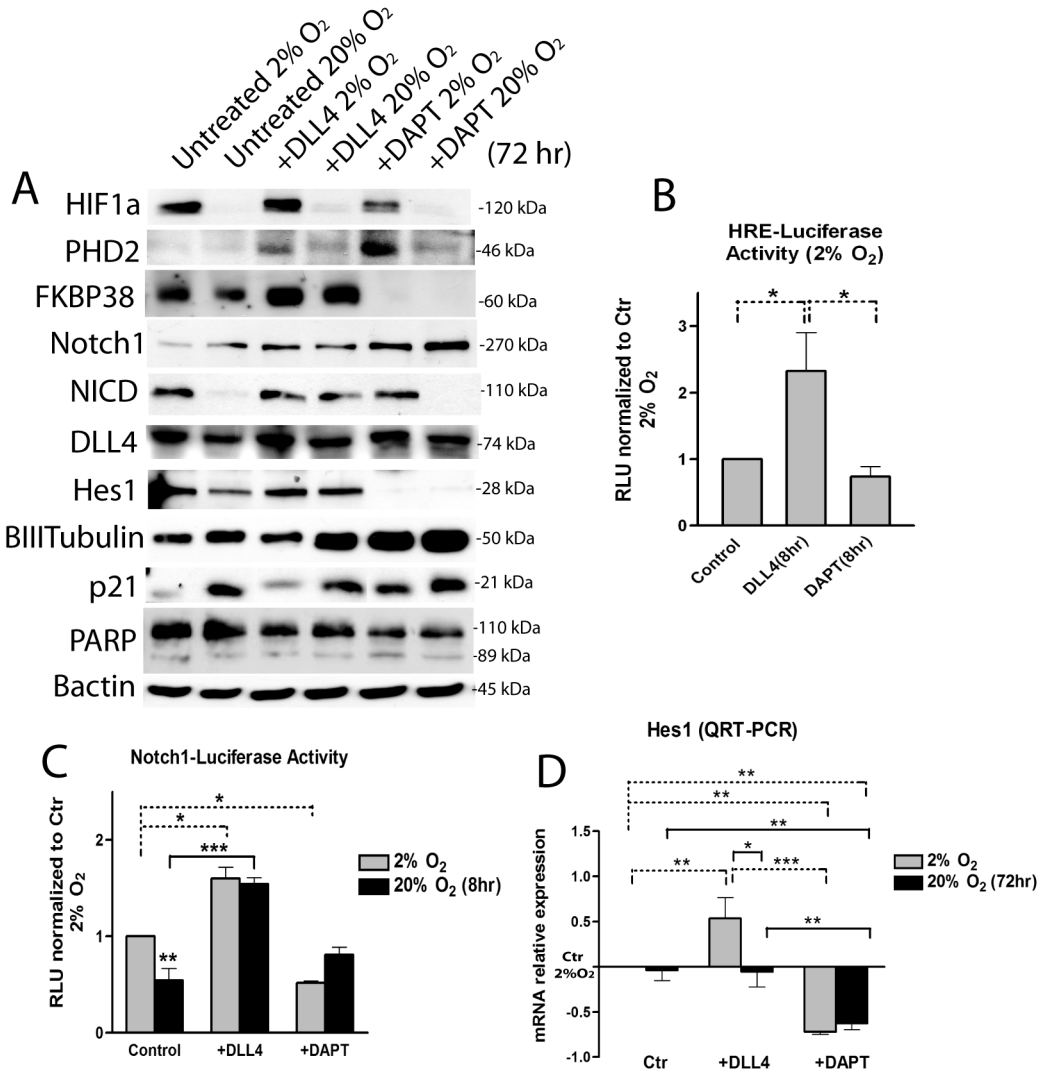

Figure 40. Effects of Notch1 signaling exogenous modulation by Dll4 and DAPT on MDB cells. (A) Representative western blot analyses of HIF-1α, PHD2, FKBP38, Notch1, NICD, Dll4, Hes1, β-III-tubulin, $p21^{cip1}$, PARP and β-actin of MDB derived cells cultured for 72 hrs in presence of either immobilized Dll4 (2 μg/ml) or DAPT (10 μM) at either 2% or 20% oxygen. (B) HRE-luciferase transfected cells in the same conditions as in (A) at 2% oxygen. (C) Notch1-luciferase transfected MDB cells treated with Dll4 and DAPT for 8 hr as described in Materials and Methods. For both B and C, values are expressed in RLU (= relative light units). (D) QRT-PCR analysis of *HES1* normalized to *GUSB* and then calibrated to 2% oxygen control. Mean ± S.E.M of 3 different MDB. *p < 0.05, **p < 0.01, ***p < 0.001.

Notch1 signaling modulation affects MDB cell phenotype depending on hypoxia.

We and others previously provided evidence that hypoxia either instructs or selects for a more primitive phenotype of tumor cell and that HIF-1α is an important factor in promoting this cell state (Gustafsson et al., 2005; Helczynska et al., 2003; Jogi et al.,

2002; Pistollato et al., 2009a). We tested whether the interaction between Notch signaling and HIF-1α regulated the relative abundance of MDB-derived precursor cells compared with more differentiated cell types. We tested this by activating Notch1 signaling with Dll4 and found an increase in $CD133^+$, marking stem cells, and $nestin^+$ cells (i.e. $nestin^+/\beta\text{-III-tubulin}^-$) in 2% oxygen but not 20% oxygen within 72 hr of treatment (Figure 41A,B,F). Interestingly, this treatment led to a decrease in $\beta\text{-III-tubulin}^+$ cells (i.e. $nestin^-/\beta\text{-III-tubulin}^+$) in 20% oxygen but not 2% oxygen (Figure 41B,F). Another cell surface marker, CD15, is used analogously to CD133 as a stem cell marker for normal and MDB-derived cells in mouse models (Panchision et al., 2007; Read et al., 2009; Ward et al., 2009), but we did not see any change in the percentage of $CD15^+$ cells following Dll4 or DAPT treatments (not shown). Interestingly, Dll4 treatment led to a decrease in mitotically active cells (measured by Ki67 expression) in both oxygen tensions relative to their control counterparts (Figure 41D), suggesting that Notch signalling promotes quiescence that is characteristic of slowly dividing stem cells (Alvarez-Buylla and Lois, 1995; Liu et al., 2010). This effect was much stronger during acute exposure to 20% oxygen, where Dll4 treatment led to a substantial reduction in both Ki67 expression and total cell number (Figure 41D,E,F). This is consistent with the anti-proliferative effect of Dll4 previously described for other cell types (Chadwick et al., 2008; Chadwick et al., 2007).

We found that inhibition of Notch signalling with DAPT, despite also having an indirect inhibitory effect on HIF-1α (Figure 40A,B), did not reduce $CD133^+$ cell numbers within 72 hr (Figure 41A); however, it did reduce numbers of $nestin^+$ cells and increase numbers of $\beta\text{-III-tubulin}^+$ cells under both 2% and 20% oxygen tensions (Figure 41B,C,F). Mitotically active cell numbers, as measured by Ki67 staining, were also reduced by DAPT (Figure 41D), while total cell numbers were slightly but not significantly reduced following DAPT stimulus compared to control group at 2% oxygen (Figure 41E). The observed decrease of total cells number is not related to increased cell death by DAPT, as shown by analysis of cleaved PARP (Figure 40A), but rather to increased cell differentiation, as shown by higher $p21^{cip1}$ expression (Figure 40A). MDB cells treated with DAPT and acutely exposed to high oxygen tension did not undergo further decrease of Ki67 expression and of total cells number compared to 20% oxygen control group (Figure 41D,E). In total, our results suggest that Notch1

activation, by promoting the un-differentiated cellular state, makes MDB precursor cells more sensitive to the effects of changing oxygen tensions.

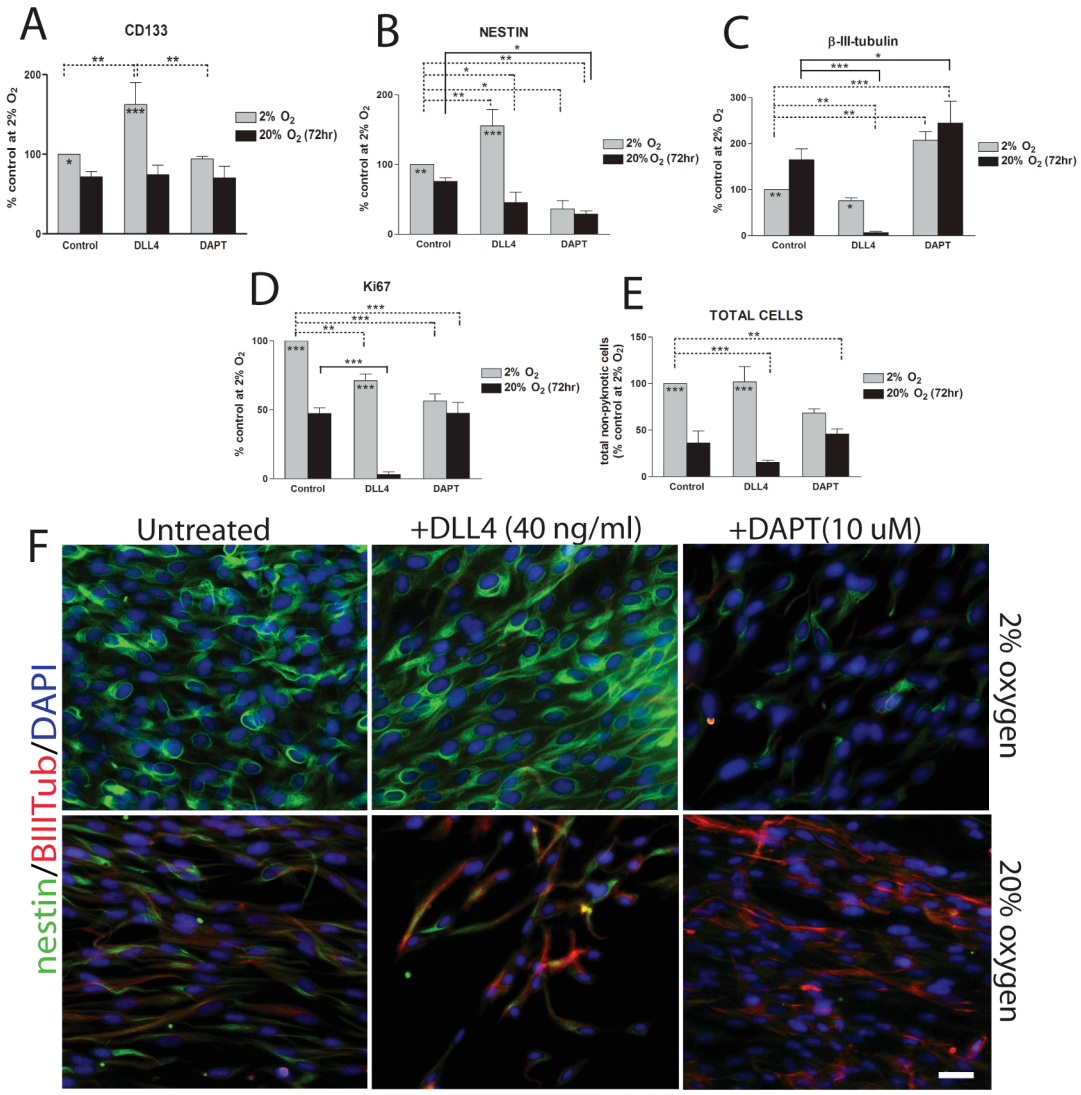

Figure 41. Notch1 signaling modulation by Dll4 and DAPT affects MDB cell phenotype depending on hypoxia. (A) Percentages of $CD133^+$ cells of MDB derived cells cultured for 72 hr in presence of either immobilized Dll4 (2 μg/ml) or DAPT (10 μM) at either 2% or 20% oxygen. Mean of 3 tumors ± S.E.M., n = 2 for each tumor. (B-E) Immunocytochemical analysis for nestin (B) β-III-tubulin (C), Ki67 (D) and total cell quantification relative to total $DAPI^+$ cells (E). MDB cells were treated as described in (A). Mean of 6 tumors ± S.E.M. (F) Representative immunocytochemical images of nestin (green)/ β-III-tubulin (red) staining. 20X pictures, bar = 40 μm. *$p < 0.05$, **$p < 0.01$, ***$p < 0.001$.

DISCUSSION PART II

There is increasing evidence that MDB, like many other cancer types, originates from and is maintained by aberrantly functioning stem cells in the cerebellum that fail to maintain proper control of self-renewal (Fan and Eberhart, 2008). Since an important feature of stem cells is their quiescence relative to their more active daughter progenitors (Alvarez-Buylla and Lois, 1995) the failure to adequately target slowly dividing "cancer stem cells" during clinical treatment may be responsible for cases of tumor recurrence. Notch signalling has been implicated in regulating MDB-derived precursors with stem cell properties (Fan et al., 2006; Fan et al., 2004; Hallahan et al., 2004; Raffel et al., 1997)and is found to promote the survival and proliferation and inhibit differentiation of tumor-derived precursors (Reya et al., 2001; Solecki et al., 2001). Our results show that Notch signalling requires hypoxia to maintain MDB-derived precursors in an undifferentiated state and suggest that Notch signalling in turn sensitizes these precursors to changes in oxygen tension. Furthermore, we show that these responses are mediated by a reciprocal interaction between components of the Notch signalling pathway and HIF-1α, a canonical effector of oxygen response signalling.

While measurements of oxygen in non-neoplastic human brain show a mean oxygen tension varying from 3.2% (23.8 ± 8.1 mmHg) at 22-27 mm below the dura to 4.4% (33.3 ± 13.3 mm Hg) at 7-12 mm below the dura (Dings et al., 1998), levels below these are a consistent feature of brain tumors (Ljungkvist et al., 2007). Several reports showed a decrease in oxygen tension in human brain tumors, including reductions of flow and oxygen utilization (Ito et al., 1982; McKenzie et al., 1978). Even though direct measurements of oxygen tension specifically in MDB tissues have not been directly performed, it is reasonable to hypothesize that MDB cells reside within a hypoxic niche. According to this hypothesis, it has been reported that intracerebral tumors and MDB are characterized by a higher percentage of hypoxic cells, compared to other neoplasms and for this reason higher doses of radiation therapy are required to get equivalent cell killing (Leith et al., 1994). Moreover, both hypoxic conditions and HIF-1α over-activation correlate with tumor aggressiveness (Azuma et al., 2003; Helczynska et al.,

2003; Jogi et al., 2002; Pistollato et al., 2009a; Smith et al., 2005). Our previous results showed that HIF-1α is an important mediator of this response, in part through its modulation of key intracellular pathways that regulate precursor cell proliferation and fate, such as BMP and Akt/mTOR signalling in glioblastoma (Pistollato et al., 2009a; Pistollato et al., 2009b). Here we show that, in MDB, hypoxia and HIF-1α also regulate Notch signalling. This interaction was previously identified in fetal mouse neural precursors (Gustafsson et al., 2005), but our work provides the first characterization of this interaction and its novel reciprocal features in MDB-derived precursors.

We show that MDB derived cells, which can be expanded successfully *in vitro* only when cultured under hypoxic condition, undergo differentiation and eventually cell death when acutely exposed to high oxygen tension. This occurs in part through Notch1 signaling inhibition. We found that Notch signaling is activated by HIF-1α, the main hypoxia intracellular sensor, while it is down-regulated following acute exposure to high oxygen or HIF-1α silencing. Our *in situ* histological analysis shows that Notch1 signaling is higher within tumor areas with low MVD, where MDB cell precursors are more abundant. Recent studies have shown that within brain tumors, cancer stem cells preferentially reside near both vasculature and in surrounding necrotic and/or less vascularized (i.e. hypoxic) tissues (Calabrese et al., 2007; Gilbertson and Rich, 2007). Consistent with our data, it has been reported that restricted oxygen conditions increase the cancer stem cell fraction and promote acquisition of a stem-like cell features (Heddleston et al., 2009). While the preferential association of cancer stem cells with both vascularized and non-vascularized regions may seem paradoxical, we have hypothesized that vascular regions may actually promote both stem cell properties and quiescence because of the combination of vascular niche factors and higher oxygenation, while specifically restricting oxygen may activate stem cells to re-enter the cell cycle and undergo self-renewal and/or transit-amplifying divisions (Panchision, 2009). In our culture conditions of low oxygen tension (2% O_2) $CD133^+$ cells derived from MDB tissues disclosed clonogenic potential in respect to $CD133^-$ MDB cells (Figure 42). $CD133^+$ cells have been isolated from different types of brain tumors including MDB and were shown to form aggressive tumors in the brain of mice when injected at low numbers (Hemmati et al., 2003; Singh et al., 2004). The utility of CD133 in the isolation of cells with tumor initiating properties has been confirmed by several

research groups (Bao et al., 2006; Piccirillo et al., 2006), but it is unclear whether this marker really identifies tumor initiating cells or a subset of cells that can resist the immune system in partially immunodeficient mice strains. Recent works reported that the $CD133^-$ population from GBM tumors is able to produce orthotopic tumors even if with a lower efficiency (Beier et al., 2007; Sakariassen et al., 2006) However, at this time no cell marker is considered absolute in identifying brain tumor stem cells (Hadjipanayis and Van Meir, 2009). Thus, since we did not evaluate the *in vivo* tumorigenicity of MDB derived $CD133^+$ cells maintained in hypoxic culture conditions, our hypotheses on the diverging role of the vascular and hypoxic stem cell niche remain speculative.

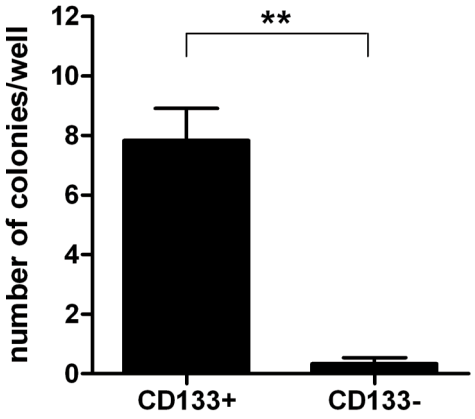

Figure 42. Clonogenic assay of $CD133^+$ MDB derived cells. $CD133^+$ and $CD133^-$ MDB cells (HuTu33 and FI25) were sorted by FACS and resuspended in the appropriate culture medium as described in Supplemental Materials and Methods. Graph indicates the number of colonies/well MTT stained MDB cells after 15 days of culture. Mean of 3 independent experiments ± S.E.M. **$p < 0.01$.

We found that HIF-1α and Notch signaling occur in a high proportion of $nestin^+$ MDB precursors, while inhibition of Notch signaling by DAPT promotes neuronal differentiation. The increase in $CD133^+$ cell numbers by Notch activation in 2% oxygen suggests that hypoxia is required for MDB stem cell maintenance. Another potential link between HIF-1α and Notch signaling is found in recent work showing that Factor Inhibiting HIF-1 (FIH-1) regulates asparagine hydroxylation of both HIF-α and Notch1-3 (Wilkins et al., 2009). Additionally, in mouse embryonic stem cells the hypoxia-induced increase of HIF-1α promotes Notch-1 activation via Wnt-1 signaling (Lee et al., 2009). Thus, there appear to be several levels of shared molecular regulatory

mechanisms between Notch and HIF1α. *Hes1*, a Notch1 target gene, is one of the gene mammalian homologues of Drosophila *Hairy* and *Enhancer of split*, which encode basic helix-loop-helix (bHLH) transcriptional repressors. In the developing central nervous system, *hes* genes are highly expressed in neural stem cells and their inactivation leads to accelerated neurogenesis and premature depletion of neural stem cells (Kageyama et al., 2008). We found that Dll4 treatment increased Hes1 protein levels in both 2% and 20% oxygen, while *hes1* transcript was upregulated by Dll4 only under hypoxia, which is consistent with HIF-1α-dependent Notch1 activation and consequentially maintenance of MDB stem cells. Additionally, DAPT treated cells undergo a decrease of HIF-1α level, phenomenon correlated to PHD2 stabilization. As a consequence, DAPT treated cells undergo neuronal differentiation, as shown by higher proportion of β-III-tubulin$^+$ cells.

Conclusion: Our results suggest that two components of the tumor microenvironment, cell-to-cell signaling through Notch and oxygen sensing through HIF-1α, regulate precursor proliferation and fate and may exert specific control on stem cell quiescence. While definitive evidence of this requires prospective isolation of these cells and testing of tumor reconstitution *in vivo*, our results provide mechanistic insight into how stem cell niche signals may be utilized by cancer stem cells to promote tumor aggression. This in turn can potentially be exploited to selectively target the cells that initiate and maintain MDB, thereby increasing the success rate of treatment.

The results of these study have been published on: Stem Cells. 2010 Nov;28(11):1918-29. doi: 10.1002/stem.518. Interaction of hypoxia-inducible factor-1α and Notch signaling regulates medulloblastoma precursor proliferation and fate. Pistollato F, Rampazzo E, Persano L, Abbadi S, Frasson C, Denaro L, D'Avella D, Panchision DM, Della Puppa A, Scienza R, Basso G.

MATERIALS AND METHODS

Isolation and gas-controlled expansion of cells.

Written informed consent for the donation of adult tumour brain tissues was obtained from patients, under the auspices of the protocol for the acquisition of human brain tissues obtained from the Ethical Committee board of the University of Padova and Padova Academic Hospital. All tissues were acquired following the tenets of the Declaration of Helsinki. Patients from which we derived GBM primary cultures are listed in Supplementary Table 2. Written informed consent for the donation of pediatric tumor brain tissues was obtained from parents, prior to tissue acquisition, under the auspices of the protocol for the acquisition of human brain tissues obtained from the Ethical Committee board of the University of Padova and Padova Academic Hospital. All tissues were acquired following the tenets of the Declaration of Helsinki. MDB precursors were derived from 13 tumors taken at surgery (Supplementary Table 3); initial pathological review was followed by secondary neuropathological review to reconfirm diagnosis. GBM and MDB precursors were derived and maintained as previously described (Pistollato et al., 2010a). Briefly, we enzymatically dissociated tumour biopsies and cultured derived cells in HAM's-F12/DME (Irvine Scientific, Santa Ana, CA) with additional BIT9500 (10% serum substitute; Stem Cell Technologies, Vancouver, Canada), in an atmosphere of 2% oxygen, 5% carbon dioxide, and balanced nitrogen.

Where indicated, GBM-derived cells were supplemented with soluble BMP2 (50 or 10ng/ml) for short time course or 72h or Wnt3a (30ng/ml, Millipore, Billerica, MA) for 4, 24, 48 or 96h or transfected by using a protocol for transient transfection of adherent cells using Effectene Reagent (Qiagen, Hilden, Germany). GBM cell were transfected with a plasmid bearing a constitutively active form of β-catenin (CA-β-catenin)(Borello et al., 2006). To evaluate Notch pathway over-activation cells were transfected with a pcDNA3.1 plasmid constitutively expressing Notch Intracellular Domain (NICD)(Weng et al., 2004). In some experiments, MDB-derived cells were supplemented with the immobilized Notch ligand Delta-Like 4 (Dll4, 2μg/ml R&D Systems, Minneapolis,

MN) or gamma secretase inhibitor X or IX (DAPT, 10μM, Calbiochem, Nottingham, UK) for 72 hr; both secretase inhibitors elicited analogous Notch1 inhibition. Normal subventricular zone (SVZ)-derived cells were cultured using the same protocol as that used for their previous extensive characterization

Immunocytochemistry

Cells were fixed in cold 4% paraformaldehyde for 15 min, rinsed and stored at +4°C prior to analysis. Primary antibody, listed in supplementary table 7, staining was performed. Cells were washed and incubated with species-specific secondary antibodies conjugated to Alexa dyes (Invitrogen, Carlsbad, CA). Cells were counterstained with DAPI to measure total cell number. Staining was visualized by epifluorescence (Vico, Nikon, Melville, NY) or confocal epifluorescence microscopy (Ti-E-A1, Nikon, Melville, NY) and images processed for figures using Adobe Illustrator (Adobe Inc., San Jose, CA).

Luciferase reporter assays on GBM or MDB cells

GBM or MDB cells were transfected using a protocol for transient transfection of adherent cells using Effectene Reagent (Qiagen, Hilden, Germany). BAT-luciferase reporter construct (BAT-lux) was kindly provided by Prof. Piccolo. It consists of seven TCF/LEF-binding sites upstream of a 0.13-kb fragment containing the minimal promoter–TATA box of the gene *siamois* (Maretto et al., 2003) driving the expression of Firefly luciferase reporter gene. The Hif-1α luciferase reporter assay was performed by using a HRE-luciferase reporter construct (wHRE) consisting of a trimerized 24-mer containing 18bp of sequence from the PGK promoter including the HE (5'-tgtcacgtcctgcacgactctagt, HE) and an 8bp linker sequence followed by a 50 bp minimal tyrosine kinase promoter in a pGL2-firefly luciferase basic Vector backbone (Promega, Madison, WI). The Notch luciferase reporter assay was performed by using a reporter plasmid (6x-RBP-Jk-luc, kindly provided by Prof. Piccolo, University of Padova) containing six copies of the CBF1 binding consensus sequence (5'-tgggaa, Notch consensus sequence) from the Hes1 promoter used to evaluate Notch mediated

transcription. Transfection with a Renilla luciferase vector was used in order to normalize luciferase detection (Promega, Madison, WI).

Twenty-four hours after transfection, a total medium change was done and cells were treated with 30ng/ml of soluble Wnt3a or 50ng/ml BMP2 and maintained at 2% O_2 or acutely expose to 20% O_2. Where indicated GBM derived cells were co-transfected with CA-β-Catenin plasmid or pcDNA3.1:NICD. Cells were processed for analysis of BAT-lux, HRE- and Notch-luciferase activity as described (Dual-Luciferase Reporter Assay System, Promega, Madison, WI) using a plate-reading luminometer (Victor, Perkin Elmer, Waltham, MA). Values reported in the graphs are expressed in "RLU" (= relative light units) and were normalized to control group at 2% oxygen.

CD133 flow cytometric analyses and cell sorting

Cells ($2x10^5$cells/ml) were incubated with anti-human CD133 (clone AC133/2-PE, MiltenyiBiotec, BergischGladbach, Germany) as previously described (Pistollato et al., 2010a; Pistollato et al., 2009b). Viability was assessed by adding 7-amino-actinomycin-D (7-AAD, 50ng/ml, BD Biosciences, Franklin Lakes, NJ) prior to analysis. Cells were analyzed on a Cytomics FC500 flow cytometer (Beckman Coulter Inc., Brea, CA). Relative percentages of different subpopulations were calculated based on live gated cells (as indicated by physical parameters, side scatter and forward scatter). Unlabeled cells and cells incubated with appropriate isotypic control antibodies were first acquired to ensure labeling specificity. In four experiment cells were analyzed on a BD FacsAria III (Becton Dickinson, Franklin Lakes, NJ) and then sorted on the basis of CD133 expression. CD133 vs. Side Scatter dot plot revealed the populations of interest that were sorted: $CD133^+$ and $CD133^-$ cell fractions were selected by setting appropriate sorting gates. Unlabeled cells were first acquired to ensure labeling specificity. Cells to be sorted were re-suspended in complete medium and kept cold until sorting. Sorted cells were collected in a tube containing growth medium. After sorting, an aliquot of the sorted cells was run on the sorter to check the purity of the two populations.

Western blot and densitometric analysis

Total protein extracts were isolated in lysis buffer as described (Pistollato et al., 2009a; Pistollato et al., 2009b). Equal amounts of protein (10–20μg) were resolved using a SDS-PAGE gel (Criterion, Bio-Rad, Hercules, CA) and transferred to PVDF Hybond-p membrane (GE Healthcare, London, Canada). Membranes were blocked with I-block™ Blocking (Tropix, Sigma-Aldrich, St. Louis, MO) for at least 1hour or overnight, under rotation at RT or 4°C respectively. Membranes were then incubated overnight at 4°C under constant shaking with the primary antibodies listed in supplementary table 5. Membranes were next incubated with peroxidase-labeled goat anti-rabbit or anti mouse IgG (1:100.000; Sigma-Aldrich, St. Louis, MO) for 60min. All membranes were visualized using ECL Advance (GE Healthcare, London, Canada) and exposed to Hyperfilm MP (GE Healthcare, London, Canada). Densitometric analysis of the films was performed using Image J densitometer software.

Real-Time PCR analysis

RNA was isolated from GBM cells or MDB cells or zebrafish larval brains using Trizol (Invitrogen, Carlsbad, CA) and 0.5µg of total RNA reverse-transcribed using SuperScriptRNAse H-Reverse Transcriptase (Invitrogen, Carlsbad, CA). Quantitative RT-PCR reactions were run in triplicate using Brilliant® SYBR® Green QPCR Core Reagent Kit (Stratagene, La Jolla, CA). Fluorescent emission was recorded in real-time (Sequence Detection System 7900HT, Applied Biosystems, Carlsbad, CA). Gene expression analysis was completed using the comparative Ct method of relative quantification. PCR amplification conditions consisted of 40 cycles with primers annealing at 60°C. Sequences of specific primers used in this work are listed in Supplementary Table 4.

Primers have been designed by using the software Primer 3 (http://frodo.wi.mit.edu/primer3/input.htm) and the specificity of the primers for the human sequences has been evaluated by using the software Human BLAT Search (http://genome.ucsc.edu/cgi-bin/hgBlat?command=start). PCR amplicons had been previously evaluated on agarose gel, and during SYBR green analyses primers dissociation curves have been checked in each run to ensure primers specificity on

human mRNA. Relative RNA quantities were normalized to *GUSB* and human GBM cells prior injection were used as the calibrating condition (ΔΔCt Method).

Chromatin immuno-precipitation assay

We performed CHIP assay on 293T cells treated with 30ng/ml of soluble Wnt3a for 48hrs or maintained in DMEM 10% FBS. Collected cells were sonicated 30sec x 8 times in water bath sonicator and immuno-precipitation was performed using total β-Catenin (rabbit, 1:5000, Abcam, Cambridge, UK) antibody. Purification of genomic DNA (ChIP samples + input) was performed by phenol/chloroform extraction and we detected specific NUMB promoter sequences from No Ab (negative control), immunoprecipitated (samples) and input (positive control) DNAs by PCR, using 2μl of each DNA sample.

Labeling of human cells with vital dye.

Cell pellets were resuspended at a density of 1×10^6/ml in serum-free DMEM/F12 (Irvine Scientific, Irvine, CA), then the cell-labeling solution (Vibrant-DiI or Vibrant-DiO; Invitrogen, Carlsbad, CA) was added at a final concentration of 5μM. Cells were gently mixed and incubated for 20 minutes at 37°C in darkness. The labeled suspension tubes were centrifuged at 1150 rpm for 7 minutes. Supernatant was removed and pellet was gently resuspended in warm (37°C) serum-free medium. Wash procedure was repeated two more times. Finally cells were resuspended in complete medium at a final concentration of 10^7 cells/ml.

Zebrafish handling for xeno-transplantation.

Zebrafish embryos were generated by natural mating of adult fish and manipulated according to the Zebrafish Handbook(Westerfield, 2000). We used Giotto and Umbria wild type strains(Pauls et al., 2007). To avoid host pigmentation at later stages of

development, we took advantage of an albino fish line (gift from Prof. H. Spaink). All strains were maintained at the Zebrafish Facility of the Department of Biology– University of Padova. Zebrafish handling and treatments were approved by the UniPD Ethical Committee on Animal Experimentation (CEASA - Project #62/2009).

Prior to injection of cancer cells, zebrafish larvae were maintained at 28°C in fishwater(Westerfield, 2000). GBM-derived cancer cells were injected in the brain *peri*-ventricular zone of 7dpf wild type zebrafish larvae. During injection, zebrafish were anaesthetized with Tricaine (0.5mM 3-aminobenzoic acid ethyl ester; Sigma-Aldrich, St. Louis, MO) and then placed in a mini-plate with multiple ramps. Zebrafish larvae were placed on their sides in 3% methyl-cellulose. Approximately 100-150 cancer cells were injected into the brain *peri*-ventricular zone and zebrafish were then transferred in fresh fish water to a 28°C incubator up to 1 hour to allow recovery of larvae from anesthesia and handling. Then transplanted zebrafish were transferred to 34°C incubator to allow human cells recovery. When the experiments were terminated, zebrafish embryos were fixed using 4% formaldehyde in PBS at 4°C overnight, washed with PBS and then transferred in 70% ethanol for immunohistochemistry analysis, dehydrated gradually into 100% methanol for *in situ* hybridization or dissolved in TRIZOL Reagent (Invitrogen, Carlsbad, CA) for subsequent RNA extraction.

In some experiments we transplanted GBM cells in *hsp70l:dkk1-GFP* transgenic zebrafish larvae (gift from Dr. G. Weidinger). This fish line is characterized by the expression of *dikkopf1b* gene under the control of the heat shock cognate protein 70 promoter. Heat shocks cause a dramatic expression of *dkk1* and the subsequent inhibition of Wnt signalling. For our experiments heat shocks were performed twice daily by transferring fish from 34°C water to preheated 40°C water with subsequent incubation in an air incubator at 40°C for 1hour(Stoick-Cooper et al., 2007).

The Wnt-Notch pathway interaction was evaluated *in vivo* by using transgenic reporter zebrafish lines. Wnt reporter zebrafish are characterized by the expression of *mCherry* (RED) under the control of seven TCF/LEF-binding sites upstream of a 0.13kb fragment containing the minimal promoter–TATA box of the gene *siamois* (Moro E. *et al*. unpublished data). Notch reporter zebrafish transgenic lines expressed GFP [Tg(Tp1bglob:eGFP)^{um14}] under the control of an element containing 12x RBP-Jκ

binding sites. The tp1blgob element consist of 6 copies of the TP1 promoter (12 Rbp-Jκ binding sites), upstream of the rabbit β-globin minimal promoter(Parsons et al., 2009).

Cell transplantation into zebrafish larvae.

Labeled cells were loaded into a pulled glass micropipette that was drawn on an electrode puller and then trimmed to form a needle. The micro-needle was attached to an air driven micro-injector. The tip of the needle was inserted into the zebrafish brain *peri*-ventricular zone and intact cells, excluding cells debris, were delivered in a double injection. Using 30–100ms pulse time and 8psi positive pressure, we optimized the number of cells injected in a range between 50/75 cells/shot, which we confirmed by dispensing cells onto a microscope slide and visually counting them. The volume of material injected was approximately 20–50nl. During injection, zebrafish larvae were examined by fluorescence microscopy (Leica, Wetzlar, Germany) to check for cell morphology and the presence of a human cell mass in the brain *peri*-ventricular zone and cells morphology. Then larvae were transferred to an incubator and maintained at 34°C to allow cells recovery. Injected cells were followed every day using a fluorescent microscope (Leica, Wetzlar, Germany) to monitor cell morphology and position.

Luciferase reporter assays on xeno-transplanted GBM cells

GBM cells were transfected as previously described with BAT-luciferase reporter construct (BAT-lux) or Notch luciferase reporter plasmid. Transfection with a Renilla luciferase vector was used in order to normalize luciferase detection (Promega, Madison, WI). Twelve hours after transfection, total medium change was done and cells were collected for zebrafish injection. To control transfection efficacy, control cells were re-suspended in Passive Lysis Buffer (PLB, Promega, Madison, WI) and luciferase activity was analysed. Zebrafish xeno-transplanted larvae and GBM cells were processed for analysis of BAT-luciferase activity as recommended (Dual-Luciferase Reporter Assay System, Promega, Madison, WI) using a plate-reading luminometer (Victor, Perkin Elmer, Waltham, MA). Values, expressed in "RLU" (= relative light units), were normalized to the values obtained from GBM cells prior to injection.

Live Imaging of zebrafish embryos/larvae

Xeno-transplanted zebrafish live larvae and reporter zebrafish were anaesthetized with Tricaine (0.5 mM 3-aminobenzoic acid ethyl ester; Sigma-Aldrich, St. Louis, MO) and then embedded in 1% low melting agarose in methylene blue free fishwater added with Tricaine. Images and stacks were acquired by using a Biorad confocal microscope and images or 3D reconstruction were processed for figures and videos using ImageJ software (Research Services Branch, National Institute of Mental Health, Bethesda, Maryland, USA.).

Immunohistochemistry on paraffin embedded sections.

Brain tumours biopsies or Xeno-transplanted zebrafish larvae were fixed in 4% paraformaldehyde, paraffin-embedded and cut in 5μm-thick sections. Sections were re-hydrated and then antigen retrieval was performed by incubation with citrate buffer 0.01M pH6 at 95°C for 20'. After saturation with 5% BSA, slides were incubated with primary antibodies listed in supplementary table 6. After incubation, sections were washed and incubated with species-specific secondary antibodies conjugated to Alexa dyes (1:1000, Invitrogen, Carlsbad, CA). Tissues were counterstained with DAPI (1:10000, Sigma-Aldrich, St. Louis, MO) to evidence cell nuclei and zebrafish morphology. Staining was visualized by epifluorescence (Vico, Nikon, Melville, NY) and images processed for figures using Adobe Photoshop or Illustrator (Adobe, San Jose, CA). The specificity of each staining procedure was confirmed by replacing the primary antibodies with the specific isotype control.

Gene expression profiling of xeno-transplanted larvae

For microarray experiments *in vitro* transcription, hybridization and biotin labeling of RNA from zebrafish larvae brainswere performed, according to Affymetrix 3'IVT Express protocol, before and at several time points after transplantation with GBM cells. GeneChip Human Genome U133 Plus 2.0 (Affymetrix, Santa Clara, CA) was used.

Microarray data (CEL files) were generated using default Affymetrix microarray analysis parameters (Command Console suite software). CEL files were normalized using robust multiarray averaging expression measure of Affy-R package (http://www.bioconductor.org). Probe sets with Present or Marginal detection calls in the zebrafish only array generated by Affymetrix Microarray Suite version 5 (MAS5) algorithm were filtered out in the analysis of the arrays after transplantation(McClintick and Edenberg, 2006). CEL files can be found at the Gene Expression Omnibus (GEO) repository (http://www.ncbi.nlm.nih.gov/geo/; Series Accession Number GSE25012), and are accessible without restrictions.

Filtering on variance (quantile 0.995) was applied to identify genes that were differently expressed along the 3 time points (4hpi, 24hpi, 48hpi) into 2 independent experiments.

Heat map was generated using R software (http://www.R-project.org) using Euclidean distance as a distance measure between genes.

Expression data have been deposited into the Gene Expression Omnibus (GEO) database under Series Accession Number GSE25012 and are accessible without restrictions.

In Situ Hybridization (ISH) on whole mount zebrafish larvae.

We performed ISH on 6dpf whole mount zebrafish larvae treated for 72h with 20μM IWR or matched controls using a zebrafish specific RNA probe recognizing the *neurod* transcript. The probe was synthesized using DIG labeled nucleotides (Roche, Basel, Swiss), and zebrafish embryos stained following standard procedures. Briefly, paraformaldehyde-fixed zebrafish were rehydrated, permeabilized, pre-hybridized with tRNAs and then hybridized with the probes O/N at 65°C. The detection of the labeled probes was achieved using anti-DIG antibodies-AP (Roche, Basel, Swiss) O/N at 4°C and then incubated with a NBT-BCIP staining solution. Larvae were not post-fixed.

REFERENCES

Al-Hajj, M., Wicha, M. S., Benito-Hernandez, A., Morrison, S. J., and Clarke, M. F. (2003). Prospective identification of tumorigenic breast cancer cells. Proc Natl Acad Sci U S A *100*, 3983-3988.

Alvarez-Buylla, A., and Lois, C. (1995). Neuronal stem cells in the brain of adult vertebrates. Stem Cells *13*, 263-272.

Arsham, A. M., Plas, D. R., Thompson, C. B., and Simon, M. C. (2002). Phosphatidylinositol 3-kinase/Akt signaling is neither required for hypoxic stabilization of HIF-1 alpha nor sufficient for HIF-1-dependent target gene transcription. J Biol Chem *277*, 15162-15170.

Azuma, Y., Chou, S. C., Lininger, R. A., Murphy, B. J., Varia, M. A., and Raleigh, J. A. (2003). Hypoxia and differentiation in squamous cell carcinomas of the uterine cervix: pimonidazole and involucrin. Clin Cancer Res *9*, 4944-4952.

Bao, S., Wu, Q., McLendon, R. E., Hao, Y., Shi, Q., Hjelmeland, A. B., Dewhirst, M. W., Bigner, D. D., and Rich, J. N. (2006). Glioma stem cells promote radioresistance by preferential activation of the DNA damage response. Nature *444*, 756-760.

Barth, S., Nesper, J., Hasgall, P. A., Wirthner, R., Nytko, K. J., Edlich, F., Katschinski, D. M., Stiehl, D. P., Wenger, R. H., and Camenisch, G. (2007). The peptidyl prolyl cis/trans isomerase FKBP38 determines hypoxia-inducible transcription factor prolyl-4-hydroxylase PHD2 protein stability. Mol Cell Biol *27*, 3758-3768.

Beier, D., Hau, P., Proescholdt, M., Lohmeier, A., Wischhusen, J., Oefner, P. J., Aigner, L., Brawanski, A., Bogdahn, U., and Beier, C. P. (2007). CD133(+) and CD133(-) glioblastoma-derived cancer stem cells show differential growth characteristics and molecular profiles. Cancer Res *67*, 4010-4015.

Berra, E., Benizri, E., Ginouves, A., Volmat, V., Roux, D., and Pouyssegur, J. (2003). HIF prolyl-hydroxylase 2 is the key oxygen sensor setting low steady-state levels of HIF-1alpha in normoxia. Embo J *22*, 4082-4090.

Birner, P., Gatterbauer, B., Oberhuber, G., Schindl, M., Rossler, K., Prodinger, A., Budka, H., and Hainfellner, J. A. (2001). Expression of hypoxia-inducible factor-1 alpha in oligodendrogliomas: its impact on prognosis and on neoangiogenesis. Cancer *92*, 165-171.

Bonnet, D., and Dick, J. E. (1997). Human acute myeloid leukemia is organized as a hierarchy that originates from a primitive hematopoietic cell. Nat Med *3*, 730-737.

Borello, U., Berarducci, B., Murphy, P., Bajard, L., Buffa, V., Piccolo, S., Buckingham, M., and Cossu, G. (2006). The Wnt/beta-catenin pathway regulates Gli-mediated Myf5 expression during somitogenesis. Development *133*, 3723-3732.

Brugarolas, J., Lei, K., Hurley, R. L., Manning, B. D., Reiling, J. H., Hafen, E., Witters, L. A., Ellisen, L. W., and Kaelin, W. G., Jr. (2004). Regulation of mTOR function in response to hypoxia by REDD1 and the TSC1/TSC2 tumor suppressor complex. Genes Dev *18*, 2893-2904.

Bruick, R. K., and McKnight, S. L. (2001). A conserved family of prolyl-4-hydroxylases that modify HIF. Science *294*, 1337-1340.

Calabrese, C., Poppleton, H., Kocak, M., Hogg, T. L., Fuller, C., Hamner, B., Oh, E. Y., Gaber, M. W., Finklestein, D., Allen, M*., et al.* (2007). A perivascular niche for brain tumor stem cells. Cancer Cell *11*, 69-82.

Casper, K. B., and McCarthy, K. D. (2006). GFAP-positive progenitor cells produce neurons and oligodendrocytes throughout the CNS. Mol Cell Neurosci *31*, 676-684.

Cau, E., and Blader, P. (2009). Notch activity in the nervous system: to switch or not switch? Neural Dev *4*, 36.

Chadwick, N., Fennessy, C., Nostro, M. C., Baron, M., Brady, G., and Buckle, A. M. (2008). Notch induces cell cycle arrest and apoptosis in human erythroleukaemic TF-1 cells. Blood Cells Mol Dis *41*, 270-277.

Chadwick, N., Nostro, M. C., Baron, M., Mottram, R., Brady, G., and Buckle, A. M. (2007). Notch signaling induces apoptosis in primary human CD34+ hematopoietic progenitor cells. Stem Cells *25*, 203-210.

Chen, B., Dodge, M. E., Tang, W., Lu, J., Ma, Z., Fan, C. W., Wei, S., Hao, W., Kilgore, J., Williams, N. S*., et al.* (2009). Small molecule-mediated disruption of Wnt-dependent signaling in tissue regeneration and cancer. Nat Chem Biol *5*, 100-107.

Chen, H. L., Pistollato, F., Hoeppner, D. J., Ni, H. T., McKay, R. D., and Panchision, D. M. (2007). Oxygen tension regulates survival and fate of mouse central nervous system precursors at multiple levels. Stem Cells *25*, 2291-2301.

Clements, W. K., Ong, K. G., and Traver, D. (2009). Zebrafish wnt3 is expressed in developing neural tissue. Dev Dyn *238*, 1788-1795.

Corada, M., Nyqvist, D., Orsenigo, F., Caprini, A., Giampietro, C., Taketo, M. M., Iruela-Arispe, M. L., Adams, R. H., and Dejana, E. (2010). The Wnt/beta-catenin pathway modulates vascular remodeling and specification by upregulating Dll4/Notch signaling. Dev Cell *18*, 938-949.

de la Iglesia, N., Konopka, G., Lim, K. L., Nutt, C. L., Bromberg, J. F., Frank, D. A., Mischel, P. S., Louis, D. N., and Bonni, A. (2008). Deregulation of a STAT3-interleukin 8 signaling pathway promotes human glioblastoma cell proliferation and invasiveness. J Neurosci *28*, 5870-5878.

Dennis, P. B., Jaeschke, A., Saitoh, M., Fowler, B., Kozma, S. C., and Thomas, G. (2001). Mammalian TOR: a homeostatic ATP sensor. Science *294*, 1102-1105.

DiFeo, A., Narla, G., and Martignetti, J. A. (2009). Emerging roles of Kruppel-like factor 6 and Kruppel-like factor 6 splice variant 1 in ovarian cancer progression and treatment. Mt Sinai J Med *76*, 557-566.

Dings, J., Meixensberger, J., Jager, A., and Roosen, K. (1998). Clinical experience with 118 brain tissue oxygen partial pressure catheter probes. Neurosurgery *43*, 1082-1095.

Dunlop, E. A., and Tee, A. R. (2009). Mammalian target of rapamycin complex 1: signalling inputs, substrates and feedback mechanisms. Cell Signal *21*, 827-835.

Fan, X., and Eberhart, C. G. (2008). Medulloblastoma stem cells. J Clin Oncol *26*, 2821-2827.

Fan, X., Khaki, L., Zhu, T. S., Soules, M. E., Talsma, C. E., Gul, N., Koh, C., Zhang, J., Li, Y. M., Maciaczyk, J., *et al.* (2010). NOTCH pathway blockade depletes CD133-positive glioblastoma cells and inhibits growth of tumor neurospheres and xenografts. Stem Cells *28*, 5-16.

Fan, X., Matsui, W., Khaki, L., Stearns, D., Chun, J., Li, Y. M., and Eberhart, C. G. (2006). Notch pathway inhibition depletes stem-like cells and blocks engraftment in embryonal brain tumors. Cancer Res *66*, 7445-7452.

Fan, X., Mikolaenko, I., Elhassan, I., Ni, X., Wang, Y., Ball, D., Brat, D. J., Perry, A., and Eberhart, C. G. (2004). Notch1 and notch2 have opposite effects on embryonal brain tumor growth. Cancer Res *64*, 7787-7793.

Favaro, E., Nardo, G., Persano, L., Masiero, M., Moserle, L., Zamarchi, R., Rossi, E., Esposito, G., Plebani, M., Sattler, U., *et al.* (2008). Hypoxia inducible factor-1alpha inactivation unveils a link between tumor cell metabolism and hypoxia-induced cell death. Am J Pathol *173*, 1186-1201.

Fuh, B., Sobo, M., Cen, L., Josiah, D., Hutzen, B., Cisek, K., Bhasin, D., Regan, N., Lin, L., Chan, C., *et al.* (2009). LLL-3 inhibits STAT3 activity, suppresses glioblastoma cell growth and prolongs survival in a mouse glioblastoma model. Br J Cancer *100*, 106-112.

Fukuda, S., Abematsu, M., Mori, H., Yanagisawa, M., Kagawa, T., Nakashima, K., Yoshimura, A., and Taga, T. (2007). Potentiation of astrogliogenesis by STAT3-mediated activation of bone morphogenetic protein-Smad signaling in neural stem cells. Mol Cell Biol *27*, 4931-4937.

Gaiano, N., and Fishell, G. (2002). The role of notch in promoting glial and neural stem cell fates. Annu Rev Neurosci *25*, 471-490.

Garcia, J. A. (2006). HIFing the brakes: therapeutic opportunities for treatment of human malignancies. Sci STKE *2006*, pe25.

Geiger, G. A., Fu, W., and Kao, G. D. (2008). Temozolomide-mediated radiosensitization of human glioma cells in a zebrafish embryonic system. Cancer Res *68*, 3396-3404.

Ghosh-Choudhury, N., Abboud, S. L., Nishimura, R., Celeste, A., Mahimainathan, L., and Choudhury, G. G. (2002). Requirement of BMP-2-induced phosphatidylinositol 3-kinase and Akt serine/threonine kinase in osteoblast differentiation and Smad-dependent BMP-2 gene transcription. J Biol Chem *277*, 33361-33368.

Gilbertson, R. J., and Rich, J. N. (2007). Making a tumour's bed: glioblastoma stem cells and the vascular niche. Nat Rev Cancer *7*, 733-736.

Gillespie, D. L., Whang, K., Ragel, B. T., Flynn, J. R., Kelly, D. A., and Jensen, R. L. (2007). Silencing of hypoxia inducible factor-1alpha by RNA interference attenuates human glioma cell growth in vivo. Clin Cancer Res *13*, 2441-2448.

Gu, F., Hata, R., Ma, Y. J., Tanaka, J., Mitsuda, N., Kumon, Y., Hanakawa, Y., Hashimoto, K., Nakajima, K., and Sakanaka, M. (2005). Suppression of Stat3 promotes neurogenesis in cultured neural stem cells. J Neurosci Res *81*, 163-171.

Gulino, A., Di Marcotullio, L., and Screpanti, I. (2010). The multiple functions of Numb. Exp Cell Res *316*, 900-906.

Gustafsson, M. V., Zheng, X., Pereira, T., Gradin, K., Jin, S., Lundkvist, J., Ruas, J. L., Poellinger, L., Lendahl, U., and Bondesson, M. (2005). Hypoxia requires notch signaling to maintain the undifferentiated cell state. Dev Cell *9*, 617-628.

Guzman, M. L., and Jordan, C. T. (2004). Considerations for targeting malignant stem cells in leukemia. Cancer Control *11*, 97-104.

Hadjipanayis, C. G., and Van Meir, E. G. (2009). Brain cancer propagating cells: biology, genetics and targeted therapies. Trends Mol Med *15*, 519-530.

Haldi, M., Ton, C., Seng, W. L., and McGrath, P. (2006). Human melanoma cells transplanted into zebrafish proliferate, migrate, produce melanin, form masses and stimulate angiogenesis in zebrafish. Angiogenesis *9*, 139-151.

Hallahan, A. R., Pritchard, J. I., Hansen, S., Benson, M., Stoeck, J., Hatton, B. A., Russell, T. L., Ellenbogen, R. G., Bernstein, I. D., Beachy, P. A., and Olson, J. M. (2004). The SmoA1 mouse model reveals that notch signaling is critical for the growth and survival of sonic hedgehog-induced medulloblastomas. Cancer Res *64*, 7794-7800.

Heddleston, J. M., Li, Z., McLendon, R. E., Hjelmeland, A. B., and Rich, J. N. (2009). The hypoxic microenvironment maintains glioblastoma stem cells and promotes reprogramming towards a cancer stem cell phenotype. Cell Cycle *8*, 3274-3284.

Helczynska, K., Kronblad, A., Jogi, A., Nilsson, E., Beckman, S., Landberg, G., and Pahlman, S. (2003). Hypoxia promotes a dedifferentiated phenotype in ductal breast carcinoma in situ. Cancer Res *63*, 1441-1444.

Hemmati, H. D., Nakano, I., Lazareff, J. A., Masterman-Smith, M., Geschwind, D. H., Bronner-Fraser, M., and Kornblum, H. I. (2003). Cancerous stem cells can arise from pediatric brain tumors. Proc Natl Acad Sci U S A *100*, 15178-15183.

Holmquist-Mengelbier, L., Fredlund, E., Lofstedt, T., Noguera, R., Navarro, S., Nilsson, H., Pietras, A., Vallon-Christersson, J., Borg, A., Gradin, K.*, et al.* (2006). Recruitment of HIF-1alpha and HIF-2alpha to common target genes is differentially regulated in neuroblastoma: HIF-2alpha promotes an aggressive phenotype. Cancer Cell *10*, 413-423.

Hulleman, E., Quarto, M., Vernell, R., Masserdotti, G., Colli, E., Kros, J. M., Levi, D., Gaetani, P., Tunici, P., Finocchiaro, G.*, et al.* (2009). A role for the transcription factor HEY1 in glioblastoma. J Cell Mol Med *13*, 136-146.

Ignatova, T. N., Kukekov, V. G., Laywell, E. D., Suslov, O. N., Vrionis, F. D., and Steindler, D. A. (2002). Human cortical glial tumors contain neural stem-like cells expressing astroglial and neuronal markers in vitro. Glia *39*, 193-206.

Ikeuchi, T., and Sisodia, S. S. (2002). Cell-free generation of the notch1 intracellular domain (NICD) and APP-CTfgamma: evidence for distinct intramembranous "gamma-secretase" activities. Neuromolecular Med *1*, 43-54.

Indraccolo, S., Roni, V., Zamarchi, R., Roccaforte, F., Minuzzo, S., Stievano, L., Habeler, W., Marcato, N., Tisato, V., Tosello, V.*, et al.* (2002). Expression from cell type-specific enhancer-modified retroviral vectors after transduction: influence of marker gene stability. Gene *283*, 199-208.

Ito, M., Lammertsma, A. A., Wise, R. J., Bernardi, S., Frackowiak, R. S., Heather, J. D., McKenzie, C. G., Thomas, D. G., and Jones, T. (1982). Measurement of regional cerebral blood flow and oxygen utilisation in patients with cerebral tumours using 15O and positron emission tomography: analytical techniques and preliminary results. Neuroradiology *23*, 63-74.

Jogi, A., Ora, I., Nilsson, H., Lindeheim, A., Makino, Y., Poellinger, L., Axelson, H., and Pahlman, S. (2002). Hypoxia alters gene expression in human neuroblastoma cells toward an immature and neural crest-like phenotype. Proc Natl Acad Sci U S A *99*, 7021-7026.

Jogi, A., Ora, I., Nilsson, H., Poellinger, L., Axelson, H., and Pahlman, S. (2003). Hypoxia-induced dedifferentiation in neuroblastoma cells. Cancer Lett *197*, 145-150.

Jogi, A., Vallon-Christersson, J., Holmquist, L., Axelson, H., Borg, A., and Pahlman, S. (2004). Human neuroblastoma cells exposed to hypoxia: induction of genes associated with growth, survival, and aggressive behavior. Exp Cell Res *295*, 469-487.

Kageyama, R., Ohtsuka, T., and Kobayashi, T. (2008). Roles of Hes genes in neural development. Dev Growth Differ *50 Suppl 1*, S97-103.

Kamegai, A., Tanabe, T., Nagahara, K., Kumasa, S., and Mori, M. (1990). Pathologic and enzyme histochemical studies on bone formation induced by bone morphogenetic protein in mouse muscle tissue. Acta Histochem *89*, 25-35.

Katoh, M., and Katoh, M. (2006). NUMB is a break of WNT-Notch signaling cycle. Int J Mol Med *18*, 517-521.

King, A., Selak, M. A., and Gottlieb, E. (2006). Succinate dehydrogenase and fumarate hydratase: linking mitochondrial dysfunction and cancer. Oncogene *25*, 4675-4682.

Korur, S., Huber, R. M., Sivasankaran, B., Petrich, M., Morin, P., Jr., Hemmings, B. A., Merlo, A., and Lino, M. M. (2009). GSK3beta regulates differentiation and growth arrest in glioblastoma. PLoS One *4*, e7443.

Koshiji, M., To, K. K., Hammer, S., Kumamoto, K., Harris, A. L., Modrich, P., and Huang, L. E. (2005). HIF-1alpha induces genetic instability by transcriptionally downregulating MutSalpha expression. Mol Cell *17*, 793-803.

Kotliarova, S., Pastorino, S., Kovell, L. C., Kotliarov, Y., Song, H., Zhang, W., Bailey, R., Maric, D., Zenklusen, J. C., Lee, J., and Fine, H. A. (2008). Glycogen synthase kinase-3 inhibition induces glioma cell death through c-MYC, nuclear factor-kappaB, and glucose regulation. Cancer Res *68*, 6643-6651.

Kranenbarg, S. (2002). Oxygen diffusion in fish embryos. (Wageningen, The Netherlands: Wageningen University Press)

Kuwabara, T., Hsieh, J., Muotri, A., Yeo, G., Warashina, M., Lie, D. C., Moore, L., Nakashima, K., Asashima, M., and Gage, F. H. (2009). Wnt-mediated activation of NeuroD1 and retro-elements during adult neurogenesis. Nat Neurosci *12*, 1097-1105.

Land, S. C., and Tee, A. R. (2007). Hypoxia-inducible factor 1alpha is regulated by the mammalian target of rapamycin (mTOR) via an mTOR signaling motif. J Biol Chem *282*, 20534-20543.

Lee, J., Son, M. J., Woolard, K., Donin, N. M., Li, A., Cheng, C. H., Kotliarova, S., Kotliarov, Y., Walling, J., Ahn, S.*, et al.* (2008). Epigenetic-mediated dysfunction of the bone morphogenetic protein pathway inhibits differentiation of glioblastoma-initiating cells. Cancer Cell *13*, 69-80.

Lee, S. H., Kim, M. H., and Han, H. J. (2009). Arachidonic acid potentiates hypoxia-induced VEGF expression in mouse embryonic stem cells: involvement of Notch, Wnt, and HIF-1alpha. Am J Physiol Cell Physiol *297*, C207-216.

Leith, J. T., Cook, S., Chougule, P., Calabresi, P., Wahlberg, L., Lindquist, C., and Epstein, M. (1994). Intrinsic and extrinsic characteristics of human tumors relevant to radiosurgery: comparative cellular radiosensitivity and hypoxic percentages. Acta Neurochir Suppl *62*, 18-27.

Liao, S. Y., Lerman, M. I., and Stanbridge, E. J. (2009). Expression of transmembrane carbonic anhydrases, CAIX and CAXII, in human development. BMC Dev Biol *9*, 22.

Lie, D. C., Colamarino, S. A., Song, H. J., Desire, L., Mira, H., Consiglio, A., Lein, E. S., Jessberger, S., Lansford, H., Dearie, A. R., and Gage, F. H. (2005). Wnt signalling regulates adult hippocampal neurogenesis. Nature *437*, 1370-1375.

Lim, J. H., Chun, Y. S., and Park, J. W. (2008). Hypoxia-inducible factor-1alpha obstructs a Wnt signaling pathway by inhibiting the hARD1-mediated activation of beta-catenin. Cancer Res *68*, 5177-5184.

Liu, X., Wang, L., Zhao, S., Ji, X., Luo, Y., and Ling, F. (2010). beta-Catenin overexpression in malignant glioma and its role in proliferation and apoptosis in glioblastma cells. Med Oncol.

Ljungkvist, A. S., Bussink, J., Kaanders, J. H., and van der Kogel, A. J. (2007). Dynamics of tumor hypoxia measured with bioreductive hypoxic cell markers. Radiat Res *167*, 127-145.

Maretto, S., Cordenonsi, M., Dupont, S., Braghetta, P., Broccoli, V., Hassan, A. B., Volpin, D., Bressan, G. M., and Piccolo, S. (2003). Mapping Wnt/beta-catenin signaling during mouse development and in colorectal tumors. Proc Natl Acad Sci U S A *100*, 3299-3304.

Martys-Zage, J. L., Kim, S. H., Berechid, B., Bingham, S. J., Chu, S., Sklar, J., Nye, J., and Sisodia, S. S. (2000). Requirement for presenilin 1 in facilitating lagged 2-mediated endoproteolysis and signaling of notch 1. J Mol Neurosci *15*, 189-204.

Mazumdar, J., O'Brien, W. T., Johnson, R. S., LaManna, J. C., Chavez, J. C., Klein, P. S., and Simon, M. C. (2010). O2 regulates stem cells through Wnt/beta-catenin signalling. Nat Cell Biol *12*, 1007-1013.

McClintick, J. N., and Edenberg, H. J. (2006). Effects of filtering by Present call on analysis of microarray experiments. BMC Bioinformatics *7*, 49.

McKenzie, C. G., Lenzi, G. L., Jones, T., and Moss, S. (1978). Radioactive oxygen 15O studies in cerebral neoplasms. J R Soc Med *71*, 417-425.

Memberg, S. P., and Hall, A. K. (1995). Dividing neuron precursors express neuron-specific tubulin. J Neurobiol *27*, 26-43.

Metzen, E., Stiehl, D. P., Doege, K., Marxsen, J. H., Hellwig-Burgel, T., and Jelkmann, W. (2005). Regulation of the prolyl hydroxylase domain protein 2 (phd2/egln-1) gene: identification of a functional hypoxia-responsive element. Biochem J *387*, 711-717.

Mosimann, C., Hausmann, G., and Basler, K. (2009). Beta-catenin hits chromatin: regulation of Wnt target gene activation. Nat Rev Mol Cell Biol *10*, 276-286.

Munoz-Descalzo, S., de Navascues, J., and Arias, A. M. (2012). Wnt-Notch signalling: An integrated mechanism regulating transitions between cell states. Bioessays.

Nakashima, K., Yanagisawa, M., Arakawa, H., and Taga, T. (1999). Astrocyte differentiation mediated by LIF in cooperation with BMP2. FEBS Lett *457*, 43-46.

Netto, G. C., Bleil, C. B., Hilbig, A., and Coutinho, L. M. (2008). Immunohistochemical evaluation of the microvascular density through the expression of TGF-beta (CD 105/endoglin) and CD 34 receptors and expression of the vascular endothelial growth factor (VEGF) in oligodendrogliomas. Neuropathology *28*, 17-23.

Nicoli, S., and Presta, M. (2007). The zebrafish/tumor xenograft angiogenesis assay. Nat Protoc *2*, 2918-2923.

Niehrs, C. (2006). Function and biological roles of the Dickkopf family of Wnt modulators. Oncogene *25*, 7469-7481.

Nowicki, M. O., Dmitrieva, N., Stein, A. M., Cutter, J. L., Godlewski, J., Saeki, Y., Nita, M., Berens, M. E., Sander, L. M., Newton, H. B.*, et al.* (2008). Lithium inhibits invasion of glioma cells; possible involvement of glycogen synthase kinase-3. Neuro Oncol *10*, 690-699.

Panchision, D. M. (2009). The role of oxygen in regulating neural stem cells in development and disease. J Cell Physiol *220*, 562-568.

Panchision, D. M., Chen, H. L., Pistollato, F., Papini, D., Ni, H. T., and Hawley, T. S. (2007). Optimized flow cytometric analysis of central nervous system tissue reveals novel functional relationships among cells expressing CD133, CD15, and CD24. Stem Cells *25*, 1560-1570.

Pardal, R., Ortega-Saenz, P., Duran, R., and Lopez-Barneo, J. (2007). Glia-like stem cells sustain physiologic neurogenesis in the adult mammalian carotid body. Cell *131*, 364-377.

Parsons, M. J., Pisharath, H., Yusuff, S., Moore, J. C., Siekmann, A. F., Lawson, N., and Leach, S. D. (2009). Notch-responsive cells initiate the secondary transition in larval zebrafish pancreas. Mech Dev *126*, 898-912.

Pauls, S., Zecchin, E., Tiso, N., Bortolussi, M., and Argenton, F. (2007). Function and regulation of zebrafish nkx2.2a during development of pancreatic islet and ducts. Dev Biol *304*, 875-890.

Perez-Caro, M., and Sanchez-Garcia, I. (2006). Killing time for cancer stem cells (CSC): discovery and development of selective CSC inhibitors. Curr Med Chem *13*, 1719-1725.

Piccirillo, S. G., Reynolds, B. A., Zanetti, N., Lamorte, G., Binda, E., Broggi, G., Brem, H., Olivi, A., Dimeco, F., and Vescovi, A. L. (2006). Bone morphogenetic proteins inhibit the tumorigenic potential of human brain tumour-initiating cells. Nature *444*, 761-765.

Pistollato, F., Abbadi, S., Rampazzo, E., Persano, L., Della Puppa, A., Frasson, C., Sarto, E., Scienza, R., D'Avella, D., and Basso, G. (2010a). Intratumoral hypoxic gradient drives stem cells distribution and MGMT expression in glioblastoma. Stem Cells *28*, 851-862.

Pistollato, F., Chen, H. L., Rood, B. R., Zhang, H. Z., D'Avella, D., Denaro, L., Gardiman, M., te Kronnie, G., Schwartz, P. H., Favaro, E*., et al.* (2009a). Hypoxia and HIF1alpha repress the differentiative effects of BMPs in high-grade glioma. Stem Cells *27*, 7-17.

Pistollato, F., Chen, H. L., Schwartz, P. H., Basso, G., and Panchision, D. M. (2007). Oxygen tension controls the expansion of human CNS precursors and the generation of astrocytes and oligodendrocytes. Mol Cell Neurosci *35*, 424-435.

Pistollato, F., Rampazzo, E., Abbadi, S., Della Puppa, A., Scienza, R., D'Avella, D., Denaro, L., Te Kronnie, G., Panchision, D. M., and Basso, G. (2009b). Molecular mechanisms of HIF-1alpha modulation induced by oxygen tension and BMP2 in glioblastoma derived cells. PLoS One *4*, e6206.

Pistollato, F., Rampazzo, E., Persano, L., Abbadi, S., Frasson, C., Denaro, L., D'Avella, D., Panchision, D. M., Della Puppa, A., Scienza, R., and Basso, G. (2010b). Interaction of hypoxia-inducible factor-1alpha and Notch signaling regulates medulloblastoma precursor proliferation and fate. Stem Cells *28*, 1918-1929.

Pu, P., Zhang, Z., Kang, C., Jiang, R., Jia, Z., Wang, G., and Jiang, H. (2009). Downregulation of Wnt2 and beta-catenin by siRNA suppresses malignant glioma cell growth. Cancer Gene Ther *16*, 351-361.

Qiang, L., Wu, T., Zhang, H. W., Lu, N., Hu, R., Wang, Y. J., Zhao, L., Chen, F. H., Wang, X. T., You, Q. D., and Guo, Q. L. (2012). HIF-1alpha is critical for hypoxia-mediated maintenance of glioblastoma stem cells by activating Notch signaling pathway. Cell Death Differ *19*, 284-294.

Raffel, C., Jenkins, R. B., Frederick, L., Hebrink, D., Alderete, B., Fults, D. W., and James, C. D. (1997). Sporadic medulloblastomas contain PTCH mutations. Cancer Res *57*, 842-845.

Rajan, P., Panchision, D. M., Newell, L. F., and McKay, R. D. (2003). BMPs signal alternately through a SMAD or FRAP-STAT pathway to regulate fate choice in CNS stem cells. J Cell Biol *161*, 911-921.

Razorenova, O. V., Ivanov, A. V., Budanov, A. V., and Chumakov, P. M. (2005). Virus-based reporter systems for monitoring transcriptional activity of hypoxia-inducible factor 1. Gene *350*, 89-98.

Read, T. A., Fogarty, M. P., Markant, S. L., McLendon, R. E., Wei, Z., Ellison, D. W., Febbo, P. G., and Wechsler-Reya, R. J. (2009). Identification of CD15 as a marker for tumor-propagating cells in a mouse model of medulloblastoma. Cancer Cell *15*, 135-147.

Reya, T., Morrison, S. J., Clarke, M. F., and Weissman, I. L. (2001). Stem cells, cancer, and cancer stem cells. Nature *414*, 105-111.

Rong, Y., Durden, D. L., Van Meir, E. G., and Brat, D. J. (2006). 'Pseudopalisading' necrosis in glioblastoma: a familiar morphologic feature that links vascular pathology, hypoxia, and angiogenesis. J Neuropathol Exp Neurol *65*, 529-539.

Sakariassen, P. O., Prestegarden, L., Wang, J., Skaftnesmo, K. O., Mahesparan, R., Molthoff, C., Sminia, P., Sundlisaeter, E., Misra, A., Tysnes, B. B.*, et al.* (2006). Angiogenesis-independent tumor growth mediated by stem-like cancer cells. Proc Natl Acad Sci U S A *103*, 16466-16471.

Sanchez, C., Diaz-Nido, J., and Avila, J. (2000). Phosphorylation of microtubule-associated protein 2 (MAP2) and its relevance for the regulation of the neuronal cytoskeleton function. Prog Neurobiol *61*, 133-168.

Sareddy, G. R., Panigrahi, M., Challa, S., Mahadevan, A., and Babu, P. P. (2009). Activation of Wnt/beta-catenin/Tcf signaling pathway in human astrocytomas. Neurochem Int *55*, 307-317.

Schroeter, E. H., Ilagan, M. X., Brunkan, A. L., Hecimovic, S., Li, Y. M., Xu, M., Lewis, H. D., Saxena, M. T., De Strooper, B., Coonrod, A.*, et al.* (2003). A presenilin dimer at the core of the gamma-secretase enzyme: insights from parallel analysis of Notch 1 and APP proteolysis. Proc Natl Acad Sci U S A *100*, 13075-13080.

Schwarzer, R., Tondera, D., Arnold, W., Giese, K., Klippel, A., and Kaufmann, J. (2005). REDD1 integrates hypoxia-mediated survival signaling downstream of phosphatidylinositol 3-kinase. Oncogene *24*, 1138-1149.

Semenza, G. L. (2002). Involvement of hypoxia-inducible factor 1 in human cancer. Intern Med *41*, 79-83.

Singh, S. K., Clarke, I. D., Terasaki, M., Bonn, V. E., Hawkins, C., Squire, J., and Dirks, P. B. (2003). Identification of a cancer stem cell in human brain tumors. Cancer Res *63*, 5821-5828.

Singh, S. K., Hawkins, C., Clarke, I. D., Squire, J. A., Bayani, J., Hide, T., Henkelman, R. M., Cusimano, M. D., and Dirks, P. B. (2004). Identification of human brain tumour initiating cells. Nature *432*, 396-401.

Smith, K., Gunaratnam, L., Morley, M., Franovic, A., Mekhail, K., and Lee, S. (2005). Silencing of epidermal growth factor receptor suppresses hypoxia-inducible factor-2-driven VHL-/- renal cancer. Cancer Res *65*, 5221-5230.

Solecki, D. J., Liu, X. L., Tomoda, T., Fang, Y., and Hatten, M. E. (2001). Activated Notch2 signaling inhibits differentiation of cerebellar granule neuron precursors by maintaining proliferation. Neuron *31*, 557-568.

Stoick-Cooper, C. L., Weidinger, G., Riehle, K. J., Hubbert, C., Major, M. B., Fausto, N., and Moon, R. T. (2007). Distinct Wnt signaling pathways have opposing roles in appendage regeneration. Development *134*, 479-489.

Tohyama, T., Lee, V. M., Rorke, L. B., Marvin, M., McKay, R. D., and Trojanowski, J. Q. (1992). Nestin expression in embryonic human neuroepithelium and in human neuroepithelial tumor cells. Lab Invest *66*, 303-313.

Trompouki, E., Bowman, T. V., Lawton, L. N., Fan, Z. P., Wu, D. C., DiBiase, A., Martin, C. S., Cech, J. N., Sessa, A. K., Leblanc, J. L.*, et al.* (2011). Lineage regulators direct BMP and Wnt pathways to cell-specific programs during differentiation and regeneration. Cell *147*, 577-589.

Vescovi, A. L., Galli, R., and Reynolds, B. A. (2006). Brain tumour stem cells. Nat Rev Cancer *6*, 425-436.

Warburg, O. (1956). On respiratory impairment in cancer cells. Science *124*, 269-270.

Ward, R. J., Lee, L., Graham, K., Satkunendran, T., Yoshikawa, K., Ling, E., Harper, L., Austin, R., Nieuwenhuis, E., Clarke, I. D.*, et al.* (2009). Multipotent CD15+ cancer stem cells in patched-1-deficient mouse medulloblastoma. Cancer Res *69*, 4682-4690.

Weng, A. P., Ferrando, A. A., Lee, W., Morris, J. P. t., Silverman, L. B., Sanchez-Irizarry, C., Blacklow, S. C., Look, A. T., and Aster, J. C. (2004). Activating mutations of NOTCH1 in human T cell acute lymphoblastic leukemia. Science *306*, 269-271.

Westerfield, M. (2000). The zebrafish book. A guide for the laboratory use of zebrafish (Danio rerio). (Eugene: University of Oregon Press).

Wilkins, S. E., Hyvarinen, J., Chicher, J., Gorman, J. J., Peet, D. J., Bilton, R. L., and Koivunen, P. (2009). Differences in hydroxylation and binding of Notch and HIF-1alpha demonstrate substrate selectivity for factor inhibiting HIF-1 (FIH-1). Int J Biochem Cell Biol *41*, 1563-1571.

Williams, C. K., Li, J. L., Murga, M., Harris, A. L., and Tosato, G. (2006). Up-regulation of the Notch ligand Delta-like 4 inhibits VEGF-induced endothelial cell function. Blood *107*, 931-939.

Wong, E. T., and Brem, S. (2008). Antiangiogenesis treatment for glioblastoma multiforme: challenges and opportunities. J Natl Compr Canc Netw *6*, 515-522.

Yang, W., Xia, Y., Ji, H., Zheng, Y., Liang, J., Huang, W., Gao, X., Aldape, K., and Lu, Z. (2011). Nuclear PKM2 regulates beta-catenin transactivation upon EGFR activation. Nature *480*, 118-122.

Yuan, G., Nanduri, J., Khan, S., Semenza, G. L., and Prabhakar, N. R. (2008). Induction of HIF-1alpha expression by intermittent hypoxia: involvement of NADPH oxidase, Ca2+ signaling, prolyl hydroxylases, and mTOR. J Cell Physiol *217*, 674-685.

Zhang, L., and Hill, R. P. (2004). Hypoxia enhances metastatic efficiency by up-regulating Mdm2 in KHT cells and increasing resistance to apoptosis. Cancer Res *64*, 4180-4189.

Zhang, N., Wei, P., Gong, A., Chiu, W. T., Lee, H. T., Colman, H., Huang, H., Xue, J., Liu, M., Wang, Y.*, et al.* (2011). FoxM1 promotes beta-catenin nuclear localization and controls Wnt target-gene expression and glioma tumorigenesis. Cancer Cell *20*, 427-442.

Zhang, P., Andrianakos, R., Yang, Y., Liu, C., and Lu, W. (2010). Kruppel-like factor 4 (Klf4) prevents embryonic stem (ES) cell differentiation by regulating Nanog gene expression. J Biol Chem *285*, 9180-9189.

Zheng, H., Ying, H., Wiedemeyer, R., Yan, H., Quayle, S. N., Ivanova, E. V., Paik, J. H., Zhang, H., Xiao, Y., Perry, S. R.*, et al.* (2010). PLAGL2 regulates Wnt signaling to impede differentiation in neural stem cells and gliomas. Cancer Cell *17*, 497-509.

Zimmerman, L. B., De Jesus-Escobar, J. M., and Harland, R. M. (1996). The Spemann organizer signal noggin binds and inactivates bone morphogenetic protein 4. Cell *86*, 599-606.

Supplementary Table 1

Down-regulated probe sets along the 3 time points in the intersection list

Probe sets	*Gene Symbol*
1556499_s_at	*COL1A1*
200077_s_at	*OAZ1*
200599_s_at	*HSP90B1*
200650_s_at	*LDHA*
200738_s_at	*PGK1*
200771_at	*LAMC1*
200773_x_at	*LOC643287 /// PTMA*
200807_s_at	*HSPD1*
200832_s_at	*SCD*
200858_s_at	*RPS8*
200886_s_at	*hCG_2015138 /// PGAM1*
200958_s_at	*SDCBP*
200966_x_at	*ALDOA*
201005_at	*CD9*
201105_at	*LGALS1*
201426_s_at	*VIM*
201464_x_at	*JUN*
201645_at	*TNC*
201667_at	*GJA1*
201669_s_at	*MARCKS*
201849_at	*BNIP3*
201938_at	*CDK2AP1*
202403_s_at	*COL1A2*
202404_s_at	*COL1A2*
202428_x_at	*DBI*
204170_s_at	*CKS2*
204469_at	*PTPRZ1*
204471_at	*GAP43*
205029_s_at	*FABP7*
205030_at	*FABP7*
205292_s_at	*HNRNPA2B1*
208628_s_at	*YBX1*
208636_at	*ACTN1*
208752_x_at	*NAP1L1*
208892_s_at	*DUSP6*
208894_at	*HLA-DRA*
209189_at	*FOS*
209389_x_at	*DBI*
209465_x_at	*PTN*
209466_x_at	*PTN*
209656_s_at	*TMEM47*
210139_s_at	*PMP22*
210512_s_at	*VEGFA*
210561_s_at	*WSB1*
211070_x_at	*DBI*
211737_x_at	*PTN*

211943_x_at	*TPT1*
211945_s_at	*ITGB1*
211959_at	*IGFBP5*
211990_at	*HLA-DPA1*
212284_x_at	*TPT1*
213011_s_at	*TPI1*
213084_x_at	*hCG_16001 /// hCG_2001000 /// RPL23A*
213428_s_at	*COL6A1*
213881_x_at	*SUMO2*
213911_s_at	*H2AFZ*
217398_x_at	*GAPDH*
217757_at	*A2M*
217871_s_at	*MIF*
221479_s_at	*BNIP3L*
221841_s_at	*KLF4*
224606_at	*KLF6*
225413_at	*USMG5*
225540_at	*MAP2*
226189_at	*ITGB8*
37892_at	*COL11A1*

Probe sets with down regulation at 24 hpi time point and upregulation at 48 hpi time point

Probe sets	***Gene Symbol***
200665_s_at	*SPARC*
201550_x_at	*ACTG1*
201876_at	*PON2*
207030_s_at	*CSRP2*
210198_s_at	*PLP1*
210968_s_at	*RTN4*
211719_x_at	*FN1*
214629_x_at	*RTN4*
221607_x_at	*ACTG1*
224585_x_at	*ACTG1*
200638_s_at	*YWHAZ*
208640_at	*RAC1*
210211_s_at	*HSP90AA1*

Up-regulated probe sets along the 3 time points in the intersection list

Probe sets	***Gene symbol***
209167_at	*GPM6B*
209170_s_at	*GPM6B*
209283_at	*CRYAB*
212097_at	*CAV1*
214247_s_at	*DKK3*
219087_at	*ASPN*
221805_at	*NEFL*
221916_at	*NEFL*

Supplementary Table 2.
Glioblastoma and Normal Neural Progenitor Cells used in study

Code	Tumor Type	Age	Gender
HuTuP01	Glioblastoma	65	male
HuTuP02	Glioblastoma	43	female
HuTuP03	Glioblastoma	n.a.	male
HuTuP05	Glioblastoma	n.a.	male
HuTuP10	Glioblastoma	75	female
HuTuP11	Glioblastoma	52	female
HuTuP12	high grade glioma	68	male
HuTuP13	high grade glioma	67	male
HuTuP14	high grade glioma	34	female
HuTuP15	Glioblastoma	76	female
HuTuP16	Glioblastoma	66	male
HuTuP17	high grade glioma	60	female
HuTuP19	Glioblastoma	43	female
HuTuP20	high grade glioma	55	male
HuTuP22	low grade glioma	19	male
HuTuP23	high grade glioma	52	male
HuTuP26	high grade glioma	62	male
HuTuP27	high grade glioma	49	male
HuTuP47	Glioblastoma	81	female
HuTu53	Glioblastoma	70	male
HuTu63	Glioblastoma	37	female
HuTu83	Glioblastoma	55	male
HuTu102	Glioblastoma	40	male
HuTu107	Glioblastoma	65	male
Post-mortem review of non-tumour tissue source			

HuSC23	Premature polycythemic twin (of a twin-to-twin transfusion) who died on the day after birth	23 gw	male
HuSC27	Premature infant who died of pulmonary complications 2 weeks after birth	23 gw	male
HuSC30	Premature fraternal twin who died on the day after birth, product of in vitro fertilization	25 gw	male
Brain tumours were acquired directly from surgery, dissociated and cells were expanded in culture. First neuropathological review of the tumour tissue was followed by a second independent review. Patient ages listed in years (y). Non tumour tissue was from premature infants, listed in gestational weeks (gw), who died shortly after birth; periventricular zone tissue from the head of the caudate nucleus was isolated and initially characterized by Schwartz et al. (2003); no gross or microscopic abnormalities were observed at this time.			

Supplementary Table 3
MDB Tumors used in study

Code	Tumor Type	Age	Gender
HuTu25	Medulloblastoma	16	male
HuTu32	Medulloblastoma	5	female
HuTu33	Medulloblastoma	1	female
HuTuP18	Medulloblastoma	34	male
F132	Medulloblastoma	1	female
F125	Medulloblastoma	1	male
HuTuP49	Medulloblastoma	4	female
HuTuP57	Medulloblastoma	8	female
11811	Medulloblastoma	28	female
14213-2	Medulloblastoma	41	male
13215-1	Medulloblastoma	31	male
14223-2	Medulloblastoma	35	female
11941	Medulloblastoma	1	male

Brain tumours were acquired directly from surgery, dissociated and cells were expanded in culture. First neuropathological review of the tumour tissue was followed by a second independent review. Patient ages listed in years (y).

Supplementary Table 4

Sequence of primers used in this study

Gene	*Sequence (5'-3')*	*Amplicon (bp)*
MAP2 forward	GGGTCACAGGGCACCTATTC	129
MAP2 reverse	GCTACAGCCTCAGCAGTGAC	
β-III-tubulin (Tuj1) forward	GGGGCCTTTGGACATCTCTT	126
β-III-tubulin (Tuj1) reverse	CACCACATCCAGGACCGAAT	
Neuro D1 forward	CAGACGAGTGTCTCAGTTCTCA	139
Neuro D1 reverse	TCCTCTTCCAGGTCCTCATCTT	
Neurogenin 1 (Ngn1) forward	CCCCTAGTCAGCAGGCAATA	72
Neurogenin 1 (Ngn1) reverse	GGTCAGTTCTGAGCCAGTC	
LDHA forward	GGCCTGTGCCATCAGTATCT	177
LDHA reverse	ACCAGCTTGGAGTTTGCAGT	
VEGF forward	AACCATGAACTTTCTGCTGTCT	129
VEGF reverse	TTCACCACTTCGTGATGATTCT	
DKK3 forward	GCCTGGTGTATGTGTGCAAG	91
DKK3 reverse	TCATACTCATCGGGGACCTC	
GPM6B forward	GCTGGGTGTGTTTGGTTTCT	84
GPM6B reverse	TGCGGTGACTTGATGACTTC	
JUN forward	CCAAGAACTCGGACCTCCT	96
JUN reverse	CCCGTTGCTGGACTGGATTA	
KLF4 forward	CTGCGGCAAAACCTACACAA	90
KLF4 reverse	CGTCCCAGTCACAGTGGTA	
Numb forward	GTCGCTGGATCTGTCACTGCT	102
Numb reverse	TCTGCTTGCGCTCTAAACAGG	
NumbLike forward	CCTTTCAAACGGCAGCTGAG	102
NumbLike reverse	AGGCTCCATCTCAGGCACTG	
Numb-1180_forward	GCTAGTAGGGCTATTTAAGAACTGC	136
Numb-1180_reverse	GCCCGGCCAGCAACTTTCTAATA	
Numb-418_forward	GCAGGAAGTGAGCTGGAGAAG	118
Numb-418_reverse	GCGCAGTAGAAAGCAAAGGAG	
β-glucuronidase (GUSB) forward	GAAAATACGTGGTTGGAGAGCTCATT	101
β-glucuronidase (GUSB) reverse	CCGAGTGAAGATCCCCTTTTTA	

PHD2 forward	GGGACATTCATTGCCTCACT	158
PHD2 reverse	TCCATGAGTGGGACACTGAG	
FKBP38 forward	GGCTGTTGAGGAAGAAGACG	187
FKBP38 reverse	TCCATGAGTGGGACACTGAG	

Primers have been designed by using the software Primer 3 (http://frodo.wi.mit.edu/primer3) and the specificity of primers for human sequences has been evaluated by using the software Human BLAT Search (http://genome.csdb.cn/cgi-bin/hgBlat).

Supplementary table 5: antibodies used for western blot in this studies

Antibody	**MW(kDa)**	**Manufacturer**	**Host**	**Dil (WB)**
4E-BP1 (S65)	15-20	Cell Signaling	Rabbit	1:1000
Akt (S473)	60	Cell Signaling	Rabbit	1:1000
Akt (T308)	60	Cell Signaling	Rabbit	1:1000
HIF-1alpha (54)	120	BD	Mouse	1:250
mTOR (S2448)	289	Cell Signaling	Rabbit	1:1000
NOTCH1 6A5	110, 270	Cell Signaling	Rabbit	1:1000
Cleaved NOTCH1 (Val1744)	110	Cell Signaling	Rabbit	1:1000
Id1	15	Santa Cruz	Rabbit	1:1000
Hes1	18	Chemicon	Rabbit	1:250
p70 S6 Kinase (T389)	70, 85	Cell Signaling	Rabbit	1:1000
Pan p53	53	Cell Signaling	Rabbit	1:1000
p53 (S37)	53	Cell Signaling	Rabbit	1:1000
p53 (S392)	53	Cell Signaling	Rabbit	1:1000
p21	21	Sigma	Mouse	1:1000
PHD2	46	Santa Cruz	Goat	1:300
PHD3	46	Santa Cruz	Goat	1:300
SMAD 1(S463/465) SMAD 5(S463/465) SMAD 8 (S426/428)	60	Cell Signaling	Rabbit	1:100
Stat3 (S727)	79, 86	Cell Signaling	Rabbit	1:1000
Phospho-β-Catenin (S33/37/T41)	90	Cell Signalling	Rabbit	1:1000

total β-Catenin	90	Abcam	Rabbit	1:5000
Phospho-GSK3α/β	62/64	Cell Signalling	Rabbit	1:1000
NUMB PAN-ISO	70/72	Upstate	Rabbit	1:500
NUMB-L	70/72	Novus Biologicals	Rabbit	1:1000
Dll4	74	Abcam	Rabbit	1:500
β-III-tubulin (Tuj1)	50	Covance	Mouse	1:1000
FKBP38	45	Novus Biologicals	Rabbit	1:1000
PARP	82/86	Cell Signaling	Rabbit	1:1000
β -actin	45	Sigma	Mouse	1:10000

Supplementary table 6: antibodies used for immunohistochemistry in this studies

Antibody	**Manufacturer**	**Host**	**Dil (WB)**
Notch1	Santa Cruz	goat	1:200
Hes1	Chemicon	rabbit	1:500
HIF-1α	BD Abcam	mouse rabbit	1:20 1:50
Nestin	Chemicon	mouse	1:100
CD34	Novocastra	mouse	1:50
CD133	Abcam	rabbitv	1:200
CAIX	Novus Biologicals	rabbit	1:1000
Dll4	Abcam	rabbit	1:200
β-III-tubulin (Tuj1)	Covance	mouse	1:500
MAP2	Sigma-Aldrich	mouse	1:100
Ki67	Dako	mouse	1:200
glial fibrillary acidic protein (GFAP)	Sigma-Aldrich	rabbit	1:500
anti-mammalian β-actin	Thermo Fisher Scientific	rabbit	1:500

Supplementary table 7: antibodies used for immunocytochemistry in this studies

Antibody	Manufacturer	Host	Dil (WB)
Nestin	Chemicon	mouse	1:200
activated caspase-3	Cell Signaling	rabbit	1:2000
$p21^{cip1}$	Calbiochem,	mouse	1:800
β-III-tubulin (Tuj1)	Covance	mouse	1:1000
MAP2	Sigma-Aldrich	mouse	1:100
Ki67	Dako	mouse	1:100
glial fibrillary acidic protein (GFAP)	Sigma-Aldrich	rabbit	1:1000

To label apoptotic cells a terminal deoxynucleotidyltransferase-mediated dUTP nick end labeling (TUNEL) staining protocol was used using the In Situ Cell Death Detection Kit (Roche Diagnostics, Basel, Switzerland) according to manufacturer's instructions on paraformaldehyde-fixed GBM cell cultures.

Abbreviations used in the text

bFGF: basic Fibroblast Growth Factor
BMP: bone morphogenetic protein
BSA: bovine serum albumin
CNS: central nervous system
DAPI: 4',6-diamidino-2-phenylindole
EGF: Epidermal Growth Factor
GBM: glioblastoma
GFAP: glial fibrillary acid protein
HBSS: Hank's Buffered Salt Solution
HGG: high grade glioma
HIF: hypoxia inducible factor
HRE: hypoxia responsive element
Ig: immunoglobulin
MDB: medulloblastoma
mTOR: mammalian target of rapamycin
NICD: notch intracellular domain
PBS: Phosphate buffered saline
PHD: proline hydroxylase
PI3K: Phosphoinositide 3-kinases
PKB: protein kinase B
RT: room temperature
SDS: sodium dodecyl sulfate
SMAD: small/male tail abnormal/mothers against decapentaplegic homolog
SVZ: sub ventricular zone